CHALMERS
UNIVERSITY OF TECHNOLOGY

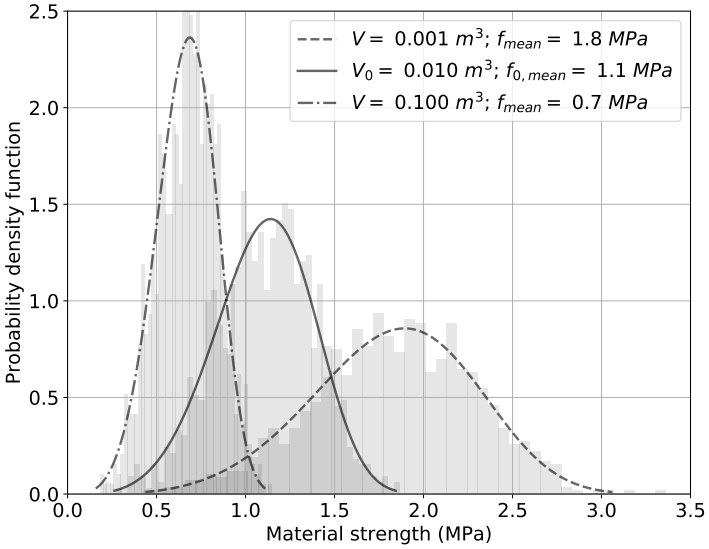

Probabilistic assessment of brittle failure modes of timber connections

A study to evaluate the load-carrying capacity of brittle failure modes and a parametric study to optimize the design of timber connections

Master's thesis in Structural Engineering and Building Technology

James C Koch

Department of Architecture and Civil Engineering
CHALMERS UNIVERSITY OF TECHNOLOGY
Master's thesis ACEX30
Gothenburg, Sweden 2020

Master's thesis ACEX30

Probabilistic assessment of brittle failure modes of timber connections

A study to evaluate the load-carrying capacity of brittle failure modes and a parametric study to optimize the design of timber connections

James C Koch

CHALMERS
UNIVERSITY OF TECHNOLOGY

Department of Architecture and Civil Engineering
Division of Structural Engineering
Research Group for Lightweight Structures
Chalmers University of Technology
Gothenburg, Sweden 2020

Probabilistic assessment of brittle failure modes of timber connections
A study to evaluate the load-carrying capacity of brittle failure modes and a parametric study to optimize the design of timber connections

James C Koch

Examensarbete ACEX30
Institutionen för arkitektur och samhällsbyggnadsteknik
Chalmers tekniska högskola, 2020

Department of Architecture and Civil Engineering
Division of Structural Engineering
Research Group for Lightweight Structures
Chalmers University of Technology
SE-412 96 Gothenburg
Telephone +46 31 772 1000

Cover: Modelling the size effect of the tensile perpendicular-to-grain wood strength.

Typeset in LaTeX
Department of Architecture and Civil Engineering
Gothenburg, Sweden 2020

Probabilistic assessment of brittle failure modes of timber connections
A study to evaluate the load-carrying capacity of brittle failure modes and a parametric study to optimize the design of timber connections
James C Koch
Department of Architecture and Civil Engineering
Chalmers University of Technology

Abstract

The growing popularity of timber as a building material fuelled by a increasing rise of both environmental and social sustainability is pushing timber structures to new heights. Taller and more complex timber structures are leading to higher capacity connections being required to continuing ensuring safe, efficient, robust, and reliable timber structural designs. Connections play an important role in the overall safety and reliability of timber structures by introducing ductility into the structural system to counteract the inherent brittle material behaviour of wood. Steel-timber connections are a common practical connection choice for high capacity connection systems to maintain ductility requirements as structures increase in height. To allow for a higher capacities, these connections are increasing not only the size of the timber members being joined together but also increasing the size and number of fasteners. Both of these two effects increase the likelihood of brittle failure mechanisms to occur; however, the likelihood of brittle failure modes is still a complex function of both material and geometric properties. The aim of this master's thesis is to develop a better understanding of when brittle failure mechanisms in high capacity timber connections occur to assist in the inclusion of explicit brittle failure models in reliable and robust timber connection design methods in tall timber structures. Simulation of material and geometric parameters of timber connections are presented to qualitatively assess the impact on capacity of the connection and the likelihood of brittle failure.

Keywords: timber engineering, tall-wood structures, structural connections, high capacity connections, brittle failure, probability of failure, ductile failure

Acknowledgements

I would like to thank the Division of Structural Engineering, Department of Architecture and Civil Engineering at Chalmers University of Technology for creating the encouraging environment to complete this master's thesis. The thesis has been performed from January 2020 to June 2020. I wish to express my sincere appreciation to my supervisor Assistant Professor Robert Jockwer: he convincingly guided and encouraged me to be professional and do the right thing even when the road got tough. Without his persistent help, the goal of this project would not have been realized. I would like to thank my opponents Maurice Kronberg and Malin Stening for their great feedback. Finally, I would like to thank all of my colleagues throughout the entire master's program.

James C Koch, Gothenburg, June 2020

Contents

1

Introduction

With the growing popularity of timber as a building material for more sustainable structures, timber buildings are being built taller and with more complexity requiring more efficient, robust, and reliable timber connections. The challenge to design timber connections to resist larger and more dynamic loads as a direct result of taller buildings is to continue to ensure a ductile structural response and minimize the probability of the types of failures which lead to catastrophic consequences should unexpected and improbable load conditions occur. As sustainable as timber is for a building material, the inherent brittle structural behaviour of timber carries a greater responsibility to ensure the catastrophic consequences of failure should a brittle material fail be properly accounted for. In large scale, mass timber connections a efficient way to increase the structure's ductility is through the structure's connection systems.

Hence, timber connections are a major consideration in the design of mass timber structures as they provide the ductility required for safe and reliable construction to any significant heights. In high-rise mass timber construction, timber-steel connectors are often used to reach the required capacity needed for the increased load associated with taller structures. These timber-steel connectors then contribute to increase the ductility of the structure by utilizing steel for the property it naturally provides better than timber which is comprised of a natural material known as wood which is inherently more brittle [1]. Brittle failure occurs suddenly and without warning often leading to severe consequences. This process of brittle failure is underscored by the theory of fracture mechanics. In contrast, ductility ensures that failure occurs only after significant plastic deformations occur where stress redistribution increases the ability of structural elements to deform further without causing failure immediately. Given the advantageous behaviour associated with ductility as opposed to brittle failure and the brittle material nature of timber, structures built using timber structural elements thus require connections to exhibit the majority of the structure's ductility [1]. As timber structures are dependent on connections to provide it with ductility to reliably and robustly carry the loads required of it, any structural design should take into account the inherent brittle nature of wood when predicting the load-carrying capacities of individual structural elements and global structural behaviour of the structure. This includes taking into account the often larger variability of brittle failure capacities than ductile failure capacities [2].

However, existing timber design standards (e.g. [3, CSA O86-14] [4, EC5] [5, NDS 2012]) rely on provisions to calculate the load-carrying capacity of connections solely using ductile failure modes described by the *European yield model (EYM)* and for example EC5 [4] only provides limited informative description of brittle failure mechanisms occurring at lower load levels. A reduction factor, n_{ef}, is included to implicitly account for brittle failure modes [4, EC5]. Fortunately with the last two decades, design standards (e.g. [3, CSA O86-14] [4, EC5] [5, NDS 2012]) have modified their design models to implicitly account for some brittle failure mechanisms through the prescription of minimum spacing requirements. Although,

there remains a lack of awareness among designers about the risks associated with neglecting to consider brittle failure modes in timber connection design [6]. By assuming the connection to fail in a ductile failure mode—the desired failure pattern—such as embedment failure of the timber members or fastener yielding, brittle failure mechanisms continue to not be fully accounted for with potential for devastating consequences. Approximately one quarter of recent collapses of timber structures are related to brittle failure of dowel-type connections with a significant number related to failure at unexpected load levels [7, 8]. It should be noted that the majority of these failures were a result of gross human errors; however, a survey conducted in the European area by Working Group 3 of the COST Action FP1402 report [9, 10] clearly shows that designers are of the opinion that connection design in the Eurocode 5 (e.g. [4, EC5]) lacks consistency (more than 15%), poorly presents technical content (more than 30%), lacks information (more than 30%), incorporates confusing statements (more than 35%), and is difficult to navigate (more than 50%). Given this reality, it is of interest to improve the robustness and reliability of timber connection design methods to promote safe and efficient usage of timber in the building industry especially given the increasing larger scale and importance of sustainable structures in today's building industry.

1.1 Types of timber connections

There are many types of timber connections employed to connect structural elements in a timber structure beginning from traditional carpentry timber joints to state-of-the-art glued-in rod timber joints. The majority of timber connections can be grouped into the following three areas of focus:

1. traditional carpentry joints,
2. dowel-type joints, and
3. adhesive joints.

Traditional carpentry joints are characterized by connecting timber elements without the use of external fasteners and rely instead on fitting two timber members together such as through the use of notches. These traditional joint techniques, however clever, are limited to seemingly low load-carrying capacities which make their use prohibitive in mass timber structures of any significant height. On the other hand, adhesive joints are uncommon due to the lack of practicality of gluing on a building site where external factors such as weather can severely degrade the integrity of such connections. By far the most common connection type used in practice are dowel-type joints, these joints connect two or more structural elements together by way of external fasteners often made of either wood or steel[1]. In the context of tall mass timber structures, steel fasteners are predominantly used to provide additional load-carrying capacity and ductility.

[1]A distinction between "dowel" and "fastener" is needed. The strict definition of a "dowel" refers only to a type of "fastener" which can be described as a smooth (unthreaded), round pin that tightly fits into a hole to fasten two adjacent members. In practice this definition is loosened to consider any type of "fastener" that fits into a hole to fasten two adjacent members and does not rely on threads to transfer load. For example, in practice nails and bolts are considered dowel-type fasteners while screws are generally classified as remaining different due to the threaded properties of screws. This thesis will take the view to use the term "fastener" instead of "dowel" except where it is explicitly meant to exclude threaded fasteners such as screws.

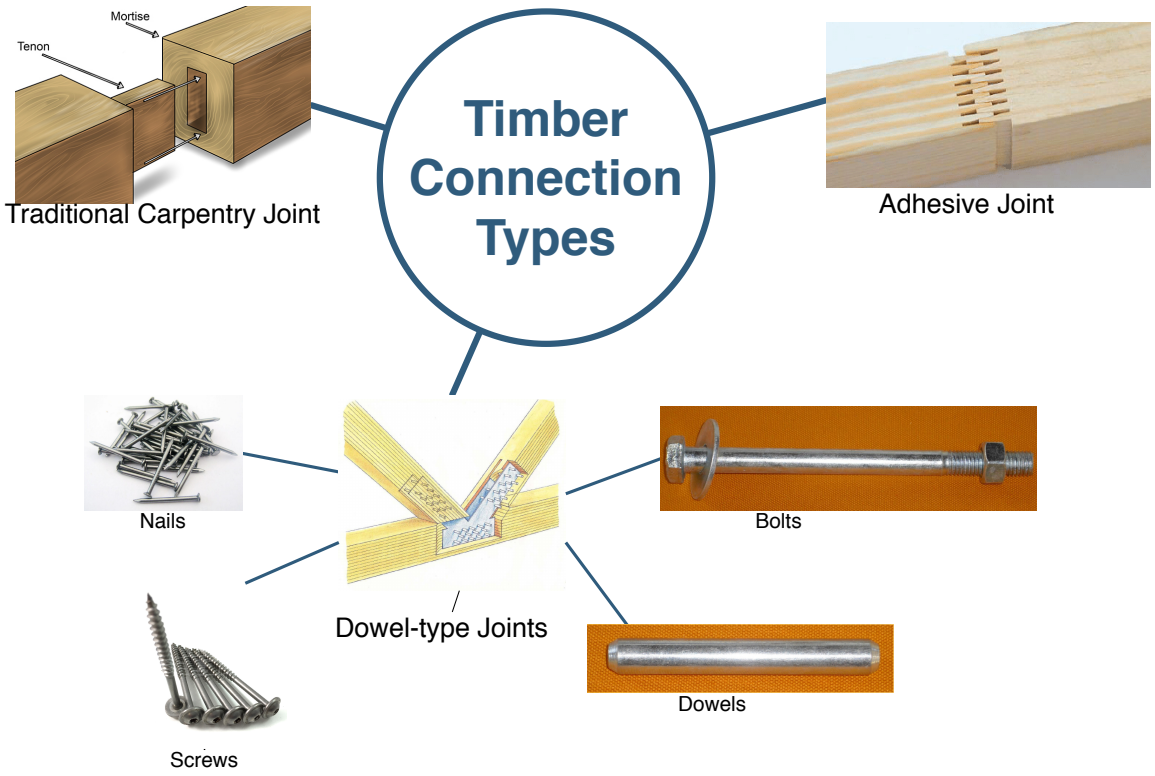

Figure 1.1: Illustration of timber connection types. Image sources (from left to right): traditional carpentry joints, nails, screws, steel dowels, bolts, structural finger joint

Fastener-type joints cover a wide and diverse range of fastener types all of which are in common use. Some fastener types which are most commonly used are nails, bolts, dowels, and screws. The difference between nails and bolts/dowels is primarily the diameter, d, of the fastener itself where nails are significantly smaller in diameter than bolts as well as pre-drilling is common for bolts/dowels. Additionally, bolts/dowels tend to have larger fastener heads. Fasteners with a $d \leq 8mm$ are commonly referred to as nails while fasteners with a $d > 8mm$ are referred to as bolts/dowels. Further, fasteners may either be unthreaded or threaded as in the case of nails/screws or bolts/dowels, respectively. Nails are often used in connections where the fastener does not extend through the entire timber members. Additionally, it should be noted that wood dowels may also be unthreaded. Figure 1.1 depicts the main groups of timber connections and various fastener types for dowelled joints.

1.2 High capacity timber connections

Recent trends to sustainable building materials such as timber has pushed timber buildings to new heights. As these structures are built taller, the loads which the structure must handle become larger requiring larger connections with higher capacities. Steel-timber connections consisting of embedded steel plates within the timber members to be joined are common connections when high capacities are required. These connections are commonly referred to as slotted-in steel plate timber connections.

The general features of these high capacity slotted-in steel plate timber connections is shown in figure 1.6 comprising of a steel plate slotted into the middle of a timber member. Often a steel backplate is then used on one end of the slotted-in steel plate where on the other side of

Figure 1.2: Images of the massive slotted-in steel plate timber connections used within the Mjøsa Tower. Source: Images from the presentation by CEO of Moelven Limtre, Rune Abrahamsen, at the Internationales Holzbau-Forum IHF in 2017

Figure 1.3: Image of the massive slotted-in steel plates of timber connections used within the Mjøsa Tower. Source: Images from the presentation by CEO of Moelven Limtre, Rune Abrahamsen, at the Internationales Holzbau-Forum IHF in 2017

the backplate a second timber member with its own slotted-in steel plate joins the connection itself. In this way, two timber structural elements are joined together. These slotted-in steel plate connections typically utilize fasteners made of steel rather than wood.

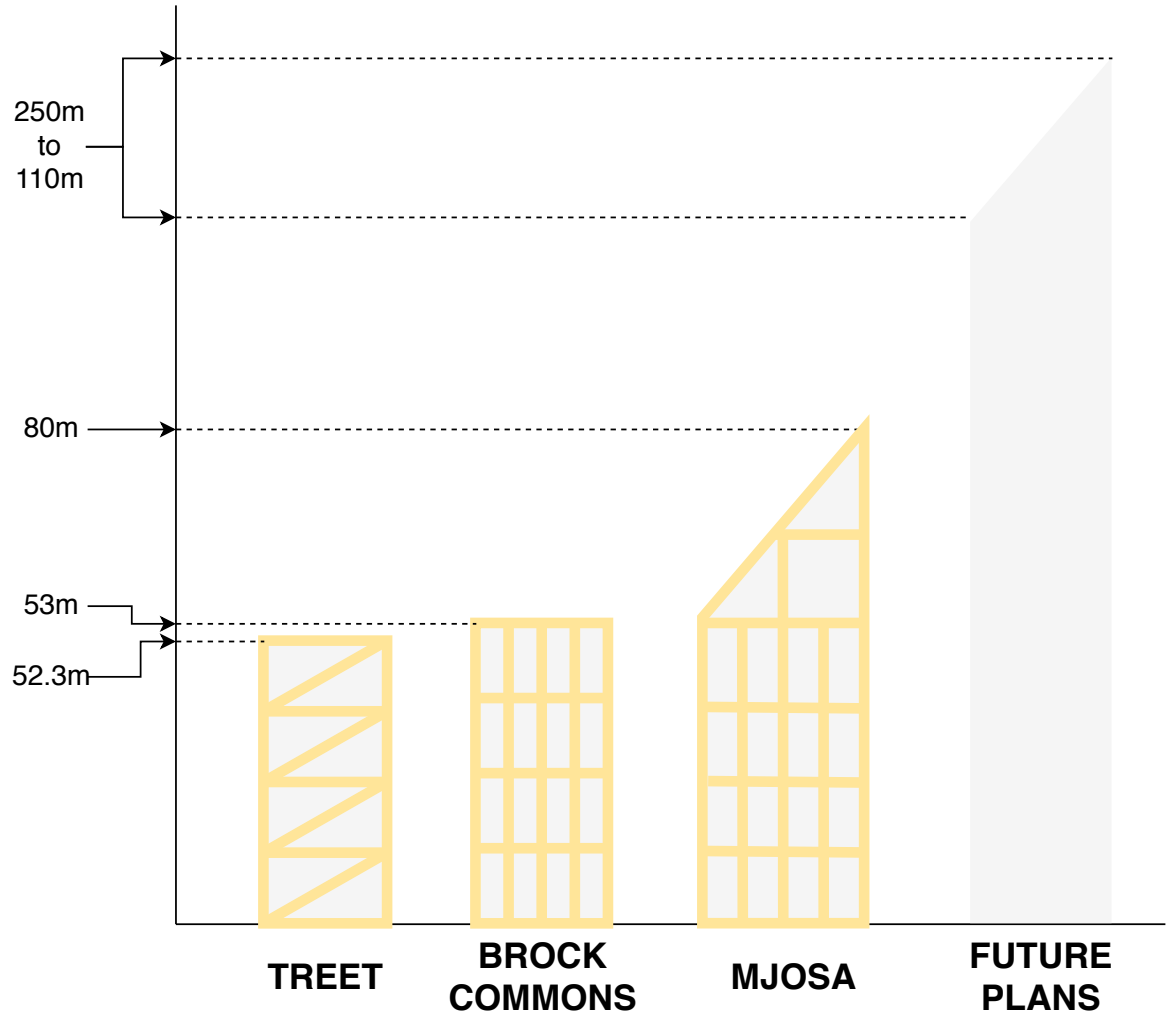

Figure 1.4: Heights attained by recent tall timber buildings.

Figures 1.2 and 1.3 shows a illustration of these type of connections as they often appear in mass timber structures. These connections are used in mass timber structures comprising of traditional post and beam construction or modern versions using glued or cross laminated engineered wood products. Traditionally, these connections only required a limited number of small fasteners to transfer load between structural elements; however, with timber structures being built taller more fasteners (and larger fasteners) are required to adequately transfer the increasing structural loads between elements. For example, recent structures shown in figure 1.4, known as Treet, Mjøsa and Brock Commons towers, built in Norway and Canada, respectively, have shown the ability for timber structures to reach heights previously thought of as unattainable. These structures reach to heights of $52.8m$, $80m$, and $53m$, respectively. These recent structures to a large degree rely on novel steel-timber connections to make their respective heights possible. At the time of this thesis there are considerable projects in progress and being planned to take the height of timber buildings to even further heights.

These timber structures are primarily possible due to innovative connection designs to accommodate for the higher loads corresponding with the increase in height. Figure 1.5 shows a sample of the engineering drawings of large scale slotted-in steel plate timber connections from the Mjøsa Tower [11]. These drawings indicate that the thickness of the connections using 6

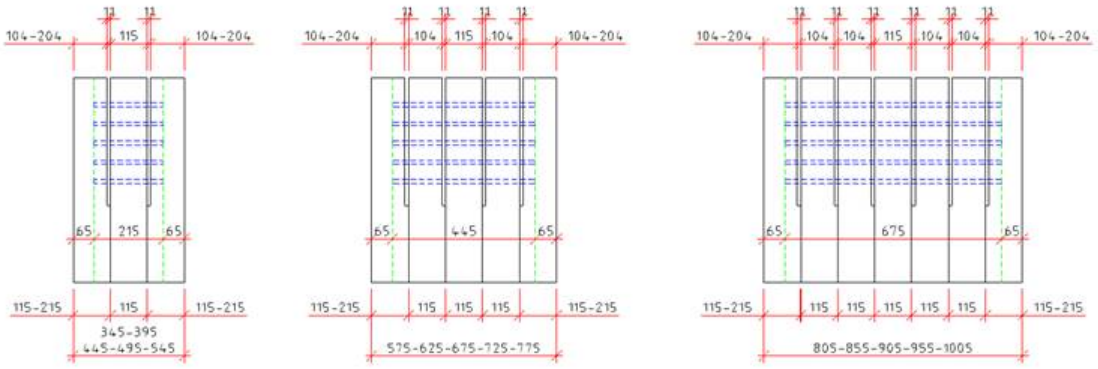

Figure 1.5: Illustration of the innovative massive connections used within the Mjøsa Tower structural system [11, Personal Communication]

multiple internal steel plates ranging in total thickness from 805mm to 1005mm. A significant challenge to safe, reliable, and robust design of these innovative, high capacity connections is that modern design standards (e.g. [3, CSA O86-14] [4, EC5] [5, NDS 2012]) are based on at most a single slotted-in steel plate (e.g. double shear) connections indicating that the assumptions of the existing models may no longer be fully applicable when multiple slotted-in steel plates are considered. Research into the applicability of existing design methods for multiple steel plate timber connections is required to be studied and how multiple steel plate timber connections exhibit structural behaviour which is different from single slotted-in steel plate (e.g. double shear) timber connections.

1.3 Objective and Scope

The aim of this master's thesis is to develop guidance to reliably and robustly design larger mass timber connections in tall timber structures such as the Mjøsa Tower. The primary behaviour shown to affect these large steel-timber connections which smaller such connections are not subjected to are brittle fracture mechanisms. Not all brittle failure mechanisms are explicitly considered in the modern timber design standards (e.g. [3, CSA O86-14] [4, EC5] [5, NDS 2012]) with many only accounting for brittle failure implicitly. Newer research efforts have been made to develop design models to aid designers to explicitly control for brittle failure possibilities when designing timber connections [12, 13, 14, 15, 6, 10, 2]. As much as these efforts have made progress to better understand when, where, how, and why some timber connections fail in a brittle fashion rather than the more desirable ductile behaviour, a lack of a unified consensus on the form of a over-reaching brittle design model compatible with the existing largely ductile design model in existing timber design standards (e.g. [3, CSA O86-14] [4, EC5] [5, NDS 2012]) is still apparent. This provides designers with significant challenges of sometimes contradictory models on which to design safe, reliable, and robust timber connections especially for larger connections employed in tall mass timber buildings without requiring advanced analyses for example incorporating finite elements.

The scope of this project is to identify and evaluate the impact of both geometric connection parameters and material variability on the load-carrying capacity—including its own variability—and resulting failure mechanism developed using a consistent and compatible failure model derived from a thorough literature review. Additionally, the project will describe a program-

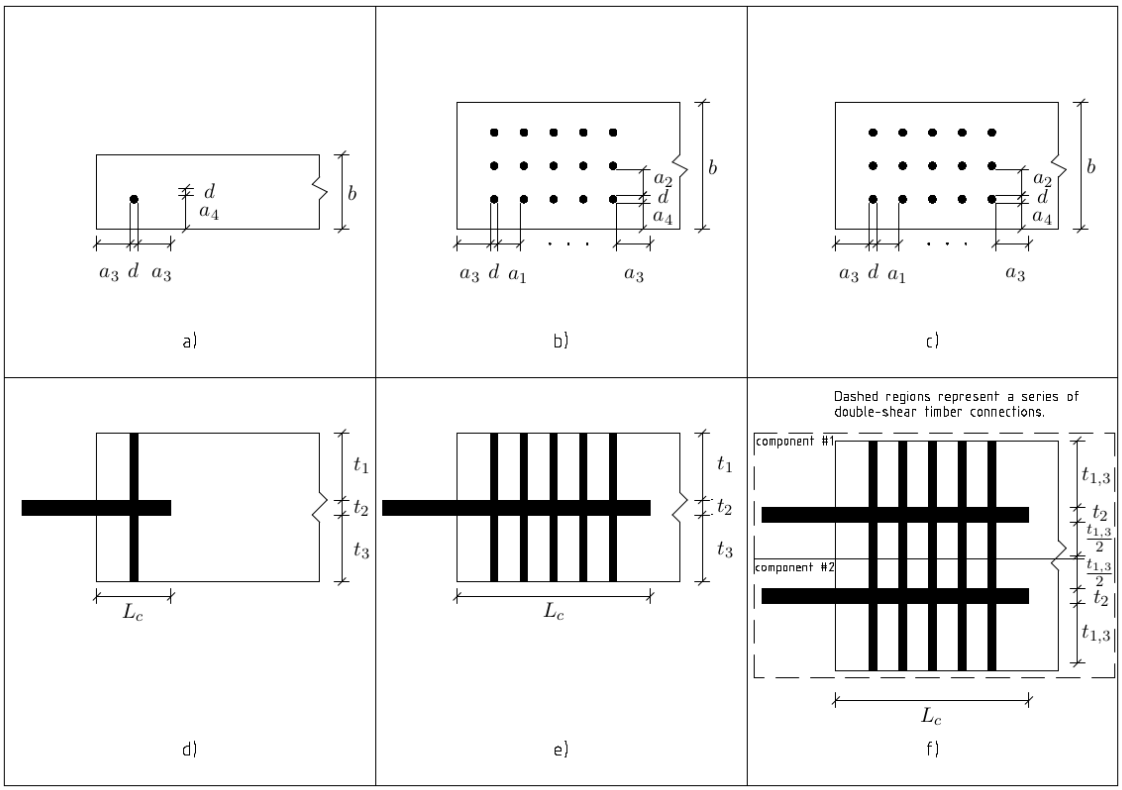

Figure 1.6: TST connection sections (top row (a-c): front section view; bottom row (d-f): lateral section view) and symbol definitions.

ming paradigm to compute the load-carrying capacity using a unified failure model for timber connections explicitly including both ductile and brittle failure mechanisms. The type of connections within the scope of this study are limited to laterally loaded timber-steel-timber connections (previously referred to as slotted-in steel plate timber connections) with fastener diameters larger than $d > 8mm$, such as those connections used in the Mjøsa Tower depicted in figures 1.2 and 1.3. Thus, massive connections are emphasized where the influence of the "size effect" is large. Figure 1.6 illustrate the relevant 2D section views and define the symbols of the geometric parameters needed to calculate the load-carrying capacity used in the remaining chapters of this thesis. The study will include the variability of material properties to include a probabilistic framework to determine the respective probability of either ductile or brittle failure governing the load-carrying capacity of each connection through the use of Monte Carlo simulation. Lastly, the study is aimed at developing practical design guidelines and equations for the accurate, safe, and simple calculation of the load-carrying capacity of dowel-type laterally loaded connections within tall timber structures.

1.4 Limitations

This study will be limited to the analysis of bolted laterally loaded TST connections with respect to ductile and brittle failure modes. The slotted-in steel plates may be of any thickness, t_2, as the fixity conditions of the fasteners are independent of the plate thickness as opposed to external steel plates where the fixity of the fasteners is dependent on the plate thickness. For simplicity, a single yet commonly used in practice steel plate thickness, $t_2 = 10mm$, is chosen. The fasteners are assumed to be completely fixed—i.e. moment transferring—with the slotted-

in steel plates. This may not always be accurate especially when considering large diameter fasteners which will affect their ductile load-carrying failure capacity; however, generally when large diameter fasteners are used in a connection design fewer number of fasteners are also used which is known to increase the likelihood of brittle failure to govern the connection design. In this case, over-estimating the ductile failure capacity—not accounting for dowel to steel plate fixity conditions correctly—is considered to be negligible when introducing a accurate brittle failure model capable of calculating the considerably lower load levels occurring brittle failure capacity.

$$f_{h,\theta,i} = \frac{f_{h,\parallel} f_{h,\perp}}{f_{h,\parallel} \sin^2 \theta + f_{h,\perp} \cos^2 \theta} \tag{1.1}$$

All connections studied in this thesis will consider loading in the parallel-to-grain wood direction to simplify the number of connection capacities to be computed. Furthermore, the theory of loading conditions at any angle with respect to the wood grain direction has been thoroughly researched culminating in the well-known Hankinson's formula (equation 1.1). It is thought that this formula could be applied to any properties in a unified failure model of timber connections to account for loading conditions at any angle.

Additionally, the failure model used within this project are analytical equations as the purpose is to promote a practical design approach to be used by designers in industry; however, the programmatic paradigm in which the failure model is computed would allow for these analytical equations to be replaced with more accurate expressions after a further detailed research on the individual failure mechanisms represented in the failure model. This thesis is limited to only considering practical algebraic equations to compute the load-carrying capacity to understand the qualitative relationship between input parameters and formulate a practical design calculation paradigm including a probabilistic framework to account for variability in material properties. Each timber connection considered in this thesis is computed with 1000 realizations of the required material properties sampled from their respective probability distributions which is considered to be sufficiently many samples to characterize the statistical distribution of the variables while considering the limited computational power available of modern desktop computer.

2

Ductile Failure

In this first chapter, the background theory of ductile failure of timber connections is considered. The existing design models included in current timber design standards (e.g. [3, CSA O86-14] [4, EC5] [5, NDS 2012]) are used as a starting point to develop the context needed for the analyses presented in this thesis. Much of the ductile failure model of modern timber connection design relies on Johansen's theory (aka the EYM) [16] which is the background of the models contained within the current design standards.

2.1 Background theory

2.1.1 European Yield Model (EYM)

The basis of the EYM as the foundation of the structural principles for the design of timber connections was developed by Johansen [16] and published in 1949. The model presented in Johansen's theory [16] is described to be the best model to fit the experimental observations of [17, Trayer] available in 1949 [18]. The structural principles developed in the EYM enabled consistent design methods to be developed through the scientific method during the 1980s leading to the current limit state design philosophy implemented in timber design standards (e.g. [3, CSA O86-14] [4, EC5] [5, NDS 2012]) today.

Johansen's theory [16] describes the structural behaviour of timber fastener-type connections loaded parallel to the grain using three elementary effects used to then derive equations to represent all possible ductile failure mechanisms. These three elementary effects are described as:

1. the resistance of timber to crushing underneath a fastener,

2. the effect of friction between the timber member and fastener, and

3. the effect of the dog[1].

The first effect is often referred to as the "dowel effect" corresponding to the resistance of the wood to the dowel trying to bend and induce local crushing deformations to occur in the timber member beneath the dowel itself. The second effect is that of friction between the surfaces of

[1]The "dog" refers to a metal device inserted between the adjacent timber members to increase the friction between the members themselves. The "dog" can be imagined as a metal bracket with teeth which embed themselves into each timber member preventing slippage due to friction.

the connected members arising from the dowel deforming and inducing a tensile force parallel to the surface connecting the members together. This "tension effect" of the fastener is then the frictional response of the two materials of each member sliding against each other as a result of the application of a load parallel to the shared surface. The third elementary effect is the effect of the dog[1] which describes the increasing effect of friction resulting from the deformation of the dowel on loading [16].

Using only the first effect, Johansen's theory [16] consists of a set of equations to calculate the load-carrying capacity of fastener-type connections when loaded laterally as a function of the embedment strength of the timber members, f_h, yield moment of the fastener, M_y, and dowel diameter, d. Johansen's theory as first proposed neglected to include the effect of friction or the effect of a toothed "dog". Frictional effects as encompassed by the second two effects identified by Johansen [16] were later studied in detail and added to the model which is now known as the European yield model (EYM) beginning with the work of Meyer [19] in 1957.

The next section 2.2 describes these parameters and their effects on the strength of connections in more details. Moreover, these load-carrying capacity equations derived by the EYM represent failure mechanisms which characterize all possible ductile failure mechanisms. Although, it has been argued in some recent literature articles [20] that the EYM failure modes which are proportional only to the embedment strength of the timber members (e.g. mode I which is defined in section 2.1.2) should be viewed as a brittle failure mechanisms or only as a quasi-ductile failure mode since wood—timber being made of the material wood—is itself a brittle material; however, most literature discussions continue to include this failure mode as one mechanism within the set of mechanisms derived by EYM [13, 21, 6, 2, 22] which is described as representing ductile failure modes.

The theoretical derivations of the EYM equations are presented in the next three sections 2.1.2 to 2.1.4 for three member symmetrical timber only connections. Additional derivations are then described to adapt these equations for TST connections focused on in this thesis. It should be noted in the following derivations presented the member which is replaced with steel as the material is always the middle member as the connections studied in this thesis are timber-steel-timber (TST), slotted-in steel plate connections. These equations are broadly based on three conditions identified as leading to failure corresponding to either zero, one, or two plastic hinges forming within the fastener, shown schematically in Figure 2.1, resulting in three mechanisms. Similar equations may be adapted for other connection types; however, this is left to the reader who is encouraged to refer to the following design guides and textbooks [23, 24] for further details. Additionally, the complete set of equations (not including their theoretical derivations) may be found in most design guides [23, 24] or design standards (e.g. [3, CSA O86-14] [4, EC5] [5, NDS 2012]).

2.1.2 Failure mechanism I: Zero plastic hinges

Failure mechanism shown in figure 2.2 defined as mode I identifies the case where no plastic hinges are formed within the fastener. This means that the dowel remains straight and does not bend; however, it should be noted that theoretically a additional possibility is that the fastener rotates while remaining straight. For the purposes of this thesis, this alternative mode I is not considered due to the type of connection studied which uses a steel plate slotted in between two timber members preventing the pure rotation of a fastener without the formation of a plastic hinge within the fastener itself. The strength of a connection governed by this first

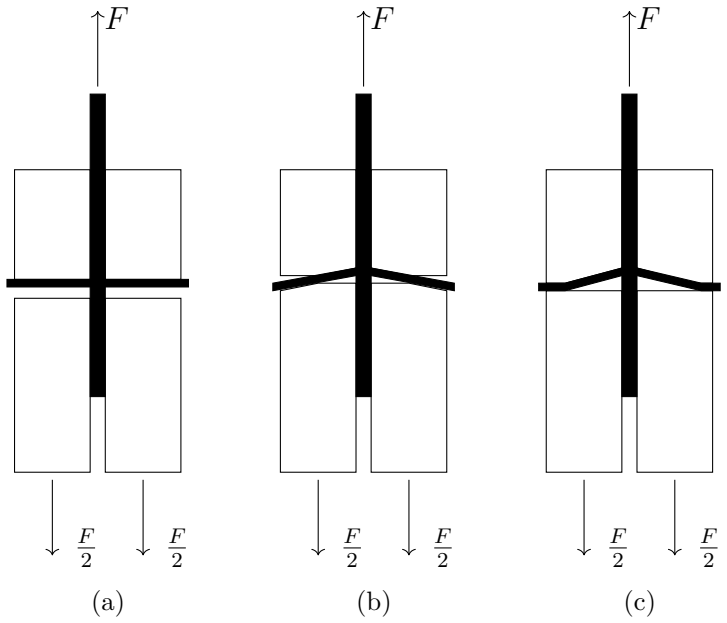

Figure 2.1: Illustration of failure modes according to the EYM for a steel-wood-steel connection with one dowel.

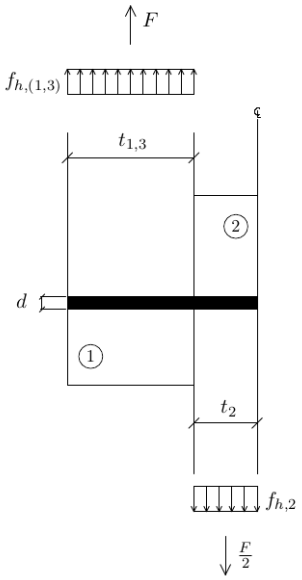

Figure 2.2: Failure mechanism I.

failure mode is then entirely a function of the f_h and the geometric properties of the timber member itself.

$$F_v = f_{h,i} t_i d \tag{2.1}$$

Equation 2.1 is given by Johansen's theory [16] to calculate the lateral load-carrying capacity per shear plane within a timber connection. The subscript, i, of equation 2.1 is introduced to account for potential differences in f_h and member thickness, t, of each timber member being joined together by the connection. The consequence is that the member which results in the lowest capacity is defined as the critical member and it is this strength for which the connection capacity is designed for with regard to the possible mode I failure mechanism.

2.1.3 Failure mechanism II: One plastic hinge

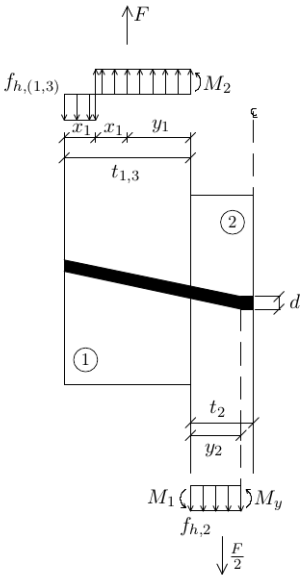

Figure 2.3: Failure mechanism II.

The second mode—shown in figure 2.3 and defined as mode II—identifies the failure mechanism where one plastic hinge forms within the fastener. For one plastic hinge to form, the fastener must bend and deform in either member present in a connection with a single shear plane.

$$F_v = \frac{f_{h,1} t_1 d}{2+\beta} \left(\sqrt{2\beta(1+\beta) + \frac{4\beta(2+\beta) M_y}{f_{h,1} d t_1^2}} - \beta \right) \tag{2.2}$$

$$F_v = f_{h,1} t_1 d \left(\sqrt{\frac{2\beta(1+\beta)}{(2+\beta)^2} + \frac{4\beta(2+\beta)}{(2+\beta)^2} \frac{M_y}{f_{h,1} d t_1^2}} - \frac{\beta}{(2+\beta)^2} \right)$$

$$F_v = f_{h,1} t_1 d \left(\sqrt{\lim_{\beta\to\infty} \left(\frac{2\beta(1+\beta)}{(2+\beta)^2} \right) + \lim_{\beta\to\infty} \left(\frac{4\beta}{2+\beta} \right) \frac{M_y}{f_{h,1} d t_1^2}} - \lim_{\beta\to\infty} \left(\frac{\beta}{2+\beta} \right) \right)$$

applying L'hopital's rule

$$F_v = f_{h,1} t_1 d \left(\sqrt{\lim_{\beta\to\infty} \left(\frac{2+4\beta}{2(2+\beta)} \right) + \lim_{\beta\to\infty} \left(\frac{4}{1} \right) \frac{M_y}{f_{h,1} d t_1^2}} - \lim_{\beta\to\infty} \left(\frac{1}{1} \right) \right)$$

applying L'hopital's rule

$$F_v = f_{h,1} t_1 d \left(\sqrt{\lim_{\beta\to\infty} \left(\frac{4}{2} \right) + 4 \frac{M_y}{f_{h,1} d t_1^2}} - 1 \right)$$

$$F_v = f_{h,1} t_1 d \left(\sqrt{2 + \frac{4 M_y}{f_{h,1} d t_1^2}} - 1 \right) \tag{2.3}$$

Equation 2.2 shows the analytically derived expression to compute the load-carrying capacity of this failure mechanism per shear plane. The connection for which the equation 2.2 is derived consists of three timber members (double shear plane connection) and thus could potentially be made of different species of wood with different embedment strengths which is captured by the ratio, $\beta = \frac{f_{h,2}}{f_{h,1}}$. To transform equation 2.2 to represent a steel-timber connection (where the central member designated with the number 2 in figure 2.3 is a steel plate), the parameter β in this instance is allowed to approach infinity due to its definition as $\frac{f_{h,2}}{f_{h,1}}$. Should the outer members be replaced with steel, the parameter β would tend to zero instead resulting in a different formulation of equation 2.3 which is, however, out of scope of this thesis. This is because steel as a material has a much higher embedment strength than timber. Allowing $\beta \to \infty$, the load-carrying capacity per shear plane is then expressed in equation 2.3.

2.1.4 Failure mechanism III: Two plastic hinges

The third and final failure mode—shown in figure 2.4 and defined as mode III—for a timber connection which may occur is when two plastic hinges form within the fastener. This is typically a very desirable governing failure mechanism as it features the highest ductility possible for a timber connection to exhibit.

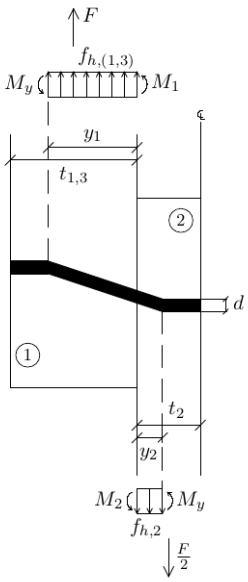

Figure 2.4: Failure mechanism III.

$$F_v = \sqrt{\frac{2\beta}{1+\beta}}\sqrt{2M_y f_{h,1} d}$$

$$F_v = \lim_{\beta\to\infty} \sqrt{\frac{2\beta}{1+\beta}}\sqrt{2M_y f_{h,1} d}$$

applying L'hopital's rule

$$F_v = \lim_{\beta\to\infty} \sqrt{\frac{2}{1}}\sqrt{2M_y f_{h,1} d}$$

$$F_v = \sqrt{2}\sqrt{2M_y f_{h,1} d}$$

$$F_v = 2\sqrt{M_y f_{h,1} d} \tag{2.4}$$

The equation representing this failure mechanism is analytically derived following the same procedure as for the previous section 2.1.3 and is shown in equation 2.4. Again, the case where $\beta \to \infty$ is utilized to consider the effect of the steel plate.

2.1.5 Load-carrying capacity of timber connections

The preceding three sections (2.1.2 to 2.1.4) have dealt and derived the base three ductile failure mechanisms which can occur in timber connections and how they may be adapted to TST connections. The equations 2.1 to 2.4 presented define the load-carrying capacity per shear plane of a TST connection because the assumption those derivations rely on consider only two members being connected. Double shear plane connections, such as those studied in this thesis, are considered by assuming each timber side member of the TST connection is symmetric with respect to the material strengths while the minimum thickness of each side member is used. Further, these failure mechanisms are derived on the basis of one and only one fastener. In typical structural mass timber connection design, multiple fasteners are used to achieve a higher capacity which is sufficiently larger than the applied loads. There are some differences in typical

designs produced depending on the geographic area where the designer resides in such that European connection designs tend to incorporate many more smaller diameter fasteners while North American designers often use fewer but larger diameter fasteners. These differences have a significant influence on the load distribution between fasteners in multiple fastener connections but also relate to differing brittle failure concerns (the latter described in detail in chapter 3).

Figure 1.6 depicts the geometry of single and multiple fastener TST connection with one or two slotted-in steel plates. Due to variability in strength properties when a connection is loaded not all fasteners will reach their load-carrying capacity at the same time. This means that load redistribution occurs if sufficient ductility can be achieved where increasing load is shifted to the least loaded fasteners from the highest loaded fasteners with increasing applied load. The possibility of load redistribution is confirmed by experimental tests reported in the literature [25, 26, 27, 28, 29, 30, 31] and more recently by numerical finite element (FE) simulations [32, 33, 21].

$$F_{multiple} = n_{ef} F_{single} \tag{2.5}$$

$$\text{, where } n_{ef} = \min \begin{cases} n \\ n^{0.9} \sqrt[4]{\frac{a_1}{13d}} \end{cases}$$

The resulting simplified design equation included in [4, EC5] to account for the load distribution between fasteners in multiple fastener connections is defined in equation 2.5 which was derived from the equations proposed by [12]. Equation 2.5 is modified to use to account for load redistribution in multiple fastener timber connections in this thesis where the fourth root term is omitted as brittle failure mechanisms are rather explicitly controlled for (refer to chapter 3 for further details).

Additionally, TST connections may contain more than one steel plate (resulting in greater than two shear planes) and thus would exhibit a greater load-carrying capacity. The superposition principle is used to determine the load-carrying capacity of the entire connection assembly for multiple steel plate connections.

Table 2.1: Description of consistent load-carrying capacities per steel plate.

Single internal steel plate	**Multiple internal steel plates**	
	Outer internal plates	Inner internal plates
$\min \begin{cases} F_I + F_I \\ F_{II} + F_{II} \\ F_{III} + F_{III} \end{cases}$	$2 \min \begin{cases} F_I + F_{Ib} \\ F_I + F_{III} \\ F_{II} + F_{Ib\} \ F_{III}+F_{Ib}} \\ F_{II} + F_{III} \\ F_{III} + F_{III} \end{cases}$	+ (n_{s} - 2) $\min \begin{cases} F_{Ib} + F_{Ib} \\ F_{III} + F_{III} \end{cases}$
Remarks	F_I: Eq. 2.1 $F_{Ib} = \frac{1}{2} F_I$ » Note 1	F_{II}: Eq. 2.3 F_{III}: Eq. 2.4
Note 1:	For symmetric connections only.	

In a simple TST connection consisting of a single steel plate, the load carrying capacity as determined on the basis of the EYM is the minimum of two times each capacity computed

using the three failure mechanisms described in sections 2.1.2 to 2.1.4. Table 2.1 describes the failure cases which must be taken into account for TST connections with multiple steel plates and comparing the set of failure modes with those of a single internal steel plate connection. These combinations of the base three failure mechanisms—mode I, II, and III—must be carefully considered to allow for a consistent set of combinations of base failure mechanisms to ensure deformation compatibility of the fastener itself. The term "consistent combinations of base failure mechanisms" refers to the requirement to ensure that the fastener deforms continuously throughout the entire connection made up of multiple steel plates. This is therefore a continuity condition which is required to be met for the fastener deformation in steel-timber connections. Only the case of symmetric connections—where the timber members are equally thick and equal in material strengths—are shown in table 2.1 for TST type connections. The failure mechanism represented by $F_{Ib} = f_h \frac{t_{1,3}}{2} d$ is only used in multiple internal steel plate connections since it divides the thickness of the timber members between two internal steel plates in half where each half is considered to contribute to the load-carrying capacity of each shear plane associated with each steel plate on each side of the timber member.

This means internal steel plate parts contribute more to the overall ductile load-carrying capacity according to the EYM failure equations than outer steel plate parts as smaller timber member thickness are needed to achieve full ductile failure as in failure mode III. The principle of superposition can then be used to compute the load-carrying capacity of any number of slotted-in steel plates by means of the equations in table 2.1, where n_s denotes the number of steel plates.

2.2 Influencing parameters

Generally, the EYM only requires 5 parameters to calculate the load-carrying capacity of any timber connection which are:

1. the side member thickness, t_1,
2. the main member thickness, t_2,
3. the fastener diameter, d,
4. the timber density, ρ, and
5. the fastener yield strength, f_y, or fastener ultimate strength, f_u.

The disadvantage of this simplicity is other influencing parameters such as minimum end spacings—between fastener and edge of the timber members—and spacing between fasteners in multiple fastener connections are neglected which can lead to brittle failure modes to occur at lower load levels [34, 13, 32, 21, 35, 6]. The simplicity of this approach is nevertheless advantageous to use in design but care must be taken to apply the EYM only in situations where it is accurate and reliable. It is of importance to then understand the base assumptions on which the theory stands especially as to how the EYM uses these few input parameters to derive representative quantities to use in the calculation of the ductile load-carrying capacity of timber connections. The embedding strength of wood, f_h, and the yield moment of fasteners, M_y, are the two main derived parameters required for the design of timber connections. The embedment strength of wood, f_h, is a vital parameter in the calculation of the ductile capacity

of timber connections according to Johansen's theory (aka EYM) [17, 16, 18]. These two main derived parameters are described in the next sections 2.2.1 and 2.2.2 in greater detail beginning with the embedment strength, f_h, and concluding with the fastener yield moment, M_y, respectively.

2.2.1 Embedment strength of wood

Given the relative high importance of the embedment strength property of wood with regard to structural connection design, a thorough understanding of the embedment behaviour of wood is needed. The properties which influence the embedment behaviour of wood are well-researched and are identified as the timber density, ρ, and the fastener diameter, d, [36, 37, 38, 39]. Less well understood are the specific relationships between these influencing properties and the embedment strength, f_h. Many studies support the conclusion that the timber density, ρ, is the only influencing material property and correlates positively and linearly with the value of the embedment strength, f_h [36, 38, 40, 41]. How the variables d and f_h are related is less well agreed upon with significant differences existing in models presented in recent studies in the literature [40, 41]. Despite the embedment behaviour of timber being complex, current provisions in modern design standards (e.g. [3, CSA O86-14] [4, EC5] [5, NDS 2012]) are comparatively simple to allow for easy application yet have been shown to be inconsistent and unreliable [40]. To reliably understand the embedment behaviour of wood in timber connections requires a more nuanced theoretical and experimental understanding of the specific statistical variation between influencing properties and the embedment strength, f_h.

An initial overview of the challenges of evaluating the reliability of existing models to predict the embedment strength of timber considers a probabilistic design framework to develop a new and more reliable prediction model [42, 43] based on existing experimental data. The main difference and challenge evaluating the embedment strength under a probabilistic design framework is to account for the non-linearity of the relationship with the influencing properties: ρ and d. Due to the variability in timber density, the relationship with the embedment strength is not perfectly linear. Additionally, the fastener diameter also does not appear to portray a linear relationship with the embedment strength since the fastener diameter is also weakly correlated with the timber density [42]. The recent literature on the embedment behaviour of wood also suggests that existing models used in design standards are inadequate to account for variability of the influencing parameters. This chapter of this thesis aims to review and summarize the most relevant findings and conclusions from the existing literature on the current scientific understanding of the embedment strength of wood by comparing existing models against each other on the basis of existing experimental results available in the literature.

A comprehensive review of the design of timber connections according the EYM is described in the previous section 2.1 while further details can be found in timber design handbooks [44, 23, 24]. The remaining part of this section considers the influence on the embedment strength, f_h, of the two properties denoted by the variables of timber density, ρ, and fastener diameter, d. Furthermore, existing models to evaluate the f_h are only valid for loading which acts parallel and perpendicular to the wood grain orientation due to anisotropic mechanical behaviour of wood.

$$f_{h,\theta,i} = \frac{f_{h,\parallel} f_{h,\perp}}{f_{h,\parallel} \sin^2\theta + f_{h,\perp} \cos^2\theta} \tag{2.6}$$

$$f_{h,\theta,i} = \frac{f_{h,\parallel}}{\frac{f_{h,\parallel}}{f_{h,\perp}} \sin^2\theta + \cos^2\theta} \tag{2.7}$$

As with any property in timber engineering design which depends on the loading angle with respect to the wood grain orientation, the existing models for the f_h parameter can be generalized to all possible loading angles using Hankinson's formula (Eq. 2.6) which relates the parallel- and perpendicular-to-grain strengths to any off-axis strengths. It should be noted that in some design standards (e.g. [4, EC5]), the variable, k_{90}, is used in place of the term $\frac{f_{h,\parallel}}{f_{h,\perp}}$ shown in equation 2.7 to simplify the calculation contained within Hankinson's formula.

$$\begin{aligned} f_{h,\parallel} &= 0.082\rho(1 - 0.01d) \\ f_{h,\perp} &= \frac{41\rho(d - 100)}{75(d + 90)} \\ k_{90} &= \frac{f_{h,\parallel}}{f_{h,\perp}} = 1.35 + 0.015d \end{aligned} \tag{2.8}$$

$$\begin{aligned} f_{h,\parallel} &= 0.082\rho(1 - 0.01d) \\ f_{h,perp} &= 0.036\rho(1 - 0.01d) \\ k_{90} &= \frac{f_{h,\parallel}}{f_{h,\perp}} = 2.27 \end{aligned} \tag{2.9}$$

$$\begin{aligned} f_{h,\parallel} &= 0.077\rho \\ f_{h,\perp} &= 0.042\rho^{1.45} d^{-0.5} \\ k_{90} &= \frac{f_{h,\parallel}}{f_{h,\perp}} = 1.8\bar{3}\rho^{-0.45} d^{-0.5} \end{aligned} \tag{2.10}$$

Equations 2.8 to 2.10 show the existing models used to evaluate f_h in three current design standards, e.g. [3, CSA O86-14] [4, EC5] [5, NDS 2012], respectively. These equations have been transformed to compute mean values of the f_h from the characteristic design equations according to the methodologies used in each design standard to relate mean and 5^{th} percentile values. This transformation of characteristic to mean value equations is based on the work by Kennedy et al. [41]. Additionally, it should be noted that the unit for density used here is $\frac{kg}{m^3}$ while articles cited herein may use different units chief among them $\frac{g}{cm^3}$. This paper also uses a reference wood moisture content (MC) of 12% which may also vary from articles referenced herein. Equations 2.8 to 2.10 were developed based on empirical mean value regression equations of extensive testing during the 1980s [45, 37, 36, 39]. For the purpose of the comparison study presented in this paper, average values will be used to compare the models to evaluate f_h in each design standard without introducing effects of different modification factors (e.g. load duration, service conditions, or treatment factors) used in each design standard.

Since the adoption of the current equations in modern design standards further research has shown that these equations may be improved to better predict the f_h as well as quantify the effect of the variability of input properties on the f_h and thus the reliability of the connection design [40, 42, 41]. Particularly, a deeper understanding of the relationship between the fastener diameter and embedment strength is investigated in recent literature [37, 45, 39] and this thesis focuses on this aspect of the current embedment strength models. The following three subsections 2.2.1.1 to 2.2.1.3 review the three most significant and relevant articles from the recent literature [40, 42, 41].

2.2.1.1 Comprehensive experimental testing of the dowel embedding strength [40]

The study reviewed here focuses on presenting an experimental testing regime to fill a gap in the literature relating to quantifying the variability of f_h parameter to enable a reliability-based design methodology. Reliability-based design requires knowledge of the variability of input parameters which allows for more efficient and accurate models to evaluate the mechanical behaviour within a certain known level of uncertainty. The embedment strength tests were done according to the EN 383 [46] standard on commonly used softwood timber species in Japan and four fastener diameters of 8, 12, 16, and 20 millimetres. Several different strength grades—structural timber is visually or machine graded according to strength—were also included in the experimental testing regime. It should be noted that structural timber is not only strength graded but is graded according to many other criteria such as modulus of elasticity and density.

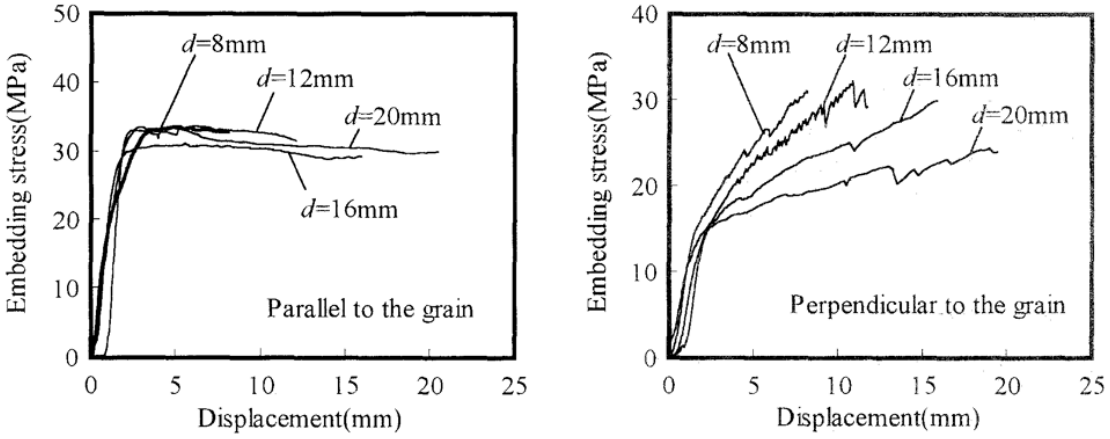

Figure 2.5: Embedding stress as a function of displacement (taken from [40]).

Firstly, embedding stress as a function of embedding displacement curves (see figure 2.5) were plotted for each test group identified in the methodology of the paper [40]. These embedding stress-displacement curves show a significant difference in response to parallel- and perpendicular-to-grain loading. Parallel-to-grain loading showed the familiar linear elastic perfectly plastic deformation response commonly assumed in analysis and design procedures. On the other hand, perpendicular-to-grain loading showed a continuing increase in load even after yielding—commonly referred to as hardening—which was significantly influenced by the fastener diameter. A larger fastener diameter was associated with more deformation and lower increase in embedding stress compared to smaller fastener diameters leading to higher ductility with larger diameter fasteners when loaded perpendicular-to-grain. The inference which is suggested is that the fastener diameter only influences embedment strength when loaded perpendicular-to-grain and not when loaded parallel-to-grain. It could also be inferred that as

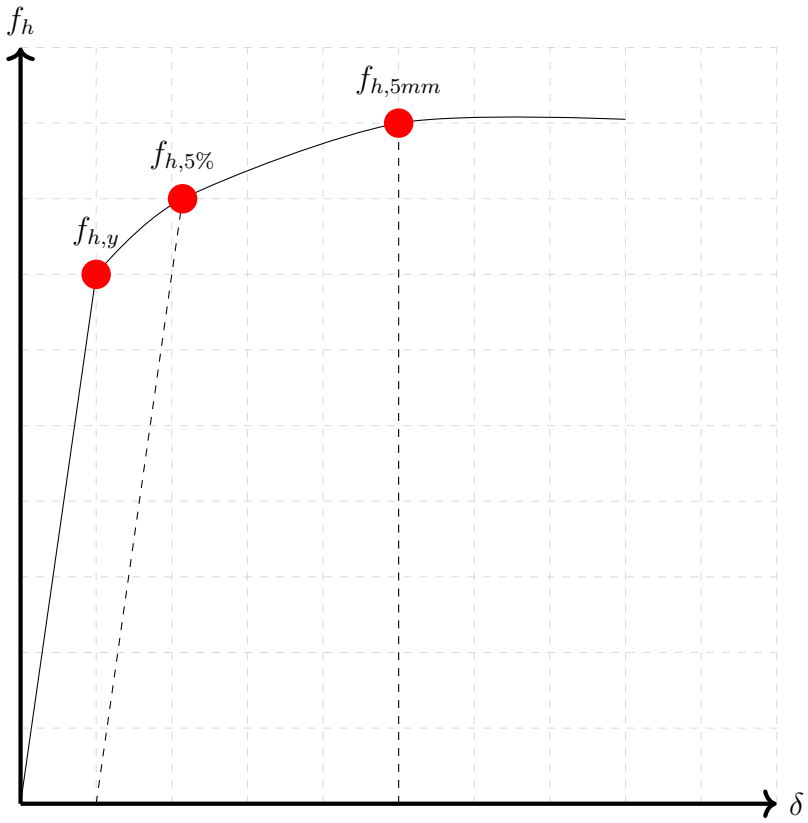

Figure 2.6: Schematic representation of methods to experimentally deterimine the embedment strength of timber.

the loading direction with respect to the wood grain orientation transitions from perpendicular- to parallel-to-grain the dependency of fastener diameter on the embedment strength decreases. Further study of loading angle is necessary to determine how the dependency of fastener diameter on the embedment strength decreases.

Secondly, two methods were discussed and compared in determining the embedment strength:

1. the 5% offset method defined by ASTM D5764 [47], and

2. the 5mm offset method defined by EN 383 [46].

Method 1 takes its cue from traditional methods to estimate the yield strength based on classical techniques of stress and strain. In this approach shown in figure 2.6, the linear elastic branch of the load deformation curve is offset by 5% and the yield point of the embedding stress is defined by the intersection of this offseted line with the experimental load deformation curve. In contrast, method 2, also shown in figure 2.6, sets the embedment strength as the strength when 5mm of deformation is recorded during a experimental embedment test. The difference in these two methods is that method 1 defines the embedment strength as a classical yield strength while method 2 defines the embedment strength as more of a ultimate strength. Regardless of the evaluation method, the embedment strength has a positive correlation with density. When considering the effect of fastener diameter, a difference is shown to exist between the two test methods only when the load acts perpendicular-to-grain. This is not surprising since the load deformation curve (Figure 2.5) showed a hardening phase when loaded perpendicular-to-grain which would not be accounted for using method 1. As d increases, the f_h decreases linearly with a slope of approximately 0.5 based on the results from method 2 which captures the

embedment strain hardening when loaded perpendicular-to-grain. The remaining three cases (i.e. parallel-to-grain loading for both methods and perpendicular-to-grain loading for method 1) show only a weak linear relation (slope less than 0.2).

It was found that the ratio of the parallel-to-grain embedment strength of method 1 over method 2 was approximately a constant value (mean of 0.968) while the same ratio for the perpendicular-to-grain embedment strength showed a positive linear relationship (mean slope of 0.016). Furthermore, ratio of parallel-to-grain strength to perpendicular-to-grain embedment strength evaluated using method 1 was again approximately constant (mean value of 2.385) and the same ratio evaluated using method 2 showed a positive linear relationship (mean slope of 0.041).

The results reported in the study reviewed here reinforce the behaviour shown in figure 2.5 that the embedment strength parallel-to-grain is not affected by the evaluation method; however, evaluation method does influence the perpendicular-to-grain embedment strength through the fastener diameter.

2.2.1.2 Probabilistic-based multi-linear regression model [42]

The second study reviewed describes a novel probabilistic framework to accurately and robustly predict the embedment strength developed by re-analyzing the existing experimental data used to develop the current models in design standards. For example, the density, ρ, of softwood—coniferous wood species—timber specimens tested to determine the embedment strength is shown in table 2.2 where the average density is approximately $425\frac{kg}{m^3}$ with average coefficient of variation of 0.11. It is this natural variation of on average 11% for softwoods that prompted the authors of this study being reviewed here to consider a probabilistic framework in the first place.

Table 2.2: Density of timber used in experimental testing from various literature sources.

Source	Coniferous wood species	Density	
		Mean (kg/mˆ3)	COV (%)
[40, Sawata & Yasmura (2002)]		396	11
[41, Kennedy et al. (2014)]	Spruce-Pine (SP)	454	
	Spruce-Pine-Fir (SPF)	399	
	Douglas Fir (D.Fir)	439	
[42, Leijten et al. (2004)]	Spruce-Pine-Fir (SPF)	411	9
	Spruce	446	12
	Sitka Spruce	393	10
	Scots Pine	458	13
	European Redwood	460	10
	European Whitewood	390	11
	Average values	424.6	10.9

Multiple linear regression analyses were conducted to better identify the influence of timber density, ρ, and fastener diameter, d, on the embedding strength of timber members. A probabilistic approach provides the advantage of the ability to characterize the probability distribution of the embedment strength parameter, f_h, which is important in a natural material like wood due to it's higher inherent variability than manufactured materials like steel or concrete.

$$f_h = A\rho^B d^C \tag{2.11}$$
$$\ln f_h = \ln A + B \ln \rho + C \ln d + \epsilon$$

Table 2.3: Regression parameters derived from embedment strength experimental testing described in [42, Leijten et al.] for parallel-to-grain loading.

Parameter	Type	μ	σ	A	B	C	ϵ
A	Normal	-2.33	0.230	1.00	-0.991	-0.244	0.00
B	Normal	1.07	0.040	-0.991	1.00	0.105	0.00
C	Normal	-0.25	0.012	-0.244	0.105	1.00	0.00
ϵ	Normal	0.00	0.110	0.00	0.00	0.00	1.00

Using existing embedment strength test data, the regression equation 2.11 was determined. The assumption of this regression equation is that the embedment strength is dependent on the timber density and fastener diameter which exhibits at least a locally linear logarithmic relationship. The test data was grouped into 8 groups based on species of wood and type of fastener (e.g. nail or dowel) and further classified into sub-groups based on the source of the data. Significant statistical differences were found between sub-groups in each group of the complete dataset and thus multivariate models were not used. However, it was assumed that each data group, if sufficiently large number of sub-groups were included, would be normally distributed. The regression and corelation parameters determined for European softwoods are shown in Table 2.3. The study described here also remarks that a significant portion of the experimental data was unsuitable for use due to differences in the definition of the embedment strength when the test member was loaded perpendicular-to-grain (confirming the conclusion reached by the article reviewed in the previous section 2.2.1.1 of this thesis).

$$F(x) = P(\exp(A + B \ln \rho + C \ln d + \epsilon) \leq f_{h,5\%}) \tag{2.12}$$

The use of equation 2.12 allows the fifth percentile embedment strength, $f_{h,5\%}$, to be computed based on probability of the underlying distribution of the embedment strength defined by equation 2.11. Then knowing the $f_{h,5\%}$ a simple timber connection can be designed more reliably since the both the mean and variance of the embedment strength is taken into consideration. Varying the variance of the timber density—affecting the shape of the embedment strength distribution—, the effect on the reliability of the connection design is derived. A coefficient of variation (COV) of 18% of the timber density results in a reliability index of approximately 4.2 which is the typical level of reliability which is designed for in structural applications [48]; however, the reliability index varies from 5.23 to 3.98 for a COV of timber density from 0.1 to 0.2. The study described here thus proposes a new model (equation 2.11) to predict the embedment strength of wood which better considers the variability of wood properties.

2.2.1.3 Statistical-based non-linear regression model [41]

This most recent study in the literature evaluates existing models to predict the embedment strength of timber by performing both a extensive statistical comparative evaluation of models

currently found in design standards [4, 5, 3] but also a experimental regime to verify the significance of existing properties, material or otherwise, used within these models to predict the embedment strength. The experimental regime comprised of embedment tests in glued laminated and cross-laminated, CLT, products using both threaded and smooth (non-threaded) fasteners done according to the ASTM D5764 [47] standard. The study claims the importance of these two research goals is to fill a gap in the literature given growing interest in designing connections for heavy timber or hybrid structures of high load bearing capacity using innovative engineered wood products such as CLT. Better understanding the embedment strength parameters for larger connections which utilize either larger fastener diameters or many smaller diameter fasteners is of critical importance to the further safe and reliable design of timber connections which this thesis focuses on.

$$f_{h,\parallel} = 77G_0 \tag{2.13}$$
$$f_{h,\perp} = \frac{f_{h,parallel}}{k_{90}}, \text{ where} k_{90} = 0.36G_0^{-0.45}d^{0.5}$$

The models used in the comparative study are taken from the Canadian (O86) [3], European (EC5) [4], and American (NDS) [5] design standards. The first two models are described generally in the previous section 2.2.1 while the model to predict the embedment strength in the NDS [5] design standard is shown in equation 2.13 converted to use SI units.

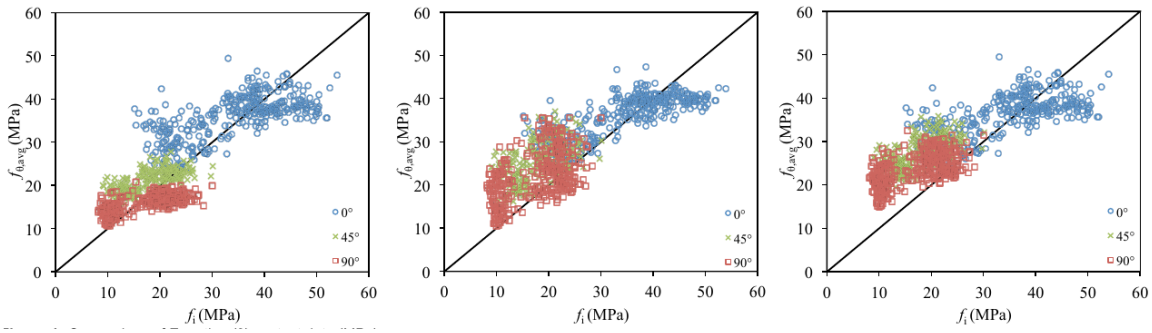

Figure 2.7: Statistical evaluation of the embedment strength equations within the O86, NDS, and EC5 timber design codes (left to right plots) taken from [41, Kennedy et al.].

A comprehensive statistical evaluation, as illustrated in figure 2.7 taken from [41, Kennedy et al.], of the differences between the embedment strength equations within the O68, NDS, and EC5 timber design codes indicates that the CSA O86 equation performs best between the models compared. The O86 equation tends to underestimate embedment strength predictions for perpendicular-to-grain loading and overestimate for 45 degree and parallel-to-grain loading. Both the EC5 and NDS embedment strength equations for parallel-to-grain loading show similar model fit to experimental data with respect to the CSA O86 equation. For 45 degree and perpendicular-to-grain loading, both the EC5 and NDS embedment strength equations show poor prediction abilities against experimental results while CSA O86 gives a reasonable fit for perpendicular-to-grain loading and a weak fit for 45 degree to grain loading.

It must also be noted that the influence of fastener diameter was statistically tested for significance. The result showed that fastener diameter had no significant influence on the embedment strength at any loading angle. This confirms the findings observed by other researchers [39, 37, 40]. However, it must be remembered this finding of no significant influence of fastener

diameter on embedment strength is presented based on data collected using the 5% fastener diameter offset method. The embedment strength test method in EN 383 [46] does show a significant influence of fastener diameter only for loading perpendicular-to-grain also described in section 2.2.1.1.

$$f_{h,\theta,i} = \frac{\beta_1 \rho_{12}^{\beta_2}}{\left(\frac{\beta_1}{\beta_2} \rho_{12}^{(\beta_2 - \beta_4)}\right)} \tag{2.14}$$

Table 2.4: Optimal parameters of the proposed design model of the study reviewed here (taken directly from [41]).

Parameter	Estimate
β_1	108
β_2	1.67
β_3	70.1
β_4	2.17

Statistically, the study argues that all of the existing prediction equations may be improved to provide more accuracy. Therefore, a new model is proposed by the study (equation 2.14) and optimal coefficients (table 2.4) are found by performing a non-linear regression analysis on the experimental data [41]. It should be noted that the proposed model by the study [41] presented by equation 2.14 requires the density, ρ, to be in the units of $\frac{g}{cm^3}$. This proposed model is advantageous as it describes the embedment strength as a material property independent of the fastener diameter; however, it also results in considerable differences in numerical values with respect to the O86 model. Additionally, the proposed model is only validated against experimental data collected using test method 1 (i.e. ASTM D5764 [47]). This would suggest that further testing and validation is required before it could be safely and reliably used in design.

2.2.2 Fastener yield moment

The fastener yield moment is considerably less complex than the embedment strength parameter of wood. According to the EYM, the load-carrying capacity depends in addition to the embedding strength of wood on the bending resistance of the fastener. Johansen's theory [16] initially assumed the bending resistance of the fastener to be equal to the elastic moment capacity of the fastener's cross-section disregarding any plastic deformations.

$$M_{y,elasitic} = f_y \frac{\pi d^3}{32} \tag{2.15}$$

$$M_{y,plastic} = 0.8 f_u \frac{d^3}{6}, \text{ where } f_u = \frac{f_y}{0.8} \tag{2.16}$$

Under this initial assumption, the moment capacity of a fastener is defined by equation 2.15. For the design equations in EC5 [4], plastic deformation of the fasteners are considered thereby defining moment capacity by equation 2.16. It should be noted here that the definition of the

yield strength of a fastener, f_y, is not defined according to classical yield strength theory—e.g. at a stress level of 0.2

By assuming that a plastic hinge is able to fully develop within the cross-section of a fastener, it follows that the fastener must bend through to a angle of 45° at a embedment limit of 15mm. It is apparent though that the bending angles of fasteners are significantly smaller than 45° for many connections which fail according to EYM failure modes II and III [12, 49]. This means that plastic hinges are not fully developed within the fasteners and the full plastic moment capacity of the fastener is never achieved. In reality, the bending resistance of fasteners in timber connections—failing by EYM modes II and III—lies somewhere between the elastic and plastic moment capacities of the fastener itself [49].

$$M_{y,ef} = 0.3 f_u d^{2.6} \tag{2.17}$$

$$M_{y,ef} = \frac{1.8}{d^{0.4}} f_u \frac{d^3}{6} \tag{2.18}$$

The EC5 standard [4] defines the fastener yield moment for fasteners with diameters greater than $8mm$ according to equation 2.17 which reduces the fastener bending capacity from the plastic moment capacity to a so-called effective bending moment capacity, $M_{y,ef}$. Re-arranging equation 2.17 to equation 2.18 it is apparent that not only is the fastener yield moment, M_y, directly proportional to the fastener diameter but the yield bending strength of the fastener is inversely proportional to the fastener diameter as well described by the term, $\frac{1.8}{d^{0.4}} f_u$. As a result, larger diameter fasteners reduce the yield moment capacity more from the plastic moment capacity than smaller diameter fasteners. It should be noted that for small diameter fasteners such as nails, the effective yield moment capacity is equal to the plastic moment capacity of the fastener itself as the factor $\frac{1.8}{d^{0.4}}$ tends to a value of 1.0 for a diameter of approximately $4.34mm$. As it does not make sense for this factor to be larger than 1.0 since the bending strength, f_u, is the ultimate bending strength of the fastener, for small diameter fasteners such as nails the effective fastener yield moment capacity equals the plastic moment capacity of the fasteners themselves. Equation 2.17 is used as is in the ductile failure model considered in the remaining analyses of this thesis since it has been shown to adequately and accurately represent the fastener yield moment of fastener-type timber connections [49].

3

Brittle Failure

Not only are ductile failures possible in timber connections but due to the inherent brittle material behaviour of wood, brittle failures are often observed in timber connections as well. As mentioned in chapter 1, a significant number of failures of timber structures have been linked to brittle failure of timber dowel-type connectors at unexpected load levels [7, 8]. There has been some efforts to qualitatively and quantitatively assess these observed brittle failure mechanisms occurring in dowel-type timber connections resulting in structural collapse; however, brittle failure mechanism are significantly complex to have so far prevented a complete theory from being developed [13, 14, 50, 51, 22, 6]. Many research efforts have been completed to provide the necessary underlying understanding of the mechanics of brittle failure mechanisms in an effort to modernize the design of timber connections by providing methods to reliably predict brittle failure capacities [20, 52, 2] using higher levels of reliability.

3.1 Background theory

Brittle failure refers to the possibility of wood—the material making up structural timber and engineered wood products—failing due to fracture as a consequence of being relatively weak in tension. To further understand this, it is necessary to understand the material composition of timber members. Timber is comprised of a natural material, wood, which exhibits anisotropic mechanical behaviour with different strength and stiffness properties in the longitudinal and transverse directions. At a microscopic level, the strength and stiffness of wood actually depends on three directions commonly referred to as the longitudinal, tangential, and radial directions which coincide with the orientation of wood fibres.

Figure 3.1 shows a sample view of a wood specimen with its inherent anisotropic natural wood fibre properties. It is common to denote the three fibre orientations of a sample of wood as the longitudinal, L, tangential, T, and radial, R, directions. The tangential and radial directions are often considered together since these two directions tend to show a similar strength and stiffness characteristic and are collectively referred to as the transverse direction. It should also be noted that the longitudinal and transverse directions are interchangeably referred to as parallel-to-grain and perpendicular-to-grain strength properties which are the terms primarily used in this thesis.

The mechanical strength of timber in the parallel-to-grain and perpendicular-to-grain directions is shown in Figure 3.1. The strength and stiffness of timber parallel-to-grain is much larger than the strength and stiffness perpendicular-to-grain. This discrepancy in mechanical behaviour in these two spatial directions of a structural timber member or connection forms the basis of

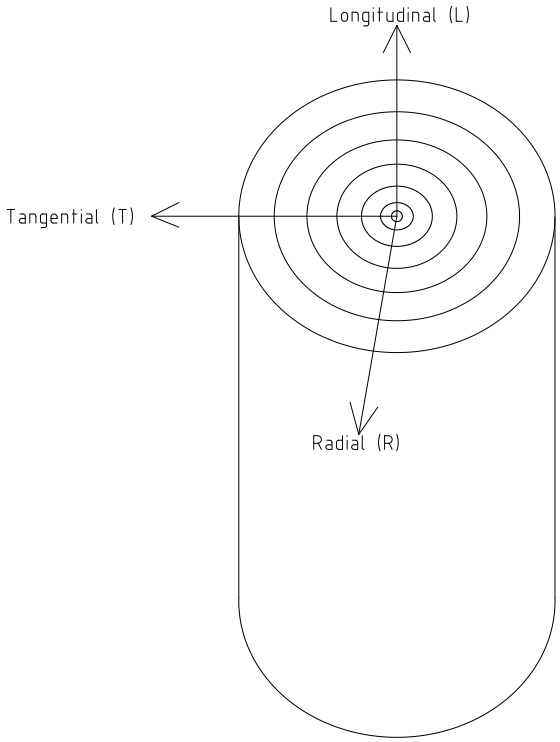

Figure 3.1: Grain/fibre directions of wood as a anisotropic material.

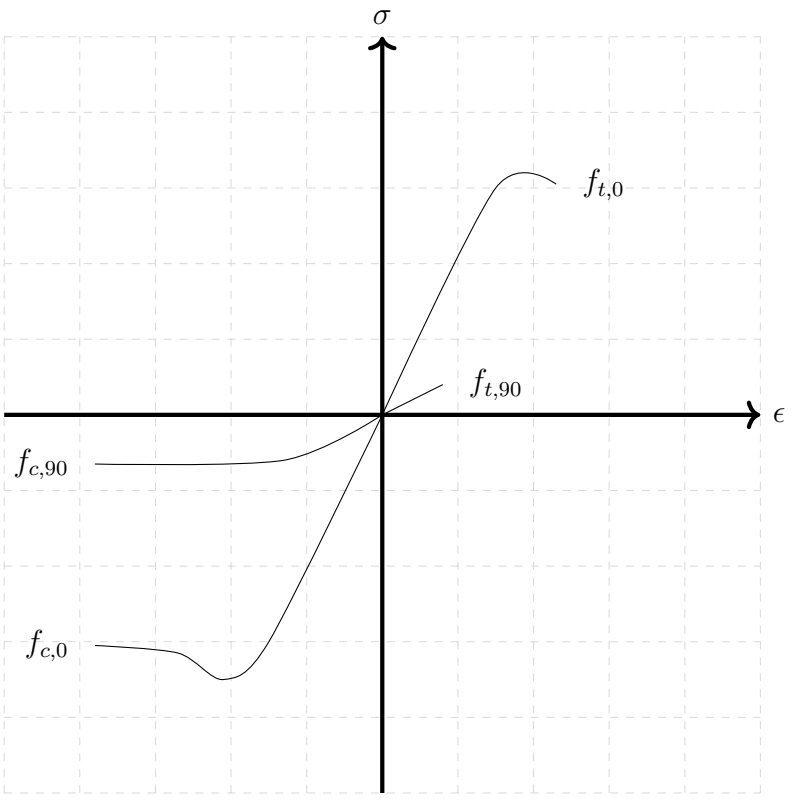

Figure 3.2: Definition of stress in different directions of a wood as an anisotropic material.

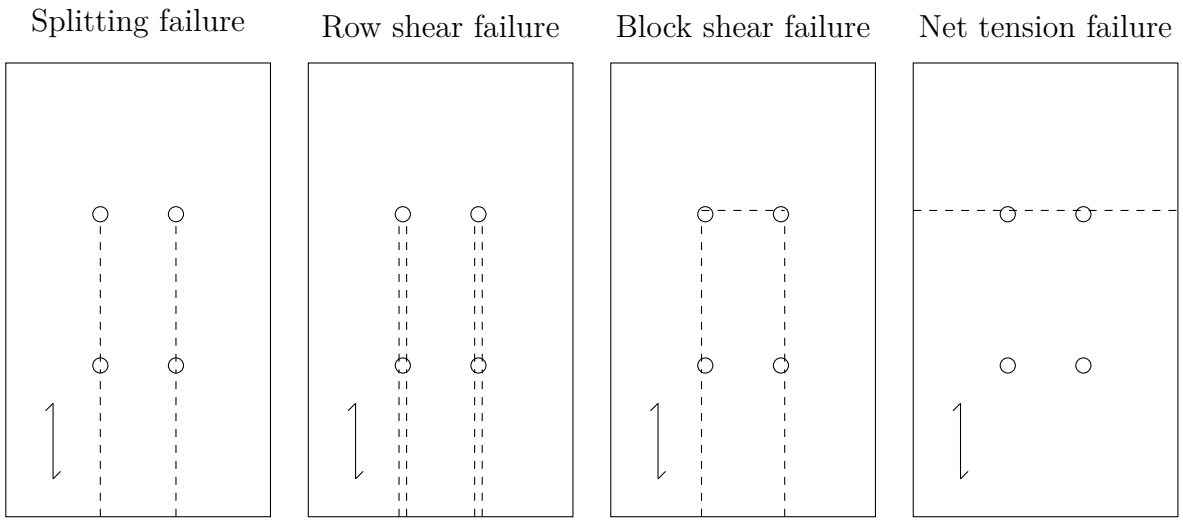

Figure 3.3: Schematic of brittle failure mechanisms of a fastener-type timber connection. Dashed lines represent where timber cracks appear.

the underlying phenomenon leading to brittle failure mechanisms which are found to occur in structural timber connections.

Brittle failure mechanisms, shown in figure 3.3, found to occur in structural timber connections loaded in the parallel-to-grain direction apart from ductile failure—described by the EYM—are:

1. splitting—tension perpendicular-to-grain stress—failure mechanism,
2. row shear—shear stress—failure mechanism,
3. net tension—tension parallel-to-grain stress—failure mechanism, and
4. mixed—block shear—failure mechanism.

Furthermore, connections are regions of complex stress states in structures with significant normal and shear stresses both parallel- and perpendicular-to-grain including interaction effects between various stress components. Timber connections generally fail due to mixed mode fracture involving both tensile perpendicular-to-grain and shear stresses if ductile failure cannot be achieved. Mixed mode fracture is a complex mechanism to model to allow for simple and practical design equations [51]; however, both experimental testing [50, 13, 35] and numerical (finite element) methods [32, 21] have been employed to determine which parameters influence the which fracture mechanism the most. To simplify the calculation of mixed mode brittle failure behaviour of timber connections, the current approach taken in the literature is to derive models to predict splitting (i.e. tension perpendicular-to-grain), shear, and tension (i.e. tension parallel-to-grain) failure mechanisms independently and consider mixed mode fracture behaviour as a interaction between these three elementary effects [12, 14, 13, 51]. The first two modes are referred to as splitting failure and row shear failure typically in traditional literature regarding timber connections while in some literature articles the terms are exchanged to use fracture mechanics terminology of mode I and mode II fracture. The third mode is referred to as net tension failure as it results from individual wood fibres breaking as a result of the tension strength parallel-to-grain being exceeded. The fourth failure mechanism identified above is included to account for timber connections with two or more rows of fasteners which often fails as a combination of the elementary failure mechanisms of shear and net tension failure. A review of the current state of the existing literature is summarized in the following sections 3.1.1

to 3.1.4 and further details may be found in [22, 6, Cabrero et al.].

3.1.1 Splitting failure mechanism

Splitting failure refers to the phenomenon of wood splitting longitudinally along wood fibres. A schematic of splitting failure as it typically occurs in timber connections is shown in figure 3.3. Pure splitting failure is characterized by fracture mechanics as a pure mode I fracture process due to tensile perpendicular-to-grain wood stresses. The predominant influencing factor according to fracture mechanics theory is the fracture energy, G_f, of wood. However, fracture mechanics approaches are often unwieldy and impractical for use in design. Thus, mode I fracture behaviour of timber connections is instead modelled analytically using a beam on elastic foundation (BEF) analogy [12]. It should be noted that Timoshenko beam theory on a elastic foundation must be considered since shear deformations are significant [12]. In the BEF model, the primary cause for the splitting mechanism to occur results from the parallel-to-grain fastener load being decomposed into a force acting perpendicular-to-grain—the wedging effect—and a moment due to eccentricity of the point of load application.

The wedging effect is defined as the relationship between parallel- and perpendicular-to-grain stresses and is dependent on the friction between the fastener and timber member. Multiple estimates of the value of the parameter associated with the wedging effect, β, are given in the literature corresponding to $\frac{1}{10}$, $\frac{1}{7}$, and $\frac{1}{4}$ [51, 53, 14], respectively. It is not clear as to which value for β is most accurate; however, a recent performance assessment of brittle failure models suggest that either $\frac{1}{7}$ or $\frac{1}{4}$ may be most appropriate and accurate [6]. The accumulated shear stresses are also accounted for in the BEF model by way of a Volkersen model. The reader is referred to details about the formulation of the fracture mechanics framework in Jorissen [12].

$$R_{t,split} = k_{t,90}\frac{1}{\beta}t_i a_3 f_{t,90} \tag{3.1}$$

The fracture mechanics based model is thus considered the best model to account for splitting failure in timber connections. Based on this fracture mechanics approach, the most recent simple model in the literature to account for splitting failure mechanism observed in timber connections is presented in equation 3.1 [52, 12]. The parameter, $k_{t,90}$, represents a stress concentration factor which is set to equal 1 based on studies of the stress distribution around a fastener in [12, Jorissen]. Further, the choice of β is left open to discussion but for the purposes of this thesis a choice of $\frac{1}{7}$ is made.

3.1.2 Row shear failure mechanism

Row shear failure unlike splitting failure is considered as technically a mixed mode fracture mechanism which acts to shear off a row of fasteners from the timber as depicted in figure 3.3. Unlike splitting failure which relies on pure mode I crack extension of fracture mechanics theory, row shear failure is a combination of mode I and II crack extension generated from both tensile perpendicular-to-grain and in-plane shear stresses. The underlying theory for which analytical models have been developed to predict the load-carrying capacity of connections where row shear failure is observed all have a basis in Volkersen's theory [12]. Many of the

models proposed in the literature deviate from Volkersen's theory by assuming that this row shear failure mechanism is a pure mode II crack extension fracture problem which significantly simplifies the analytical modelling [35, 14]. These simple models based on pure shear (i.e. mode II crack extension) fracture are a function of the shear strength, f_v, of timber, the fastener spacing, and the timber member thickness, t_i.

$$R_{v,split} = 2k_v t_i a_{L,min} f_v \tag{3.2}$$

Equation 3.2 represents this simple model to predict the capacity of a connection which is governed by the row shear failure mechanism. This simple model for a single fastener connection encapsulates the current understanding of shear failure mechanisms of timber connections in the literature [54, 55, 14, 13]. Considering mechanics based principles, stress concentrations are unavoidable in cases such as connections utilizing two different materials (e.g. steel dowels to connect two or more timber members). This stress concentration results from the changing stress distribution around a fastener which is accounted for in the proposed simple model here by the factor, k_v. The value of this stress concentration factor, k_v, is not well agreed upon in the literature [55, 14, 13] and values ranging from 0.5 to 1.0 are all reported. It is apparent that a stress concentration factor should be applied to account for shear stress concentrations which do appear near the fastener location and are correctly modelled using a Volkersen model approach [12]. For the purposes of this thesis, the shear stress concentration factor, k_v, is set to 0.5 as a conservative estimate.

Table 3.1: Three simple models to account for the row shear failure mechanism in multiple fastener connections.

Source	$R_{v,split}$	Remarks
[14]	$2k_v \frac{n^{0.9}}{n_c} L_c t f_v$	n: number of fasteners
		n_c: number of fasteners in a row
[56, 57]	$2k_v n_c n_r t a_{L,min} f_v$	n_r: number of rows of fasteners
		$a_{L,min} = \min a_1, a_3$
[54, 51, 58, 35]	$\min 2n_c n_r t a_1 f_v, 2n_c n_r t a_3 f_v$	

The simple model to account for row shear failure of timber connections, in equation 3.2, is also a function of geometric considerations such as the fastener spacing. At the simplest level of a single fastener connection, the distance between the end of the timber member and the fastener itself—defined as the end spacing, a_3—has been shown to be directly proportional to the row shear failure load. Multiple fastener connections are more challenging to determine a relationship between fastener spacing and the row shear failure load. Numerous studies have presented models and results using linear elastic fracture mechanics and quasi non-linear fracture mechanics approaches to extend these simple row shear failure mechanism models developed for single fasteners to multiple fastener connections [32, 54, 58, 35, 13]; however, further studies are required. Some simple extensions for multiple fastener connections to the simple model shown in equation 3.2 for single fastener connections exist in the literature [14, 54, 56, 57]. These extensions are summarized in table 3.1 where the major features which are included beyond the simple model of equation 3.2 are that the number of fasteners in total, n, and in a row, n_c, within the connection are considered as various terms such as $\frac{n^{0.9}}{n_c}$ or $n_c n_r$. For example, the ratio of $\frac{n^{0.9}}{n_c}$ takes into consideration that at low load levels, when row shear failure mechanisms occur, the load is distributed unevenly among fasteners in a

multiple fastener connection while other extensions of the simple shear splitting model which only multiply by the number of fasteners, $n_c n_r$, do not account for this load redistribution between fasteners. Load redistribution has been shown to significantly affect the capacity of multiple fastener connections both in terms of ductile and brittle failure mechanisms [12].

Furthermore, in multiple fastener connections the fastener from which row shear failure is triggered depends on the stress state near each fastener. Since at low load levels a uneven load distribution among fasteners exist, row shear failure is triggered at highest loaded fastener in shear when considering this mechanism to behave as a pure mode II fracture process [32, 12]. This is not the case in general since row shear failure behaviour is a mixed mode fracture process whereby tensile perpendicular-to-grain stresses–involved in splitting failures–introduce a interaction effect [12, 51, 35]. For example, connections with two or more rows of fasteners are much more likely to fail by a row shear than splitting behaviour; however, it is apparent that for a large number of fastener rows it is difficult to pinpoint whether failure was triggered due to splitting or shear failure [13, 35]. This leads to the fourth failure mechanisms defined above which is often observed in timber connections and is known as block shear failure. Block shear failure thus is most probable when two or more fastener rows exist but is traditionally assumed as a combination of the row shear and net tension failure mechanisms. Section 3.1.4 describes the block shear failure mechanism in more details. The next two sub-sections 3.1.2.1 and 3.1.2.2 describe the differences in the two approaches to model the row shear failure mechanism for multiple fastener timber connections.

3.1.2.1 Row shear failure mechanism: Approach 1

This first approach to extend models of single fastener connections considering a brittle shear failure mechanism to multiple fastener connections involve substituting the end spacing parameter with the spacing between fasteners. The approach is represented by the second and third rows of table 3.1. This approach relies on the understanding that brittle failure triggered by shear stresses occurs at a single fastener first and occurs at low load levels if minimum fastener spacings are not satisfied. Given the literature sources on load distribution between fasteners [12, 26, 27], it motivated the development of this approach since the capacity of a connection which is governed by this shear mechanism would be limited in its capacity by when cracking is triggered.

$$R_{v,split} = 2k_v n_r a_{L,min} n_c t f_v \tag{3.3}$$

This approach uses the expression, $a_{L,min} = \min(a_3, a_1)$, to determine a characteristic length over which the shear strength of wood must be overcome to trigger a brittle shear failure [13]. Equation 3.3 defines this approach as an equation for use in design. This equation has been rewritten under a common nomenclature especially given the similarities in the proposed models following this approach in the literature [13, 59, 51, 35, 58, 54]. The advantage of this approach is that it focuses on the load level when this failure mechanism is triggered as the basis to calculate the capacity of a connection limited by this failure mechanism.

3.1.2.2 Row shear failure mechanism: Approach 2

The second approach found in the literature to extend models to predict the load-carrying capacity with respect to a brittle shear failure mechanism is by considering the failure plane involved [14]. The key difference in this approach to the previous approach is that the exact fastener which triggers the brittle shear failure mechanism is unimportant. The approach instead focus on defining the area of the failure plane in shear of a row of fasteners similar to existing models for block shear failure included in Annex A of EC5 [4]. The area of the failure plane in shear is calculated as a characteristic length, $L_c = (n_c - 1)a_1 + a_3$, multiplied by the thickness of the timber member and by two to account for each side of the fastener with respect to the load direction.

$$R_{v,split} = 2k_v \frac{n^{0.9}}{n_c} L_c t f_v \tag{3.4}$$

Equation 3.4 shows the mathematical expression this approach uses to predict the load-carrying capacity of timber connections which are theoretically governed by a brittle shear failure mechanism. This approach, although on first appearance similar to the first approach (equation 3.3), is significantly different since the load distribution between fasteners is considered using a effective number of fastener term, $n_{ef} = n^{0.9}$, rather than considering that this failure mechanism is triggered at a specific fastener. It is clear this approach is advantageous in that less information is required to be known about how and where the failure is triggered while on the other hand may not be able to adequately predict the uneven load distribution between fasteners occurring at low load levels where this failure mechanism tends to govern the capacity of timber connections especially for small fastener spacings.

3.1.3 Net tension parallel-to-grain failure mechanism

Net tension failure is a mechanism similar to splitting failure in that both are a result of tensile stresses; however, the net tension failure mechanism described here relates to the parallel-to-grain tensile strength of wood and not the perpendicular-to-grain tensile strength involved in splitting failure. The difference between tension and splitting failure can be visualized in figure 3.3. The main difference is that net tension failure involves individual wood fibres to break themselves—a function of the tensile strength parallel-to-grain—while splitting failure mechanisms operate by wood fibres being pulled apart transversely. Given the characteristics of wood as a material, tension parallel-to-grain strength is much higher than tension perpendicular-to-grain strength and thus splitting failure is typically much more of a concern except in cases of connections with large groups of fasteners in multiple fastener rows. In that case, interactions between splitting, shear, and tensile failure mechanisms play a more important role to determine the mixed mode failure pattern.

$$R_{t,tension} = k_{t,0} n_c (n_r (a_2 + d)) t f_{t,0} \tag{3.5}$$

The common equation to represent this mechanism contributing to failure is defined in equation 3.5 and is directly proportional to the area in tension multiplied by the tensile strength of

timber parallel-to-grain. A further factor, $k_{t,0} = 1.25$, is used to account for the size effect as the tensile stress acts locally on a small volume. Finally, the factors, n_c and n_r, relate to the number of fasteners in a row and number of fasteners rows, respectively. The factor, n_r, is used as a part of the expression to calculate the area where the tensile stress acts while n_c acts as a factor to consider the load distribution between fasteners which may be also replaced with the fraction $\frac{n_c^{0.9}}{n_c}$ to more accurately represent this load distribution [14]. Even though, the form of equation 3.5 is typically still used to represent a net tension failure.

3.1.4 Block shear failure mechanism

The fourth failure mode of timber connections is truly a mixed failure mechanism since it is assumed to involve either splitting or row shear failure and net tension failure mechanisms described in the previous sections 3.1.2 and 3.1.3 in combination. Block shear failure, as this mechanism is known, is a mechanism whereby a whole group of fasteners is torn from the connection and involves 3 failure planes of which two are lateral planes and one head plane.

A typical block shear failure pattern is shown in figure 3.3. This type of failure mode is only observed for two or more rows of fasteners since connections while a connection with only one fastener row is assumed to fail either by splitting or row shear failure. In this sense, block shear failure is a feature of multiple fastener row timber connections only. The lateral failure planes fail according to either a splitting or shear failure mechanism depending on the whether or not the each fastener row is constrained by rows of fasteners on each side of it. It is further noticed that the block shear failure mechanism is a mixed mode fracture process and the effect of splitting should be taken into account since the outermost rows of fasteners are likely to experience splitting behaviour; however, the BEF model, described in section 3.1.1, explains the observation that timber connections with two or more rows of fasteners seldomly experience splitting as a separate failure mechanism leading to complete failure of the timber connection [14, 51]. On the other hand, a shear failure mechanism is possible on any row of fastener but a pure shear failure mechanism [14] resulting in only one fastener row leading to failure of the connection to be triggered at much lower load levels than a tension failure of the head plane is more likely.

As mentioned in the previous section3.1.3, net tension failure of the head plane is a different failure mechanism from splitting failure since it does not result from tensile perpendicular-to-grain failure but depends on tensile parallel-to-grain failure. Tensile parallel-to-grain failure requires wood fibres to break which corresponds to a stronger stress-strain response than the weaker response of wood in tension perpendicular-to-grain—requiring wood fibres to pull apart in the transverse direction—is. Therefore, block shear failure can be considered a combination of the three more elementary mechanisms (sections 3.1.1 to 3.1.3) and if accurate prediction models to represent these failure mechanisms are developed then a accurate prediction model for block shear failure may also be developed as only interaction effects between the 3 elementary mechanisms must be determined. For the purposes of this thesis, these interaction effects are not considered further as the focus is to provide an analysis of existing models to predict the brittle failure capacity of TST connections.

3.2 Literature review of existing brittle failure models

Existing models to predict brittle failure mechanisms have been developed in the literature recently to better account for brittle failure mechanisms and promising models are summarized in the previous section 3.1. Recently assessments as to the performance of these models have been conducted in the literature [60, 22, 6]. Given that current design methods of timber connections inadequately inform the designer of the risk of catastrophic brittle failure of connection designs [2, 8, 7], there is a need to assess the reliability—in other words the risk of failure—of proposed models in the literature to account for brittle failure mechanisms to minimize the risk of brittle failure in relation to ductile failure [2]. When assessing the reliability of proposed models to account for brittle failure mechanisms, probabilistic methods are a useful tool to rationally minimize the probability of brittle failure in relation to the probability of ductile failure. Ductile failure is the desired behaviour of timber connections in order to achieve sufficient levels of ductility of the overall timber structure with regard to structure robustness and safety [2]. As opposed to steel structures which are built using a material—steel—with significant ductility as a material property, timber as a material does not exhibit the same level of ductility on a material level and requires structural engineers to provide ductility in timber structures differently. The predominant way to provide sufficient ductility in timber structures is through the structure's connections particularly in high capacity connections necessary in large scale, mass timber, high-rise towers. Accurate models to predict the capacity of brittle failure mechanisms and reliable understanding of the relationship to the capacity of ductile failure mechanisms in timber connections is necessary to increase safety and risk to human injuries.

The two main approaches being considered in the literature are to calibrate using probabilistic methods a brittle over-strength factor or to explicitly include the governing equations of brittle failure mechanisms refined through a code calibration process to ensure a intended level of reliability in the design of timber connections [2]. The first approach is intended to ensure that the design capacity associated with brittle failure is significantly higher than the design capacity of ductile failure thereby ensuring the probability of brittle failure is as low as possible. The disadvantage of this approach is that any brittle over-strength factor should take into account the differences in consequences between brittle and ductile failure which relies on subjective conditions. Additionally, this approach would continue to implicitly consider brittle failure mechanisms in the design of timber connections which could lead to further exacerbating the issue raised in the literature regarding possibly more than 30% of designers not knowing even of the existence of brittle failure mechanisms [10].

The second approach considers including governing equations of brittle failure mechanisms directly into the design method of timber connections through code calibration processes to ensure the reliability of each failure mode known. Ensuring a acceptable level of reliability can be achieved by following the guidelines and recommendations developed in the Probabilistic Model Code by the Joint Committee on Structural Safety (JCSS) [48]. This approach would be advantageous since it focuses on understanding the underlying material mechanics and explicitly includes brittle failure mechanisms in design methods for use in designing timber connections. Although, arguably this approach requires more effort to develop it would result in a stronger model to design timber connections with since the assumptions of this approach are decidely stronger than those of the first approach. This second approach does not require any prior knowledge of the relationship between the differences in consequences of ductile and brittle failure whereas the first approach would require designers and clients to be comfortable with knowing that certain failure modes are achieved with possibly differing levels of reliability. The

second approach of explicit inclusion of brittle failure mechanisms represents a model where the overall probability of failure of any timber connection is known with certainty to be as low as intended with respect to any failure mechanism and any level of uncertainty in input parameters of the model.

3.2.1 Impact of varying material and geometric properties [52, 53]

The development of models to account for brittle failure mechanisms described in chapter 3 were in general validated on specific timber connections (i.e. with distinct and limited material and geometric parameters). For use in structural design, the reliability of models is typically required to be shown independently of material variability or varying geometric conditions.

$$R_{connection} = \min \begin{cases} f_{h,i} t_i d \\ f_{h,i} t_i d \left[\sqrt{2 + \frac{4 M_y}{f_{h,i} d t_i^2}} - 1 \right] \\ \sqrt{4 M_y f_{h,i} d} \\ 2 k_v a_3 t_i f_v \\ k_{t,90} \frac{1}{\beta} a_3 t_i f_{t,90}, \text{ where } \beta = \frac{1}{7} \end{cases} \tag{3.6}$$

Jockwer [52] and Jockwer et al. [53] have investigated the impact of both material variability and varying geometric conditions on the capacity of TST connections. For example, the load-carrying capacity of single fastener TST connections were calculated while varying the timber member thickness, $t_{1,3}$, and end spacing of the fastener, a_3, was evaluated for 5 failure modes consisting of the 3 relevant ductile failure modes according to the EYM, a brittle splitting failure mode, and a brittle shear failure splitting mode [52]. Equation 3.6 describes the 5 failure modes used in the study described by [52, Jockwer]. It was found that larger $t_{1,3}$ increases the likelihood of ductile failure to govern the capacity while brittle failure governed the capacity of the connection for smaller $t_{1,3}$. The same was found to be true for the fastener end spacing, a_3 [52]. It was also found from experimental tests that the load-carrying capacity decreases with decreasing fastener spacing, a_1, and end spacing, a_3 while the load-carrying capacity increases with increasing tensile strength of steel fasteners. Furthermore, ductile failure modes are characterized with smaller variability than brittle failure modes [52]. Influencing factors on the variation of the load-carrying capacity are such that the variation increases with decreasing spacing, a_1, and end spacing, a_3 [52].

The capacity of connections which are governed by brittle failure modes display a greater variability and this requires different partial safety factors according to limit state theory. It is suggested that optimal partial safety factors depend on the governing failure mode and its variability [52]. The main conclusions presented by Jockwer [52] are that in general brittle failure modes require larger safety margins than ductile failure modes which suggests that currently economic and reliable connection designs should be chosen to obtain high load-carrying capacities with small variability (i.e. sufficient fastener spacing incl. end spacing and thicker timber members) [52].

3.2.2 Probabilistic study of brittle failure models [2]

Probabilistic studies of brittle failure mechanisms are an important step towards more accurate inclusion of brittle failure within modern design methods and two main approaches are being explored in the recent literature studies. Following the approach of considering brittle over-strength factors, the probability density functions associated with the changing variation of brittle and ductile failure modes shows less variation of ductile failure modes and as the timber member thicknesses or fastener spacing increases, ductile failure becomes governing [2]. Both cases of wood-steel-wood (aka TST) and steel-wood-steel (aka STS) connections are studied[1]. It must be noted that the connection studied by [2, Cabrero et al.] consisted of a multiple fastener connection—comprising of 3 rows and 5 fasteners per row—while the brittle failure model chosen corresponds to the proposed model for the New Zealand draft standard [55]. Since the connection studied does consist of 5x3 group of fasteners, a brittle failure model consisting of lateral and head failure plane capacities—such as developed for the New Zealand standard—is appropriate since multiple fastener connections are more probable to experience brittle failure related to shear—row shear—failure or mixed-mode—block shear—failure mechanisms.

In the case of TST connections, it was demonstrated that the probability that brittle failure is more likely to occur than ductile failure happens for a normalized timber thickness, $\frac{t_{1,3}}{d}$, less than approximately 6 and is further significant for normalized timber thicknesses less than 10 [2]. Additionally, the variability of the governing failure mode depends entirely on the failure mode with brittle failure accounting for a coefficient of variation of approximately 25% and ductile failure exhibiting a coefficient of variation of approximately 10% within the distribution of load-carrying capacity as a result of material variability [2]. The likelihood of brittle or ductile failure was determined as a function of a normalized parallel-to-grain fastener spacing, $\frac{a_1}{d}$, which indicated similar results with timber thickness. The likelihood of brittle failure as a function of $\frac{a_1}{d}$ is probable when the normalized parallel fastener spacing is less than 2 [2]. For the second type of connections (i.e. STS) similar trends are shown to exist except are more pronounced. Both the normalized timber thickness and parallel fastener spacing where brittle failure is more likely increases with respect to TST connection to approximately 20 and 3, respectively [2]. The limits below with brittle failure is more likely described in the preceding paragraph were determined by varying either the normalized timber thickness or parallel-to-grain fastener spacing while holding the other parameter constant [2]. It was also shown that the decision boundary between the probability of brittle and ductile failure governing the load-carrying capacity of a TST or STS connection exhibits non-intuitive interaction between timber member thickness and fastener spacing [2].

The trends depicted by [2, Cabrero et al.] are useful and interesting and the authors conclude that further studies are required before these trends can be implemented in standards. For example, benchmarking of existing brittle failure models against experimental test results, model uncertainties, and load effects including their variability need to be further studied before brittle over-strength factors are implemented to ensure the higher consequences of brittle failure are minimized.

[1]The abbreviations used in the paper referenced are WSW and SWS but for the purposes of a consistent nomenclature in this thesis these abbreviations are switched to TST and STS, respectively.

3.2.3 Impact of the size effect on brittle failure models

One aspect which has not been studied much in the literature is how the so-called size effect phenomenon of wood applies to timber connections and especially TST connections this thesis is concerned with. The size effect of wood is a phenomenon where larger wood specimens break at a lower average stress than smaller wood specimens. This is known to be a phenomenon of tensile stresses when present in brittle materials and is typically explained by the weakest link theory. The analogy used often to describe the weakest link theory—aka Weibull theory—is that of a chain subjected to tension [61]. The theory states that such a chain subjected to tension is never stronger than its weakest link. In the context of a brittle material such as wood, Weibull theory states that a specimen of wood is never stronger than its weakest part (i.e. a defect). It naturally follows that the probability of a larger defect occurring in the most loaded part of a wood specimen is greater for a large wood specimen than for a small wood specimen. The reasoning is that Weibull theory assumes a material is brittle and defects are randomly distributed within the specimen. Therefore, if the specimen is larger in volume, the probability that the a worse defect occurs in the most loaded part of the wood specimen becomes greater [61].

$$\left(\frac{f_2}{f_1}\right) = \left(\frac{V_1}{V_2}\right)^{\frac{1}{k}} \tag{3.7}$$

Weibull theory applied to wood leads to equation 3.7 to relate the ratio of the strength of wood with the volume of the wood specimen. Equation 3.7 requires a reference volume where the strength of wood is known to then determine the strength of wood at other volumes. The parameter, k, refers to the shape parameter of the underlying Weibull distribution. The weakest link theory is underscored by modelling the distribution of the strength parameter of a brittle material using a Weibull distribution. The Probabilistic Model Code developed by JCSS [48] for timber proposes to use a 2 parameter Weibull distribution.

$$f(x;\lambda,k) = \begin{cases} \frac{k}{\lambda}\left(\frac{x}{\lambda}\right)^{k-1} \exp -\left(\frac{x}{\lambda}\right)^{k} & \text{for } x \geq 0 \\ 0 & \text{for } x < 0 \end{cases} \tag{3.8}$$

$$m = \lambda\Gamma\left(1+\frac{1}{k}\right) \tag{3.9}$$

$$v = \sigma^2 = \lambda^2\left[\Gamma\left(1+\frac{2}{k}\right) - \left(\Gamma\left(1+\frac{1}{k}\right)\right)^2\right] \tag{3.10}$$

The 2 parameter Weibull distribution is most often defined using the probability density function shown in equation 3.8, where λ is the scale parameter and k is the shape parameter of the distribution [62]. The distribution parameters, λ and k, are related to the sample mean, m, and variance, v, of any representative sample of the real statistical population of strength values in equations 3.9 and 3.10 [62, 63]. Random sampling of statistical distributions thus allows for simulation of brittle material properties and the impact on the variation of the failure capacity to be identified.

Tensile strengths of brittle materials—such as wood—are commonly known to include a size effect phenomenon which is the basis of the weakest link theory. Given the weakest link theory as it relates to brittle materials, the size effect of timber is examined by utilizing Weibull distributed random variables for the tensile strength perpendicular-to-grain only to calculate the brittle failure capacity (equations 3.1). Only the tensile strength perpendicular-to-grain is considered as being affected by the size effect modelled using a Weibull distribution despite some evidence that the tensile strength parallel-to-grain and shear strength of wood are also affected by the size effect [64, 65, 66, 67, 13, 68] in accordance to the suggested modelling of mechanical strengths of wood in the Probabilistic Model Code [48].

4

Modelling methodology

As described in chapter 1, the objective and scope of this thesis concerns developing a reliable and robust design method for large mass timber connection systems becoming more prevalent as timber buildings reach new heights. Additionally, figure 1.6 defines the connection system studied which are timber-steel-timber (TST) fastener-type connections. To extend and develop a complete design model for mass timber connection systems, the modelling is divided into three stages:

1. input parameter definitions,
2. failure mechanism models, and
3. consistent global failure model.

The three stages of modelling a reliable and consistent failure model are broken into smaller methodologically steps shown in figure 4.1. The connection type for which this modelling methodology is derived for are TST mass timber connections with one or more internal steel plates connected using steel fasteners. Despite the focus on just one type of connection system, the methodology used to model TST connections presented within this thesis can be generalized and easily adapted to other connection systems. To adapt this design failure model to other connection systems, the first and second stages of the methodology presented need not be modified except to include additional or neglect existing input parameters for the failure model depending on which parameters are required for the connection system being considered. Further, stage I proposes a methodology to model material properties as random variables to capture the variability of wood within the resulting failure model. The third stage of the modelling methodology should be modified to combine the failure mechanisms, described by stage two, such that the real failure behaviour of the connection system considered is represented by the failure model.

This methodology is then used to compute the failure capacity of a specific connection design including the variability of the failure capacity due to uncertainties in the material properties. The thesis then computes the failure capacity of a large set of connection designs where the geometric parameters are varied to provide the ability to qualitatively assess the impact of the failure model with regard to geometric parameters. The impact of geometric parameters is particularly relevant, as discussed in chapter 3, for connections failing according to a brittle failure mechanism.

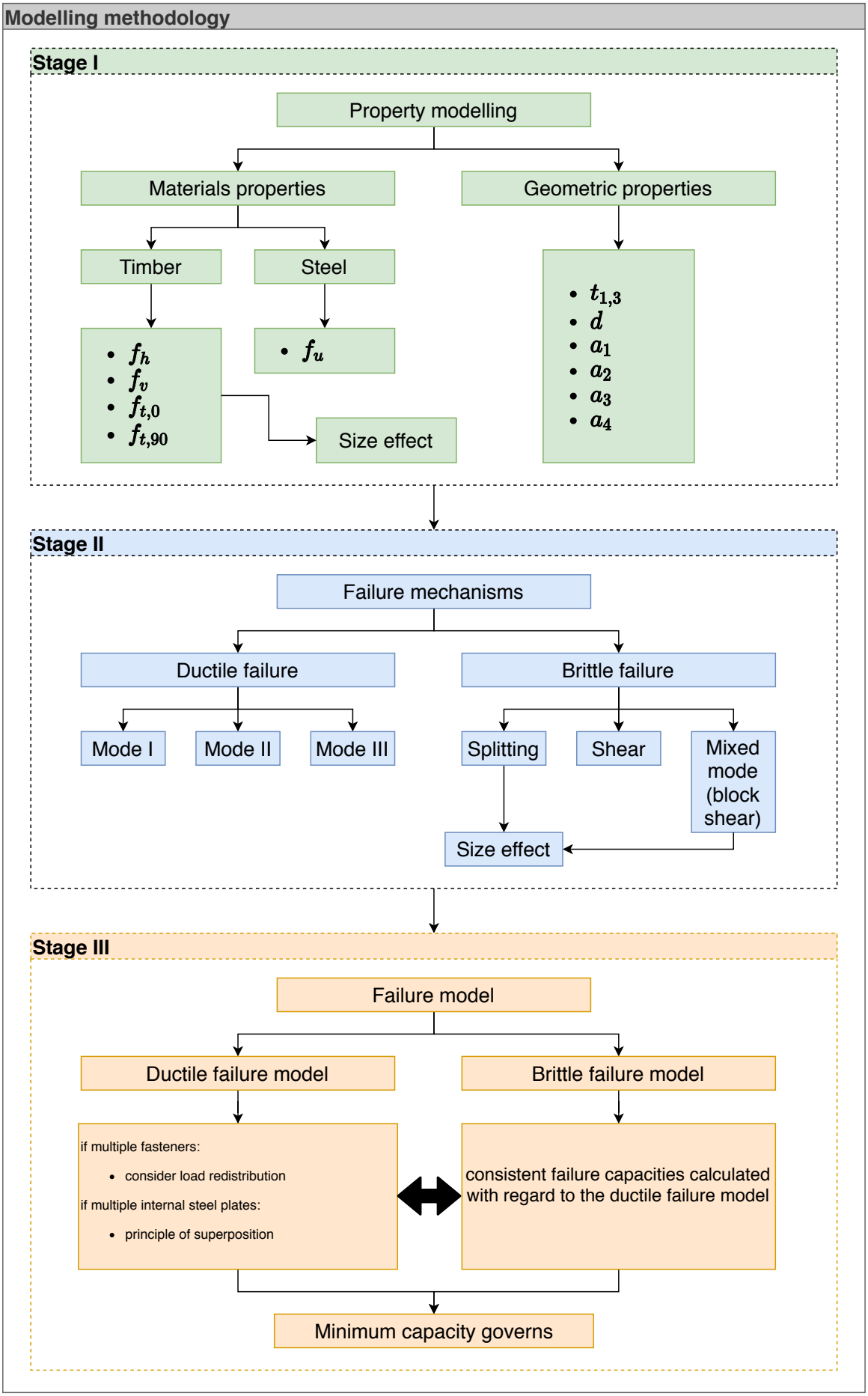

Figure 4.1: Modelling methodology.

4.1 Stage I: Input—parametric—parameter modelling

4.1.1 Geometric parameters

The geometric parameters modelled for TST connections are the timber member thickness, $t_{1,3}$, the fastener diameter, d, and various spacing between fasteners. The symbols used to represent these parameters are defined in figure 1.6. Furthermore in multiple fastener connections, fasteners may be arranged in a rectangular grid with n_c fasteners in one row parallel to the wood fibre orientation and n_r number of rows of fasteners perpendicular to the wood fibre orientation. For TST connections, there may also be more than one steel plate within the connection which is further denoted by the symbol, n_s.

Table 4.1: Discrete variation of geometric parameters considered for single fastener TST connections studied.

Parameter	Minimum Value	Maximum Value	Number of choices
d	8	20	12
$\frac{t_{1,3}}{d}$	5	25	20
$\frac{a_1}{d}$	n/a	n/a	n/a
$\frac{a_2}{d}$	n/a	n/a	n/a
$\frac{a_3}{d}$	2.1	26.25	20
$\frac{a_4}{d}$	0.9	4.5	20
n_c	n/a	n/a	n/a
n_r	n/a	n/a	n/a
n_s	2	4	2

Table 4.2: Discrete variation of geometric parameters considered for multiple fastener TST connections studied.

Parameter	Minimum Value	Maximum Value	Number of choices
d	8	20	12
$\frac{t_{1,3}}{d}$	5	25	10
$\frac{a_1}{d}$	5	15	4
$\frac{a_2}{d}$	4	15	4
$\frac{a_3}{d}$	2.1	26.25	4
$\frac{a_4}{d}$	0.9	4.5	4
n_c	2	5	4
n_r	1	5	3
n_s	2	6	3

Tables 4.1 and 4.2 define the specific discrete variation of the geometric parameters of all TST connections studied. The discrete variation, as described by tables 4.1 and 4.2, is defined by a minimum and maximum value and the number of choices within the given interval.

```
connections = np.array(np.meshgrid(<"input␣feature␣vectors">))
```

Listing 4.1: Implementation to generate a set of connections each with unique geometric parameters.

To generate, m unique combinations of geometric parameters to represent m unique TST connections, a programming technique is used to generate a discrete mesh over the x input

feature variables which in this case refer to the geometric parameters. This is easily programmed using the Python [69] programming language where the relevant pseudo-code is shown in the code snippet 2.

4.1.2 Material properties

To enable a probabilistic framework for the evaluation of the failure mechanisms described in the previous two chapters 2 and 3, the required material properties are sampled from their corresponding statistical distributions. The distribution types, mean, and variance parameters are taken to be in line with those proposed by the Probabilistic Model Code [48].

Table 4.3: Example material properties considered in the analysis of a complete failure model of both ductile and brittle failure modes.

Property	Material	Distribution Type	Mean, $\bar{x}$ (MPa)	COV (%)
ρ	timber	Normal	455	0.18
f_u	steel	Lognormal	800	0.04
f_v	timber	Lognormal	5.0	0.25
$f_{t,0}$	timber	Lognormal	32.5	0.3
$f_{t,90}$	timber	2pt. Weibull	1.1	0.25

Table 4.3 describes the distribution parameters of the fundamental material properties required by the modelling methodology to compute the failure capacity for the various failure mechanisms possible. The ρ is set to a mean value of $455\frac{kg}{m^3}$ with a coefficient of variation (COV) of 18% to match commonly used softwood species in Europe (refer to section 2.2.1 for further details concerning the variability of ρ). The timber material mechanical strength properties are taken to approximate the strength of glued-laminated timber of grade GL24h similar to recent probabilistic literature studies on brittle failure modes [2]. The ultimate bending strength of steel is included since it is a required parameter to calculate the fastener yield moment.

4.1.2.1 Monte Carlo simulation: Fundamental material properties

The modelling methodology consists of sampling N realizations from the material properties for each connection defined with unique geometric parameters to result in a distribution of load-carrying capacities per failure mechanism. This allows for a better understanding of the variability of the failure capacity of each failure mechanism model to properly define partial safety factors in load and resistance factor design (LRFD) methods which are not overly conservative or unconservative. In classical reliability analysis and statistics, two approaches are commonly referred to where the distribution characteristics of the input parameters are either known beforehand or are unknown. In this thesis, it is assumed that prior knowledge of the sample mean and variance of each material property is known (e.g. the designer is provided with strength testing data by a material supplier). The Probabilistic Model Code [48] was used to ensure that the chosen mean and variance for the material properties specified in table 4.3 is an accurate representation of the statistical population it is meant to simulate. The assumption not only simplifies the methodology described here but is similar to the method of designing connections in practice by utilizing the characteristic strengths of the wood material implemented in design standards which are typically based on at least rudimentary reliability analyses to determine the value of the characteristic strengths in design standards.

$$\mu = \ln\left(\frac{m^2}{\sqrt{s^2+m^2}}\right) = \ln\left(\frac{m^2}{\sqrt{COV^2+1}}\right) \tag{4.1}$$
$$\sigma = \sqrt{\ln\left(\frac{s}{m}^2+1\right)} = \sqrt{\ln(COV^2+1)}$$

$$m = \lambda\Gamma\left(1+\frac{1}{k}\right) \tag{4.2}$$
$$v = \lambda^2\left[\Gamma\left(1+\frac{2}{k}\right) - \Gamma^2\left(1+\frac{1}{k}\right)\right]$$

To compute the distribution parameters—μ, σ or λ, k—for each material property needed to sample from, the equations 4.1 and 4.2 are used to calculate either the parameters of the lognormal and 2 pt. Weibull distributions, respectively. Normal distributions simply use the mean, $\mu \approx \bar{x}$, and variance, $\sigma^2 = \bar{x}COV$, as its distribution parameters. Equation 4.2 must be solved simultaneously for the Weibull distribution parameters, λ and k, given a mean and variance of the random variable representing the uncertainty of the material property in question.

```
import sympy as sp

def weibull_parameters(m, v, initial_guess=[0.7297, 0.3932]):
    """
    Symbolic numerical procedure to derive the parameters
    of a Weibull 2-parameter distribution given the aggregate
    statistics of the mean, m, and variance, v.
    """
    x, alpha, betai, mu, sigma2 = sp.symbols('x alpha betai mu sigma2')

    expr1 = alpha**(-1*betai) * sp.gamma(1+betai)
    expr2 = alpha**(-2*betai) * (sp.gamma(1+2*betai) - (sp.gamma(1+betai))**2

    eqn1 = sp.Eq(expr1, m)
    eqn2 = sp.Eq(expr2, v)
    eqns = [eqn1, eqn2]

    Si = sp.nsolve(eqns, [alpha, betai], initial_guess)

    Lambda = float(Si[0]**(-Si[1]))
    k = float(1/Si[1])

    initial_guess = [float(Si[0]), float(Si[1])]

    return(Lambda, k, initial_guess)
```

Listing 4.2: Symbolic solver to compute distribution parameters of a 2pt. Weibull distribution using Python.

The solution to equations 4.2 is not straightforward due to the gamma functions, $\Gamma(x)$, and therefore a symbolic non-linear solver is implemented in Python [69] shown in code listing 26.

This relatively simple procedure has the advantage that the distribution parameters, λ and k, can be found for any known sample mean and variance of the material property. In the age of access to significant computational resources, solving the equations 3.8 is sufficiently possible as to not provide any significant hurdle to include the size effect—section 4.1.2.3 describes more details—in the design of timber connections beyond that of simple rules.

Table 4.4: Correlation matrix of material properties from table 4.3.

	ρ	f_u	f_v	$f_{t,0}$	$f_{t,90}$
ρ	1.0	0.0	0.6	0.4	0.4
f_u	0.0	1.0	0.0	0.0	0.0
f_v	0.6	0.0	1.0	0.6	0.6
$f_{t,0}$	0.4	0.0	0.6	1.0	0.2
$f_{t,90}$	0.4	0.0	0.6	0.2	1.0

The material properties discussed in table 4.3 are also correlated with each other and the correlation matrix is shown in table 4.4. These correlations are taken directly from those tabulated in the Probabilistic Model Code [48]. Though it should be intuitive, the property, f_u, is not correlated with any of the timber material properties since it is a property of the steel fastener alone; however, it is included in the correlation matrix here due to the specific implementation of the programming method to generate the correlated random variables[1].

$$RV = RV \times correlation \tag{4.3}$$

First, n standard normal random variables (RV) are generated with N samples as an array of size, n by N, and the correlation is applied through matrix multiplication with the correlation matrix described by equation 4.3. Before the cross-correlation is applied to the n standard normal RV, the correlation matrix is converted to the nearest positive definite matrix form and Cholesky factorization is applied which are required steps to correctly compute cross-correlated random variables. Secondly, the uniform marginal joint distribution of the cross-correlated RVs is then computed using the normal cumulative density function which is then used in conjunction with the distribution parameters computed beforehand to scale and shift each the RV to represent the material property it is meant to simulate. By implementing this procedure in Python [69], any percentile (e.g. characteristic value) can be easily computed from the object storing the calculated, cross-correlated statistical distribution of each material property and different N-sampled RVs can easily be computed. Figures 4.2 and 4.3 depict the distributions of the simulated material properties based on the mean and coefficient of variation specified in tables 4.3 and 4.4.

4.1.2.2 Monte Carlo simulation: Derived material properties

As per the description of ductile failure mechanisms above (section 2), the EYM requires the knowledge of two derived properties: embedment strength, f_h, and yield moment, M_y. These parameters are described in depth in section 2.2. Similar to the previous section 4.1.2.1, these derived material properties should also represent N sampled realizations from a statistical distribution. To ensure consistency with respect to the simulation technique used, N sampled realizations of the derived parameters are computed using deterministic equations from either design standards or literature sources.

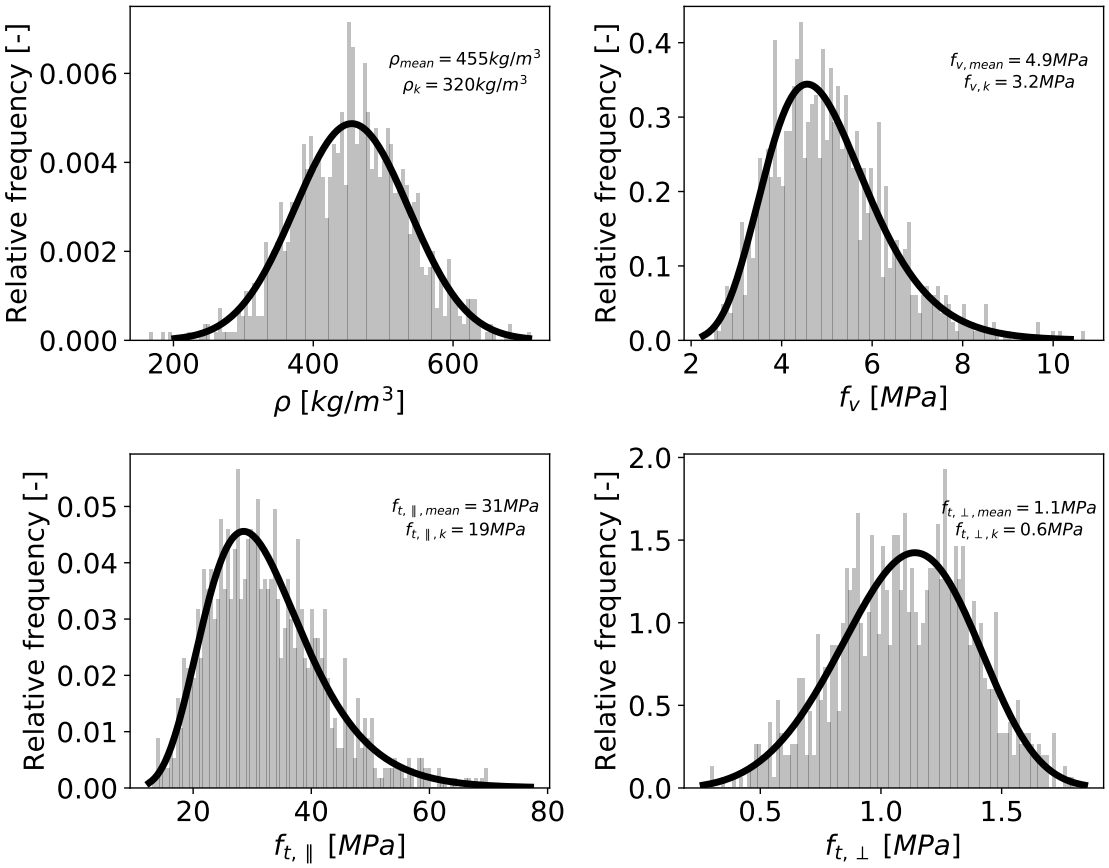

Figure 4.2: Distribution of timber material properties.

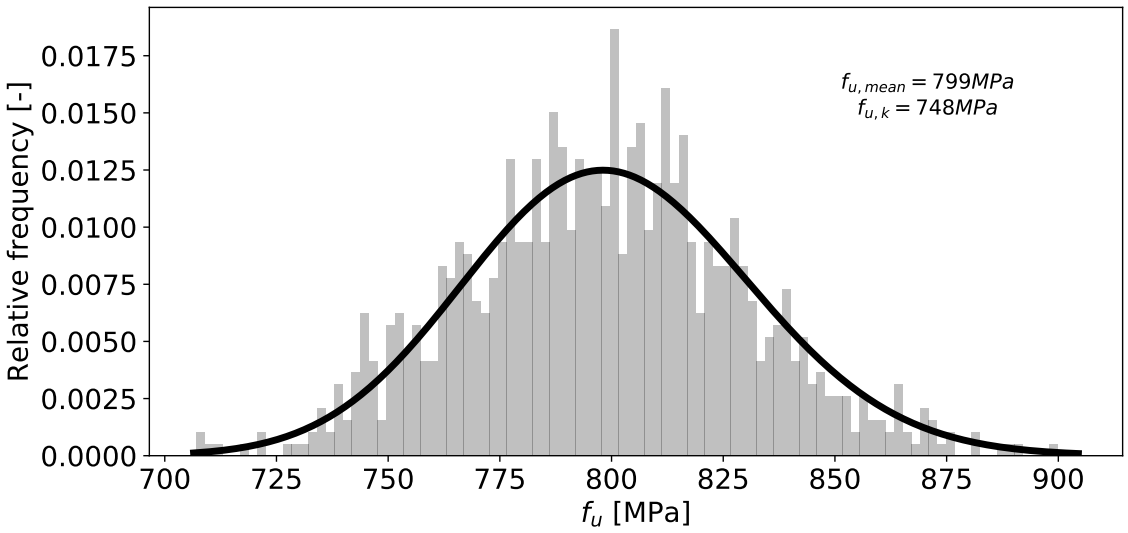

Figure 4.3: Distribution of steel fastener ultimate bending strength.

Table 4.5: Model to derive the embedment strength, f_h, of wood.

Model	$f_{h,\parallel}$	$f_{h,\perp}$
EC5 [4, EC5]	$0.082\rho(1-0.01d)$	$\frac{41\rho(d-100)}{75(d+90)}$
O86 [3, CSA O86-14]	$0.082\rho(1-0.01d)$	$0.036\rho(1-0.01d)$
Leijten et al. [42]	$A_\parallel \rho^{B_\parallel} d^{C_\parallel} D_\parallel$	$A_\perp \rho^{B_\perp} d^{C_\perp} D_\perp$
Kennedy et al. [70]	$108\left(\frac{\rho}{1000}\right)^{1.7}$	$70\left(\frac{\rho}{1000}\right)^{-0.5}$

As an additional step in the modelling methodology, table 4.5 describes four models to predict the embedment strength, f_h, of timber and a model comparison against available data from the literature is conducted to determine the most accurate model to use in the parametric study of TST connections including Monte Carlo simulation of material properties. To ensure a fair comparison of these models, the same distribution of predictor variables, ρ and d, as present in the experimental datasets available are simulated to generate a larger sample set on which to compare (refer back to section2.2.1.2. Using this larger sampled set of predictor variables following the same distribution present in the existing experimental datasets, the embedment strength parameter is computed for each model using these generated predictor variables.

$$\begin{aligned} f_h &= A\rho^B d^C \\ \ln f_h &= \ln A + B\ln\rho + C\ln d + \epsilon \end{aligned} \tag{4.4}$$

The third row in table 4.5 defines a multiple linear regression model for the f_h which will be explained in the next few paragraphs while the remaining rows of table 4.5 define algebraic models from design standards or literature sources. Using the existing data available in the literature, a multiple linear regression analysis is performed to verify the regression parameters defined by Leijten et al. [42] shown in equation 4.4. Using machine learning techniques to split the dataset into training and test sets, the linear regression analysis was performed to return the best fit model. More specifically, linear regression analysis of the logarithm of the design parameters, ρ and d, are used. This assumption of a logarithmically linear relationship between influencing parameters and the embedment strength, f_h, is taken directly from reported results in the literature indicating linear relationships with ρ and d separately but taken together a interaction exists [40, 42].

$$\hat{\beta} = \underset{\beta}{\operatorname{argmin}} J(\beta) \tag{4.5}$$

$$\hat{\beta} = (X^T X)^{-1} X^T y \tag{4.6}$$

Machine learning is then applied in the form of the ordinary least squares (OLS) method using 80% of the dataset available as a training set and the remaining 20% as the test set. Ordinary least squares is an algorithm to estimate the parameters, β[1], of a linear equation which best fits the dataset. The optimal parameters, β, are computed using the quadratic minimization

[1] β refers to the parameters A, B, C, and D of equation 4.4.

problem in equation To understand the quadratic minimization problem and specifically the objective function, $J(\beta)$, it is necessary to understand that OLS algorithm is a special case of a larger class of algorithms, least mean squares (LMS). Gradient descent is a more general algorithm belonging to the LMS class from which the objective function, $J(\beta)$, can be derived as $J(\beta) = \frac{1}{2}(X\beta - y)^T(X\beta - y)$. The value of $\beta = \hat{\beta}$ which minimizes the objective function, $J(\beta)$, is given in standard statistical texts as the closed form solution in equation 4.6.

```
from sklearn..linear_model import LinearRegression
from sklearn.model_selection import train_test_split
from sklearn.metrics import explained_variance_score

X_train, X_test, y_train, y_test = train_test_split(X, y, train_size=0.8)
regressor = LinearRegression()
regressor.fit(X_train, y_train)
y_pred = reg_leijten.predict(X_test)
R2[i] = explained_variance_score(y_test, y_pred)
```

Listing 4.3: Relevant lines of code implementing a OLS regression in Python.

To perform the OLS regression on the embedment strength, f_h, data available, the machine learning module, `sklearn`, of the Python programming language [69] is used. This module, `sklearn`, provides a easy, programmatic application of least squares regression theory in a few lines of code (the relevant lines shown in the code snippet 10 above).

Table 4.6: Model to derive the yield moment, M_y, of steel fasteners.

Model	Function
f_h	$\ln(A) + B\ln(\rho) + C\ln(d) + D$
M_y	$0.3 f_u d^{2.6}$

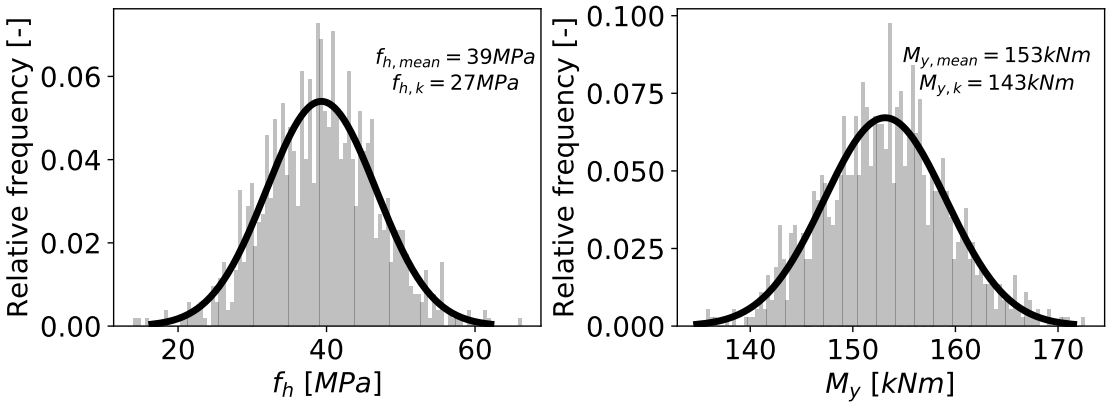

Figure 4.4: Distribution of derived material properties.

Returning to the consideration of these two derived parameters as requirements for the parametric study of the failure capacity of TST connections, table 4.6 describes the models used to derive N-sampled values for f_h and M_y. N-sampled values are needed for the Monte Carlo simulation of the material properties to define the variability of the failure capacity per TST connection (refer to the previous section 4.1.2.1). The diameter of the fasteners, d, also appears in these equations and therefore, these derived variables are computed for each connection with a different fastener diameters, d. The model to evaluate the embedment strength, f_h, is derived

from the recent literature study in [42, Leijten et al.]. Figure 4.4 shows the distributions of these two derived material properties using the models for f_h and M_y in table 4.6.

4.1.2.3 Size effect model

The size effect is a significant phenomenon of brittle materials such as wood as described in section 3.2.3. To account for this size effect when simulating material properties as outlined in section 4.1.2.1, it is necessary to update the mean and variance of the material property as per the size effect. That is to say that larger volume connections typically experience a lower mean strength—especially tensile strengths of brittle materials—than smaller volume connections which often can fail at a much higher strength. The material property most dependent on the size of the timber connection and most susceptible to cause brittle failure to govern the TST connection capacity is the tension strength perpendicular-to-grain, $f_{t,90}$, of wood. For this reason, the $f_{t,90}$ strength is the only material property where a explicit size effect dependency is implemented in the generation of the N sampled realizations of the simulated material property. This is in line with the Probabilistic Model Code [48] where the $f_{t,90}$ strength is the only timber mechanical material property defined to be represented as a 2 pt. Weibull distribution.

$$\begin{aligned} f_{t,90} &= \frac{f_{t,90,ref.}}{(V/V_{ref.})^{\frac{1}{k_0}}}, \text{ where} \\ f_{t,90,ref.} &= 1.1MPa \\ V_{ref.} &= 0.01m^3 \end{aligned} \tag{4.7}$$

By applying equation 4.7, the mean $f_{t,90}$ strength is adjusted for any volume, V, can be calculated according to a reference strength, $f_{t,90,ref.}$, and volume, $V_{ref.}$. Then, the standard normal, cross-correlated RV from the simulation procedure described in section 4.1.2.1 is used to shift and scale the RV using the 2pt. Weibull distribution parameters computed as a function of the adjusted mean $f_{t,90}$ strength and its coefficient of variation. It should be noted that the variance of the $f_{t,90}$ is considered to be constant with respect to the size effect which results in the shape parameter, k, of the 2pt. Weibull distribution being constant with only the scale parameter, λ, being affected. For a reference mean $f_{t,90,ref.} = 1.1MPa$ and $COV = 0.25$, the shape parameter, k, approximately equals a constant value of 4.542. The change in distribution shape of the size effect adjusted $f_{t,90}$ random variable is shown in figure 4.5.

4.2 Stage II: Failure mechanism models

The failure mechanism models used to evaluate the load-carrying capacity of the TST connections considered in this thesis are taken from the models presented in chapters 2 and 3 where a comprehensive review of the existing literature inclusive of current design standards (e.g. [3, CSA O86-14] [4, EC5] [5, NDS 2012]) is described. Chapter 3 provides a thorough review of recent literature sources on the development of various approaches to consider brittle failure mechanisms explicitly in design methods as opposed to existing design standards (e.g. [3, CSA O86-14] [4, EC5] [5, NDS 2012]) implicit narrative.

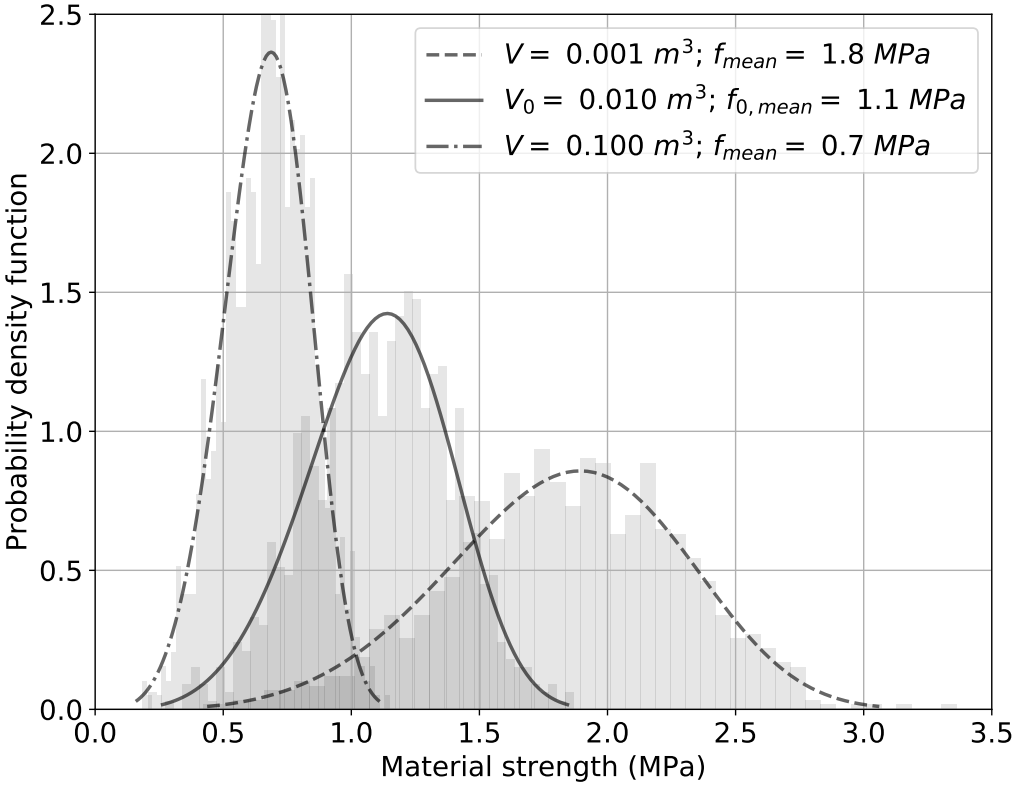

Figure 4.5: Corresponding size effect on the $f_{t,90}$ strength of timber.

Table 4.7: Failure mechanism models used in this thesis.

Failure mechanism	Model
EYM mode I	$R_I = f_{h,i} t_i d$
EYM mode II	$R_{II} = f_{h,1} t_1 d \left(\sqrt{2 + \frac{4M_y}{f_{h,1} d t_1^2}} - 1 \right)$
EYM mode III	$R_{III} = 2\sqrt{M_y f_{h,1} d}$
Splitting	$R_{t,split} = k_{t,90} \frac{1}{\beta} t_i a_3 f_{t,90}$, where $\beta = \frac{1}{7}$
Shear	$R_{v,split} = 2 k_v n_r n_c t_i a_{L,min} f_v$
Net tension	$R_{t,tension} = k_{t,0} n_c (n_r (a_2 + d)) t f_{t,0}$
Mixed mode (block shear)	$R_{\text{mixed mode}} = 2R_{v,split} + R_{t,tension}$

Table 4.7 summarizes the seven failure mechanisms (three ductile and four brittle mechanisms) which are considered in this thesis to be combined into a failure model to predict the governing load-carrying capacity of the studied TST connections. The main considerations taken into account to choose the equations to represent all possible brittle failure mechanisms were their simplicity for use in practical design applications, compatibility with the spirit of the EYM, and the computational ease to calculate. The methodology of the analysis presented here is to provide a framework to develop a consistent, reliable, and robust method to predict the load-carrying capacity of timber connections especially with regard to size effects and qualitatively assess the impact of varying geometric input parameters and variability in material properties on the failure model described in the next section 4.3. It is recognized that accuracy of the failure mechanism models themselves are important as well and for that reason a thorough literature review was conducted to justify the use of the relatively simple models summarized in table 4.7.

The EYM is used to model the three possible ductile or quasi-ductile failure modes. Brittle failure mechanisms were generally described in the literature as resulting from the complex stress state which arise in timber connections when loaded. The predominant stresses which are shown in the literature to lead to brittle failure of timber connections are tensile and shear stresses and their interaction. Therefore, it seems logical that any brittle failure model would take into account brittle failure resulting from tensile stresses either parallel- or perpendicular to the fibre orientation of wood or from shear stresses becoming larger than the strength of wood either in tension or shear, respectively. As a result, the failure mechanism models summarized in table 4.7 describe three separate models to represent a failure caused by the tensile perpendicular-to-grain strength, $f_{t,90}$, being exceeded, a failure caused by the shear strength, f_v, being exceeded, and a failure caused by the tensile parallel-to-grain strength, $f_{t,0}$, being exceeded. The last mechanism described by table 4.7 is to consider multiple fastener connections where a "block" failure could occur; however, this mechanism is a combination of a tension parallel-to-grain and shear stress exceeding their respective strengths. It makes sense, in that case to consider this "block" failure mechanism as a combination of the shear and net tension brittle failure mechanisms. Further, net tension brittle failure is highly improbable to occur as a separate distinct failure since the tensile strength parallel-to-grain is significantly higher than either the tensile strength perpendicular-to-grain or shear strength.

4.3 Stage III: Failure capacity model

The capacity of the various possible failure mechanisms spanning from ductile to brittle failure modes are computed for TST connections using N-sampled realizations of the material properties required. Sampling from the distributions of the input material properties allows for a probabilistic evaluation of the governing failure capacity of timber connections. By sampling from distributions, the exact distribution characteristics of each material property can be controlled to represent the real distribution of material strengths and the resulting failure mechanism distributions. In this way, it is possible to study the effect of the so-called size effect of wood on the failure capacity of timber connections. The specific details of the methodology of sampling from different distribution types which are correlated is described in the next section 4.1.2.1 and more details with regard to implementing a size effect study is described in section 4.1.2.3. Furthermore, the failure capacity model is evaluated for many configurations of connections to identify the impact of various geometric variables including the change in probability of brittle over ductile failure behaviour. The methodology presented here is a

continuation of existing trends in the literature to not only account for brittle failure modes in structural timber connection design methods but to do so within a probabilistic framework to ensure a safe, robust, and reliable design methods.

$$R_{\text{single internal plate}} = \min \begin{cases} F_I + F_I \\ F_{II} + F_{II} \\ F_{III} + F_{III} \end{cases}$$

$$R_{\text{multiple internal plates}} = \min \begin{cases} F_I + F_{Ib} \\ F_I + F_{III} \\ F_{II} + F_{Ib} \\ F_{III} + F_{Ib} \\ F_{II} + F_{III} \\ F_{III} + F_{III} \end{cases} + \min \begin{cases} F_{Ib} + F_{Ib} \\ F_{III} + F_{III} \end{cases}$$

$$R_{\text{ductile failure}} = R_d = n_{ef} R_{\text{single internal plate}} \text{ or } n_{ef} R_{\text{multiple internal plates}} \tag{4.8}$$

$$R_{\text{brittle failure}} = R_b = \begin{cases} R_{t,split} \\ R_{v,split} \\ R_{t,tension} \\ R_{\text{block shear}} \end{cases} \tag{4.9}$$

Using the failure mechanism models presented in the previous section 4.2, the mean failure capacity as a distribution—based on N material property realizations—is computed for both the governing ductile and brittle failure mechanisms as per equations 4.8 and 4.9.

$$P(\text{Brittle failure} \leq \text{Ductile Failure}) = P(R_b - R_d \leq 0) \tag{4.10}$$

Then the probability that brittle failure occurs instead of ductile failure is computed by subtracting the governing mean ductile failure capacity from the governing brittle failure capacity (equation 4.10) and sorting the result from smallest to largest values. Using a normal cumulative density function for the variable, $R_b - R_d$, the probability is computed for all TST connections studied with varying geometric parameters. Using the variable, $R_b - R_d$, and counting the number of instances where the variable is less than zero and dividing by the number of realizations/samples for which the failure capacity is computed, the probability that brittle failure is less than ductile failure can be determined as the final step in the crude Monte Carlo simulation described by this modelling methodology. Since the probabilities computed according to the crude Monte Carlo simulation technique, the opposite probability that ductile failure is more likely is then calculated as $1 - P(R_b < R_d)$.

5

Results & Discussion

The methodology described in chapter 4 to evaluate the effect of geometric connection parameters and the natural variability of wood on TST connections are presented next. First, several models to predict the embedment strength, f_h, of wood described in section 5.1 are compared. Existing experimental data available from previous literature sources [45, 37, 36, 39, 40] is used to compare four models for the embedment strength parameter: the EC5 design model, the O86 design model, the proposed probabilistically derived model in [42, Leijten et al.], and the proposed model based on a statistical non-linear regression analysis in [41, Kennedy et al.]. Secondly, a parametric study is performed while varying geometric parameters to determine their impact on the type of failure: brittle versus ductile. Additionally, a probabilistic framework is described in the chapter 4 to determine changes in the variability of the failure capacity as geometric connection parameters are varied. The results of the parametric study are presented and discussed in section 5.2. The discussion is split into two distinct groups consisting of single fastener and multiple fastener TST connections. Furthermore, multiple steel plate connections are mentioned and the challenge of evaluating multiple steel plate connections with existing failure modes

5.1 Comparison study of existing f_h models

As described in the previous section 2.2.1, recent literature has cast doubt on the reliability of existing models to predict the embedment strength of timber. As the embedment strength is a key parameter to determine the capacity of timber connections and a trend towards incorporating higher levels of probabilistic design methods, more reliable models for parameters such as f_h are needed. A thorough comparison of existing models is presented next to help facilitate the shift towards more reliable models. This comparison study is done using existing experimental data which was used initially to deterministically derive the existing models which are compared here [36, 42]. Additional data is also used to enhance the comparison to statistically better represent real conditions [41, 40].

Tables 5.1 summarizes the mean and coefficient of variation of the timber density and embedment strength of the experimental data available in the literature [36, 71, 40, 72, 42, 41]. To enable a comparison including the variability of the embedment strength, the timber density and fastener diameter are modelled as distributions. Timber density, ρ, for each group of data described in table 5.1 is modelled as a normal distribution with mean and coefficient of variation (COV) which statistically describes the experimental data group. The fastener diameter, d, is modelled using a discrete random variable which takes on values corresponding to the fastener diameters of the experimental data group with equal probabilities. Using these simulated dis-

Table 5.1: Summary of existing experimental data grouped into 8 groups [36, 42].

Wood Type	Fastener Type	Angle	n	ρ (kg/mˆ3) Mean	COV	f_h (MPa) Mean	COV
coniferous	dowels [36, 40]	0	940	412.483973	0.129912	33.977533	0.174046
		90	506	397.576638	0.113168	17.992405	0.207521
	nails [36, 40]	0	397	425.517710	0.123388	24.740077	0.249965
		90	319	419.543389	0.124208	26.233059	0.244636
	lag screws [41]	0	345	497.014493	0.129034	34.107420	0.278013
		45	237	478.818565	0.117221	17.730549	0.259062
		90	235	504.760563	0.119429	17.486817	0.319340
deciduous	dowels [71, 72]	0	215	855.956404	0.188584	70.852769	0.260445
		90	110	772.995361	0.185544	59.359608	0.252547
	nails [71, 72]	0	120	769.232411	0.142897	68.351997	0.252361
		90	80	805.487024	0.138684	61.662984	0.311836

tributions for ρ and d, the embedment strength, f_h, is computed for the existing models used in current design standards (e.g. [3, CSA O86-14] [4, EC5] [5, NDS 2012]) for each data group identified in table 5.1 as described by the methodology in chapter 4. Using the experimental data, a linear regression analysis of each data group is performed under the assumption that the f_h is at least locally logarithmically linear with respect to variables, ρ and d, similar to the procedure outlined in [42, Leijten et al. (2004)].

First, characteristics of the relationship between input parameters, ρ and d, are determined and conclusions drawn from the previous literature [40, 39, 36, 41] are verified graphically in figure 5.1 for the experimental data measured using test method 1[1]. It is evident that the relationship between variables ρ and f_h is significantly a positive linear relation for all cases. However, the relationship between variables d and f_h depends highly on the data group and loading situation considered. For both parallel- and perpendicular-to-grain loading, deciduous woods (i.e. hardwoods) with varying fastener diameters, d, exhibits a constant relationship with the embedment strength, f_h, when taking the variability into account. On the other hand, coniferous woods (i.e. hardwoods) with varying fastener diameter, d, exhibits a weakly positive relationship with the embedment strength, f_h, when loaded parallel-to-grain and a negative relationship when loaded perpendicular-to-grain. This last phenomenon of coniferous woods is dependent on the test methodology (here using test method 1), where the embedment strength, f_h, is defined as the 5mm embedment strength, which includes a increase in fastener diameter dependent load hardening as the diameter decreases when loaded perpendicular-to-grain. This is also illustrative of the need to account for the test methodology by which experimental data was conducted with since in [41, Kennedy et al.] the second test method is used where fastener diameter, d, was found to not be statistically significant predictor of the embedment strength, f_h.

This phenomenon that the relationship between variables d and the perpendicular-to-grain f_h of wood is dependent on the wood embedment strength testing method is further evident in figures 5.2 to 5.5 where the experimental data from [42, Leijten et al.] is compared to simulated predictions of the embedment strength. The figures 5.2 to 5.5 depict the cumulative distribution functions of the embedment strength computed for each existing model (refer to table 4.5 for

[1]Test method 1 refers to the experimental method defined in EN 383 [46] to determine the embedment strength in contrast to test method 2 defined in ASTM D5764 [47]. Further details of the differences between the two test methods is described in section 2.2.1.1.

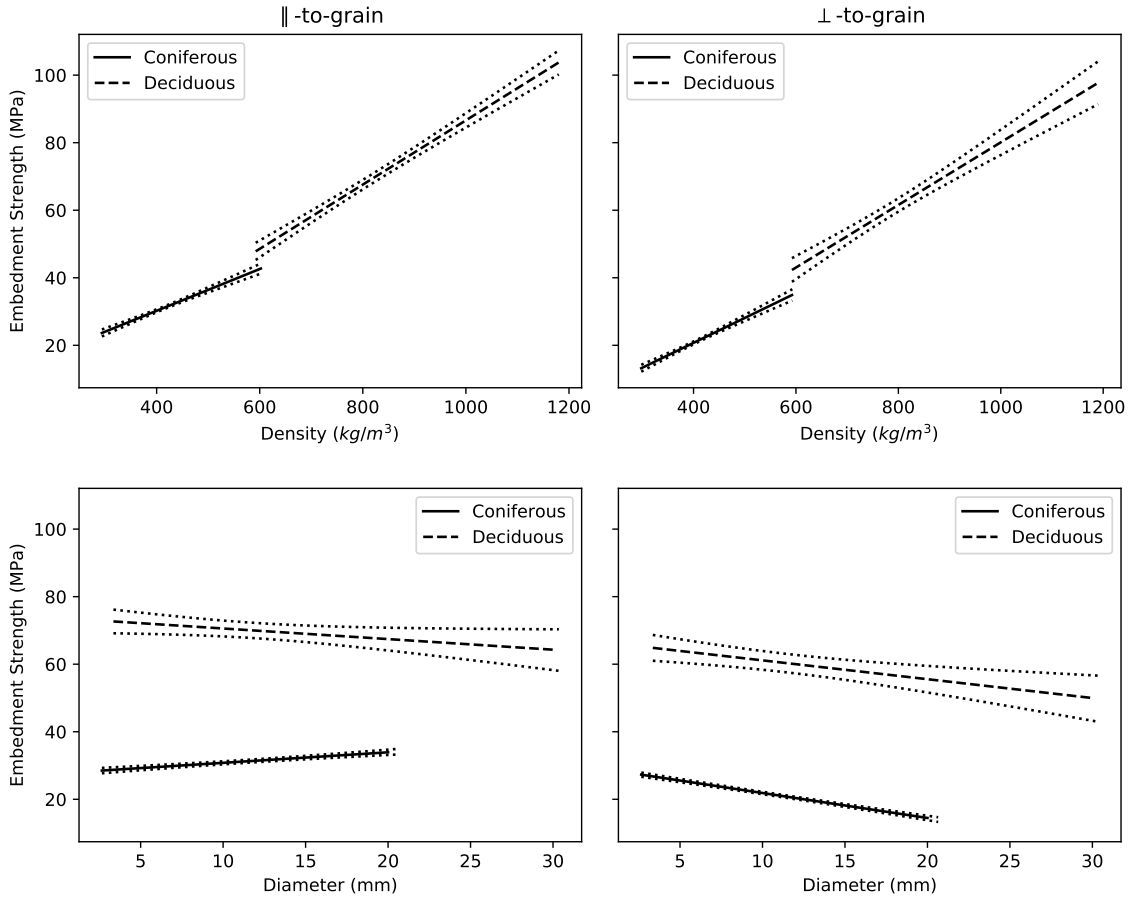

Figure 5.1: Relationship between ρ and d with f_h.

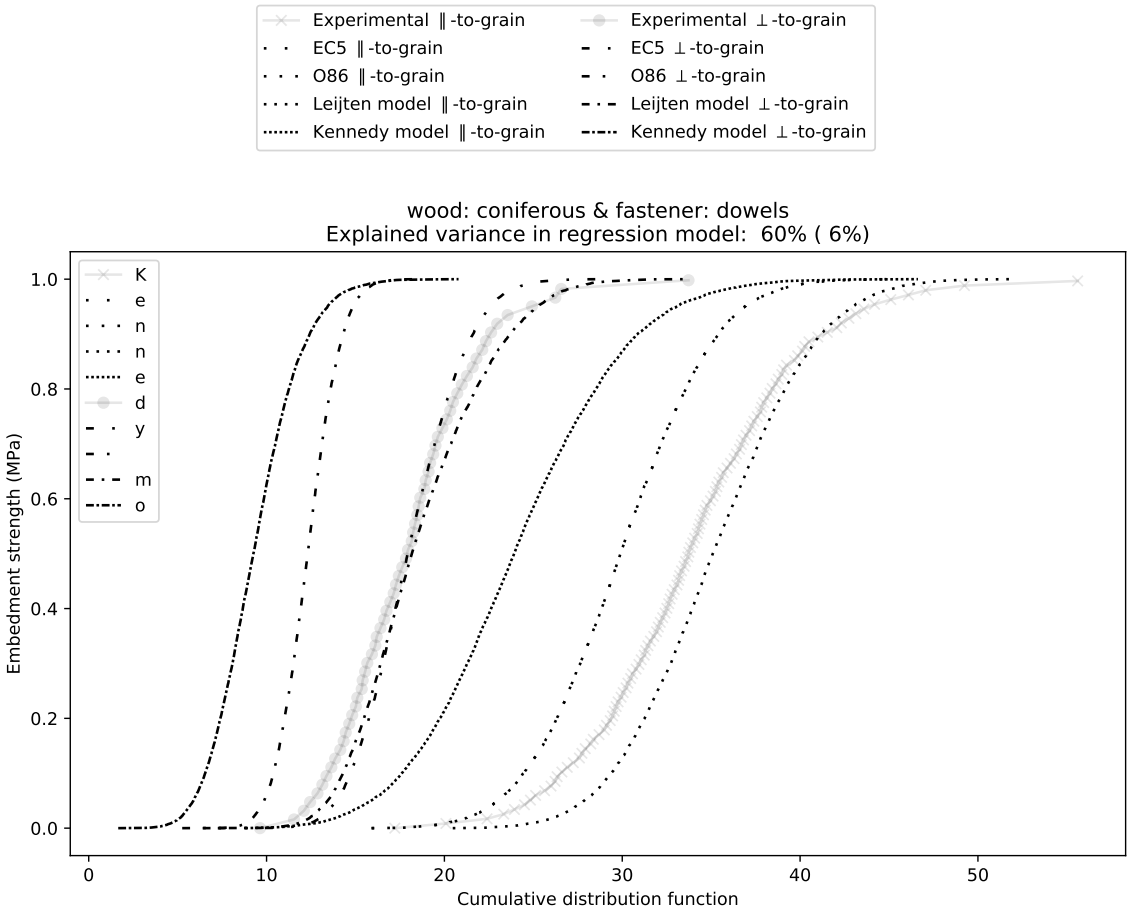

Figure 5.2: Comparison of existing models to predict the f_h of timber for coniferous (softwoods) with dowel-type fasteners.

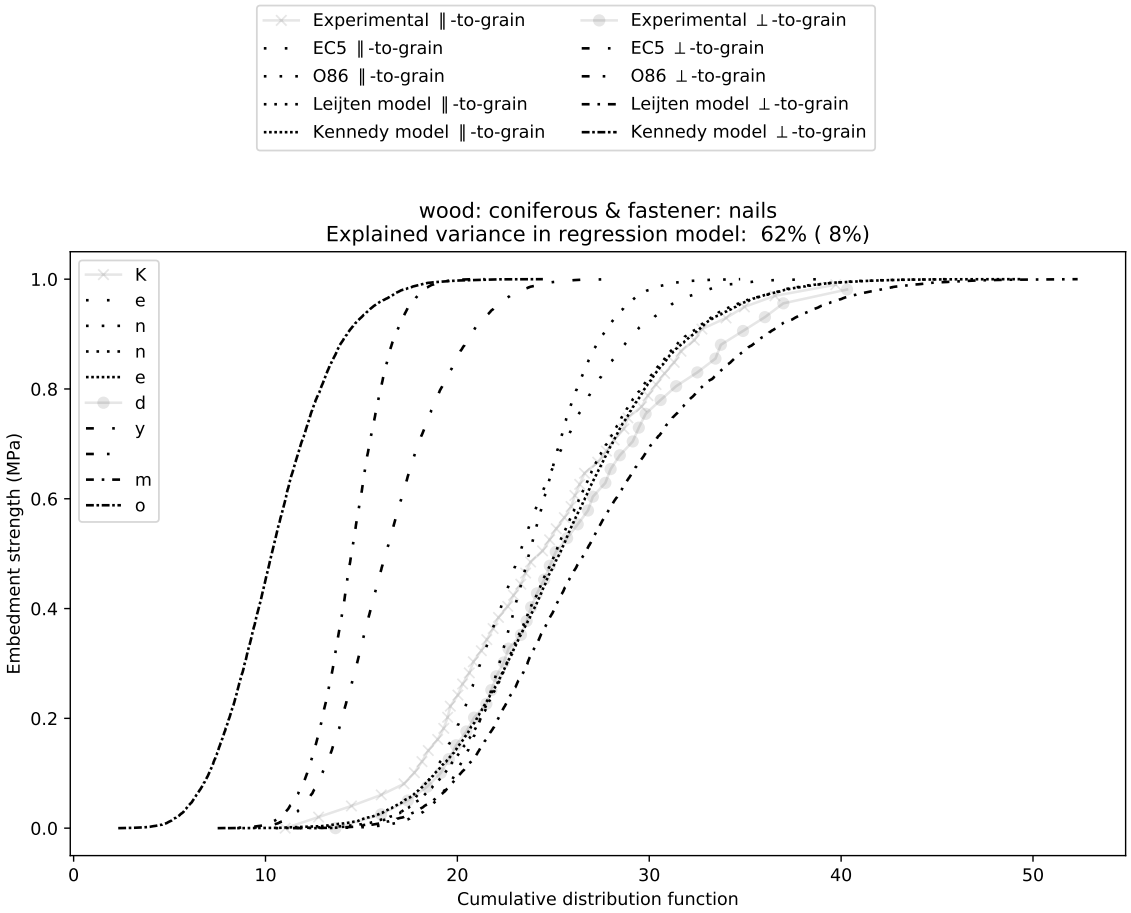

Figure 5.3: Comparison of existing models to predict the f_h of timber for coniferous (softwoods) with nail-type fasteners.

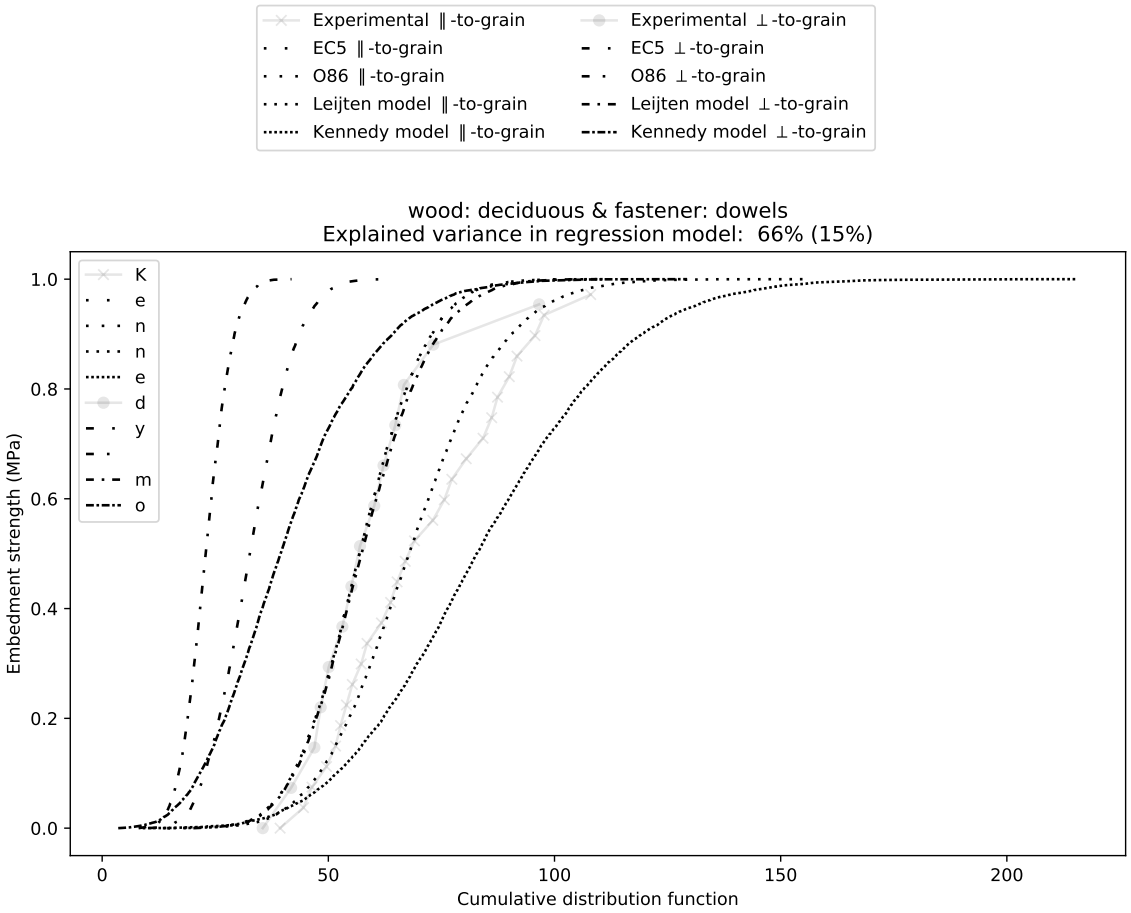

Figure 5.4: Comparison of existing models to predict the f_h of timber for deciduous (hardwoods) with dowel-type fasteners.

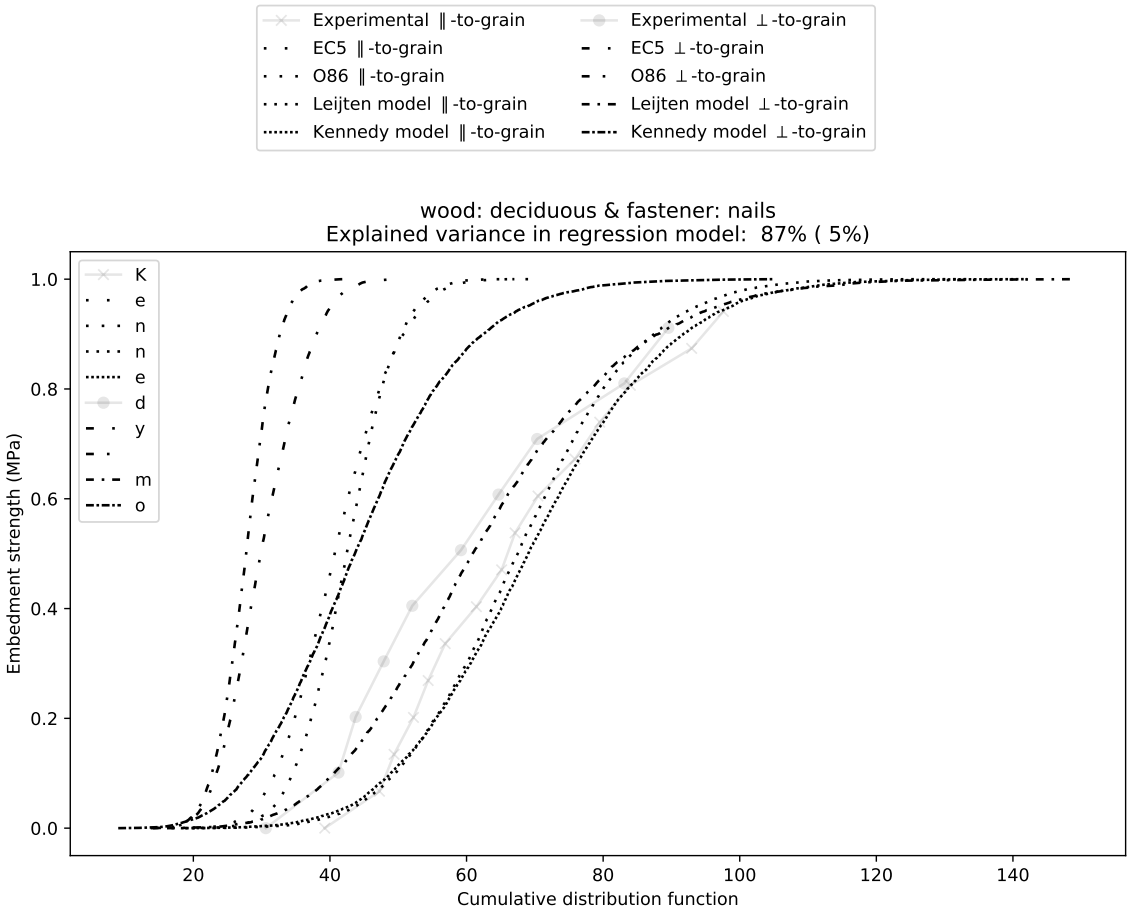

Figure 5.5: Comparison of existing models to predict the f_h of timber for deciduous (hardwoods) with nail-type fasteners.

the specific models) as a function of simulated predictor variables, ρ and d, and compared with the plotted empirical cumulative distribution function of available data. Further, figures 5.2 to 5.5 show the results of each model with respect to four data groups: coniferous (softwood) wood and deciduous (hardwoods) wood with both dowels and nails. The simulation of the predictor variables is described in section 4.1.2.2. The models which were derived using either test method correspond naturally better with the experimental data measured using the respective test method for which the model was derived for. That is to say that the European models, EC5 [4] and [42, Leijten et al.], perform better as evident when compared to the experimental curves in figures 5.2 to 5.5 and the latter model performs the best regardless.

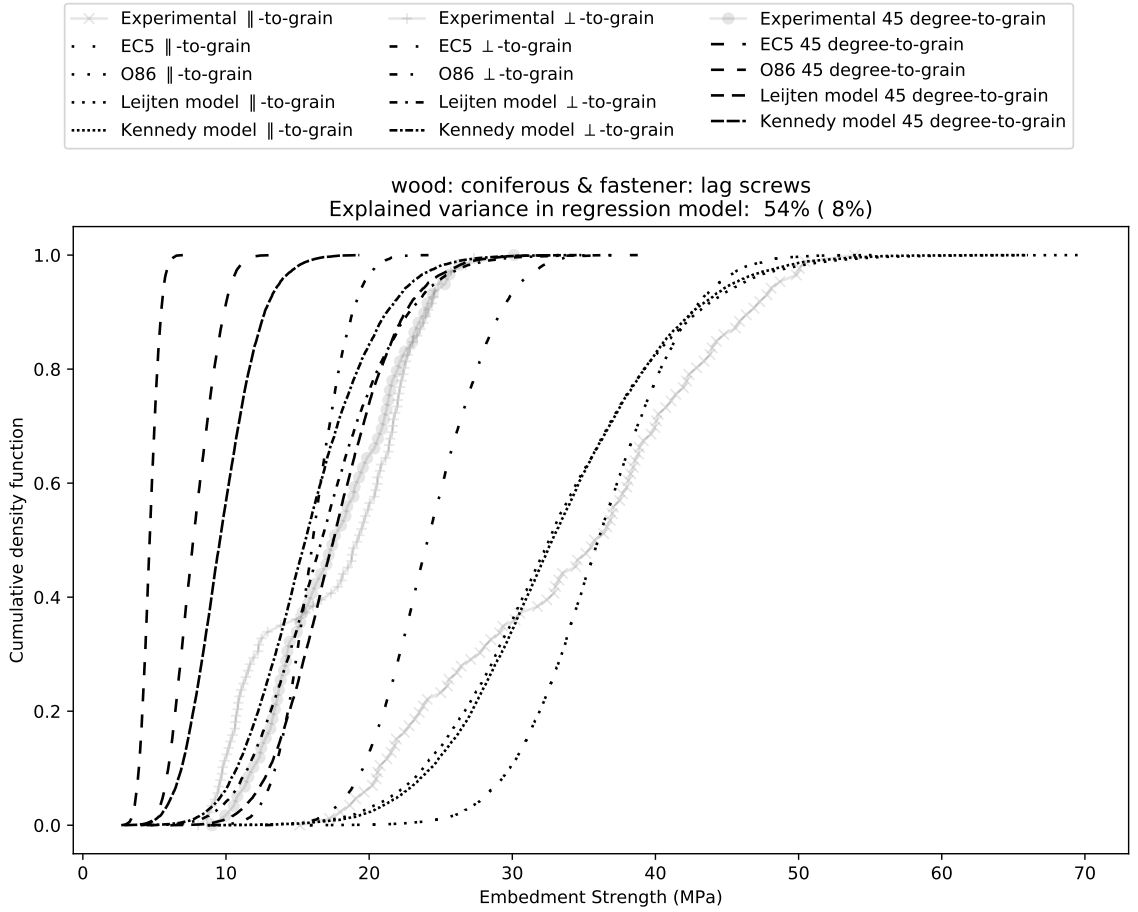

Figure 5.6: Comparison of predicted f_h using existing models with respect to experimental data collected using test method (method 2) defined in ASTM D5764 [47].

Considering only the data group of coniferous (softwood) dowelled data (figure 5.3) and the additional figure 5.6 where the empirical cumulative density function is based on data collected using test method 2 (ASTM D5764 [47]) [41], the probabilistic multiple linear regression based model [42] continues to perform best when compared to the empirical cumulative density functions derived using experimental data collected regardless of the test method. Although still dependent on the test method used to collect the embedment strength experimental data, the probabilistic linear regression model [42] is the least dependent as evident through the figures 5.3 and 5.6. A prime example of this difference is especially apparent on figure 5.6 when considering perpendicular-to-grain loading where the O86 [3] model performs much better against the experimental data collected using test method 2 (ASTM D5764 [47]) as opposed to the EC5 [4] model which was derived using data collected with test method 1 (EN 383 [46]).

Figure 5.2 to 5.5 shows the comparison of the existing f_h models in terms of the cumulative

distribution function of the resulting distribution of the computed f_h for both coniferous (softwood) and deciduous (hardwood) wood species as well as both nail and bolt fasteners. It should be noted that figure 5.2 to 5.5 only includes the European [4] and Canadian O86 [3] models and the NDS [5] model is not shown since it gives the least accurate results compared to the majority of the experimental dataset used here collected using test method 1.

The models to predict the embedment strength of wood compared indicate that simple linear equations as prescribed in current design standards (e.g. [3, CSA O86-14] [4, EC5] [5, NDS 2012]) may be inaccurate and potentially unsafe. This is primarily a result of the natural variability inherent to wood as a material which introduces a non-linearity in the embedment behaviour of wood in timber connections. Furthermore, as described in the existing literature the primary parameters influencing the embedment strength are the density of timber, ρ, and fastener diameter, d, are reasonable to predictors. However, simple models containing only linear predictors, ρ and d, of the embedment strength are not sufficient to use with Hankinson's formula (equation **??** to compute the embedment strength for any load applied at any angle with respect to the wood fibre orientation). For example, the off-axis embedment strength such as perpendicular-to-grain loading scenarios suggest a more complex non-linear behaviour as a function of d and interaction effects between d and the variability of ρ. The framework presented conducts a review of the probability approach in [42, Leijten et al.] and provides a methodology for which further experimental testing can derive and calibrate models to better explain the variability of the embedment strength parameter, f_h, as a function of the primary influencing parameter of timber density, ρ, and fastener diameter, d, for any on- or off-axis loading condition. The analysis to compute the cumulative density functions is further described in appendix A.

5.2 Parametric TST connection study

The results of the parametric study of TST connections is presented next. It should be reminded that the primary purpose of this study is to identify the difference between ductile and brittle failure modes and qualify the difference in variability of these two very different failure mechanisms. Furthermore, this study also aims to provide evidence as to the failure capacity trends for very large TST connections which are being used as high capacity connections in tall mass timber structures recently. To perform a useful study on the failure capacity of these timber TST connections, two distinct sets of connections are studied. The first group of TST connections concerns single fastener connections while the latter group concerns itself with multiple fastener connections. To add complexity to the parametric study, multiple steel plates are also considered for both groups of connections where the both groups are limited to a one and two internal steel plates. The next two sections 5.2.1 and 5.2.2 present and discuss the results of these parametric studies. Appendices B and C describe the input files for the analysis of single and multiple fastener TST connections, respectively, for the various analyses presented in the next two sections 5.2.1 and 5.2.2.

5.2.1 Single fastener TST connections

The parametric study of single fastener TST connections is used to present both the variability of the failure capacity and the likelihood of brittle over ductile failure as a function of the

timber member thickness, $t_{1,3}$, and fastener end-spacing, a_3. By describing and characterizing the relationship between these two varying geometric parameters on single fastener connections, a baseline can be established to identify values for which multiple fastener (i.e. larger TST connections) should be studied at.

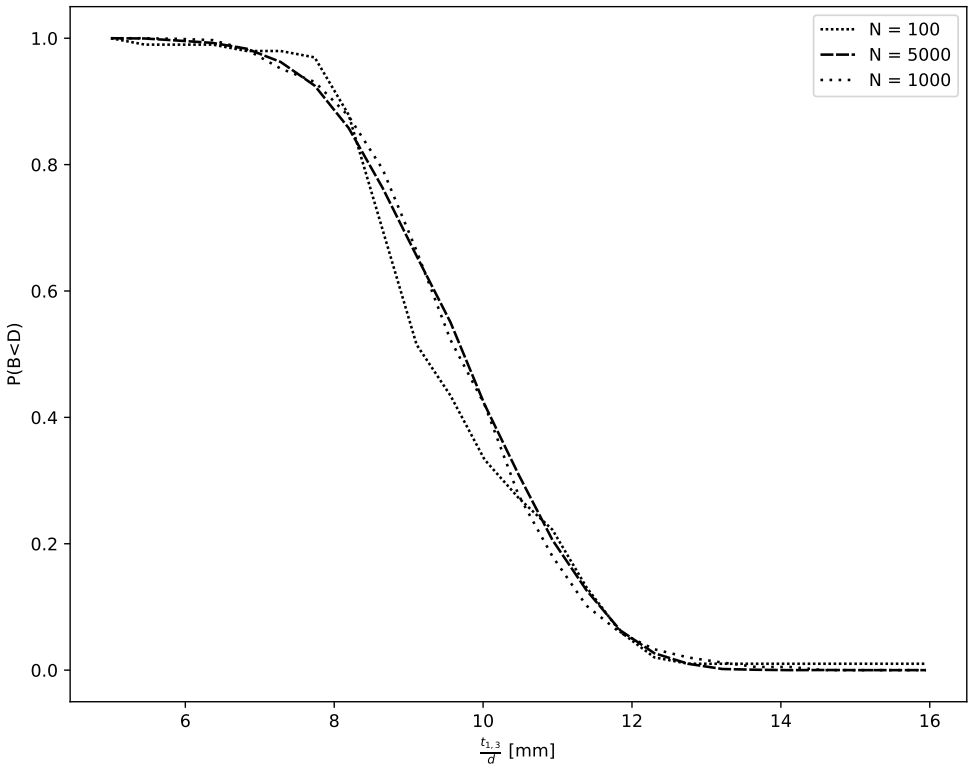

Figure 5.7: Convergence of P(B<D) for TST connections with varying $\frac{t_{1,3}}{d}$ and for three iterations with different number of realizations of Monte Carlo simulated variables.

To begin it is necessary to show that the number of realizations of each material property is sufficient and converges, figure is provided to justify the use of only 1000 samples in the crude Monte Carlo simulation process described in chapter 4 to in a larger part to allow for smaller computational run times. As evident in figure , three different number of samples were used on single fastener TST connections when only $t_{1,3}$ is varied with all other parameters held constant. The probability of brittle failure less than ductile failure appears to already converge between 1000 and 5000 realizations of the Monte Carlo simulated material properties and therefore, the remaining analyses were performed with 1000 realizations.

The importance of respecting minimum end-spacing requirements in modern design standards (e.g. [3, CSA O86-14] [4, EC5] [5, NDS 2012]), cannot be overstated as is readily apparent in figure 5.8. Small normalized—with respect to fastener diameter—end-spacings of 2.1mm at any thickness of the timber member shows a predicted probability of brittle failure at 100%. It is also apparent that smaller timber member thickness require a larger minimum end-spacing as depicted by the second column of subplots in figure 5.9. This leads to potential severe consequences in larger TST connections with multiple internal steel plates as the thickness of the 3 member connections which these larger connections are made of can become significantly smaller. The consequence would be that current minimum end-spacing requirements such as

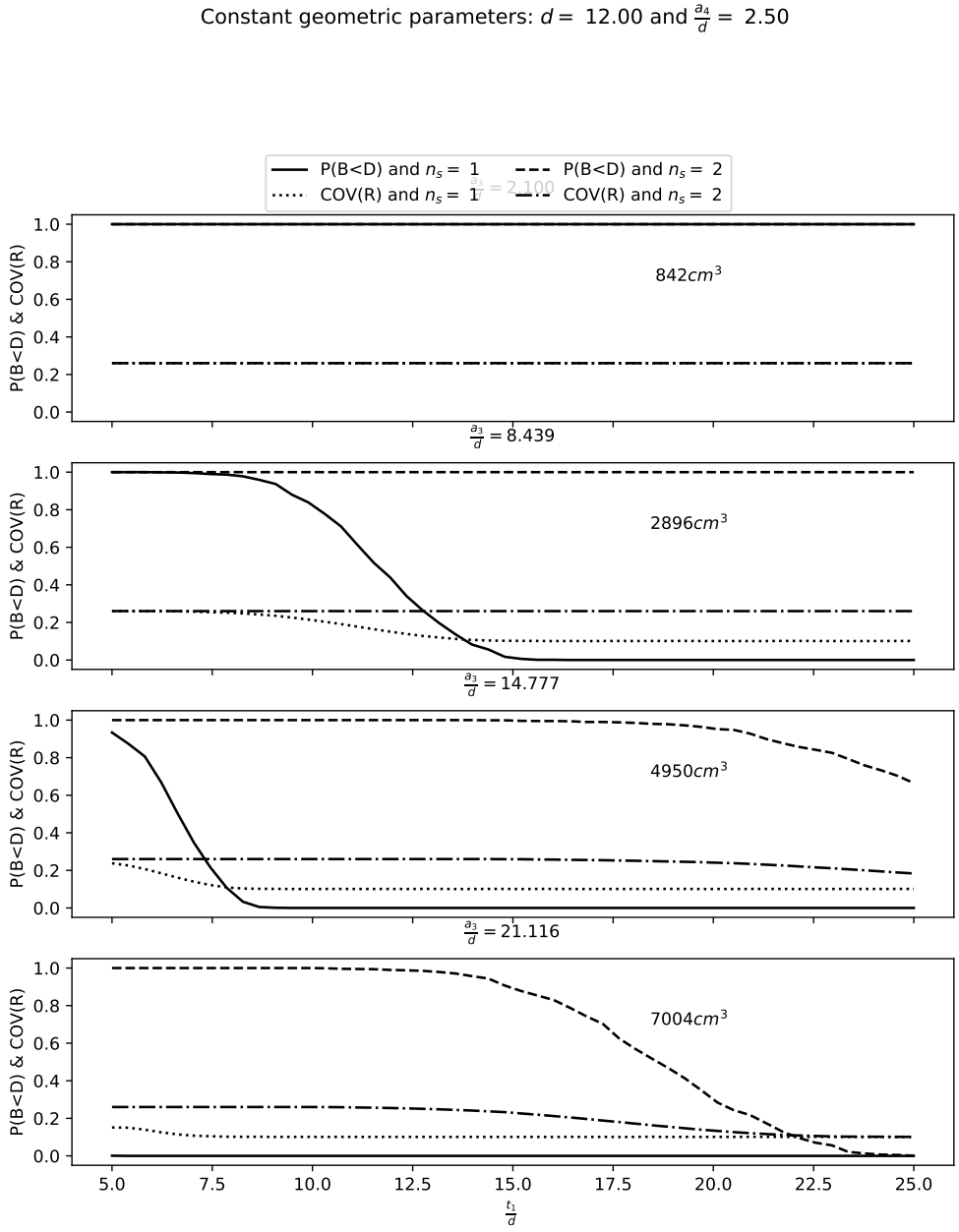

Figure 5.8: P(B<D) as a function of $\frac{t_{1,3}}{d}$ without the size effect on $f_{t,90}$ for 4 different values of $\frac{a_3}{d}$.

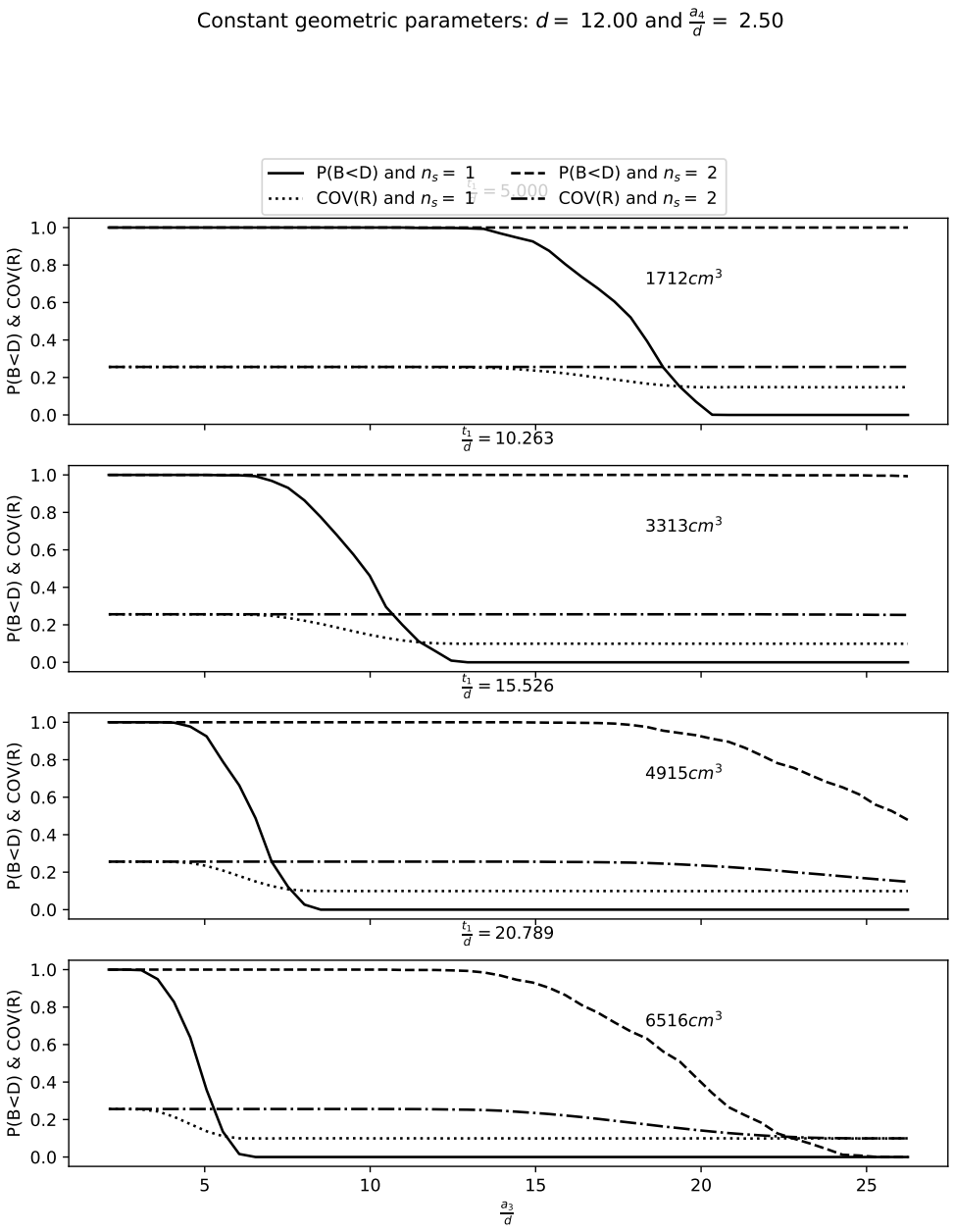

Figure 5.9: P(B<D) as a function of $\frac{a_3}{d}$ without the size effect on $f_{t,90}$ for 4 different values of $\frac{t_{1,3}}{d}$.

$a_3 \geq \min(7d, 80mm)$ in [4, EC5] would be significantly too small and brittle failure of these connections still occurs for larger timber thickness (figure 5.9). On the other hand when the $\frac{a_3}{d} \gtrapprox 21mm$ regardless of the timber member thickness the probability of brittle failure drops to 0%. Thus, for the range of end-spacing, $2.1mm \lessapprox \frac{a_3}{d} \gtrapprox 21mm$, and timber member thickness is approximately less than $21mm$, a significant probability of brittle failure occurring would not be prevented using existing minimum end-spacing requirements. These ranges of end-spacing, a_3, and timber thickness, $t_{1,3}$, parameters are used further in the next section 5.2.2.

Furthermore, the failure model described in section 4 also includes a size effect component. The size effect phenomenon is taken into account by modifying the mean tensile strength perpendicular-to-grain of wood. However, the single fastener TST connections described within this section are not in general large enough for the size effect to influence the failure capacity as can be seen in figures 5.8 and 5.9 by the volumes printed on each subplot. The largest volumes these single fastener connections reach is approximately $0.00075m^3$ (as seen in the bottom subplot of figures 5.8 and 5.9) which is significantly smaller than the reference volume used in the analysis of $0.01m^3$ and no significant decrease in the $f_{t,90}$ strength is observed. Therefore, no size effect on single fastener TST connection is observed.

Considering the possibility of brittle failure, the question then becomes does the variability of the failure capacity when governed by brittle or ductile modes change. The variability of the failure capacity does differ between brittle and ductile modes such that brittle failure modes correspond to a mean coefficient of variation, COV, of approximately 25% while ductile failure modes correspond only to a COV of approximately 10%. These values of the COV may be estimated from figures 5.8 and 5.9 as the parameters $\frac{t_{1,3}}{d}$ and $\frac{a_3}{d}$ vary while the other parameter is held constant, respectively. Both figures 5.8 and 5.9 show a trend for intermediate ranges of $\frac{t_{1,3}}{d}$ and $\frac{a_3}{d}$, the COV is between the value associated with brittle and the value associated with ductile failure. The consequence being that there is a range where either brittle or ductile failure is close to equally probable; however, the previous two figures 5.8 and 5.9 can only demonstrate the variability per TST connection at a mean level. That is to say that the COV and probability, $P(B < D)$, are computed per TST connection on the aggregate statistics of the result of 1000 simulations of the failure model to calculate the capacity using material properties defined as random variables.

To accurately capture and discuss the consequences of the variation in COV for TST connections of varied geometric parameters, the distribution of the failure capacity of representative TST connections are considered. The distribution of the failure capacity of 15 TST connections are presented in figures 5.10, 5.11, and 5.12. These 15 representative TST connections are uniquely determined by a fastener diameter of $8mm$, $12mm$, and $16mm$ with a end-spacing, $\frac{a_3}{d} = 10mm$, and perpendicular-to-grain end-spacing, $\frac{a_4}{d} = 2.5mm$ while the timber member thickness varies. The leftmost subplot in each of the three figures 5.10, 5.11, and 5.12 represents only brittle failure while the two rightmost subplot in each figure represent only ductile failure. The meaning of only brittle or ductile failure then corresponds to where the probability of failure is either 100% or 0%, respectively, in figure 3.2.2.

The distribution of the failure capacity, when either brittle or ductile failure modes are completely probable at the expense of the other, appears to follow either a lognormal or normal distribution, respectively. Most interesting, though, is the resulting failure capacity distribution for intermediate values of $\frac{t_{1,3}}{d}$ which is considerably non-parametric as shown in figures 5.10, 5.11, and 5.12 for $\frac{t_{1,3}}{d} = 7.74$ or $\frac{t_{1,3}}{d} = 10.47$. For the three fastener diameters, d, specified in each of the three figures, the distribution of the failure capacity approaches a normal distribution for the larger $\frac{t_{1,3}}{d} = 10.47$ as the d increases suggesting that ductile failure is more likely.

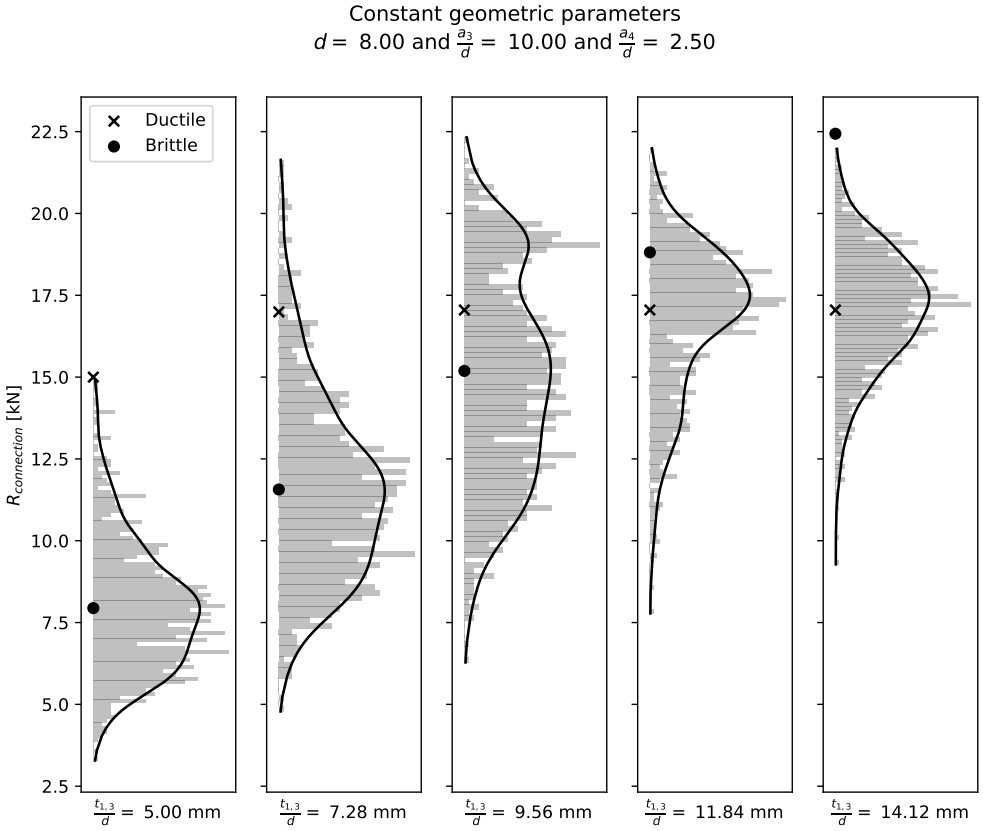

Figure 5.10: Variability of the failure capacity for a single fastener TST connection while varying $t_{1,3}$ with $d = 8mm$, $\frac{a_3}{d} = 10mm$, and $\frac{a_4}{d} = 2.5mm$. "x" denotes the mean ductile failure capacity; "o" denotes mean brittle failure capacity.

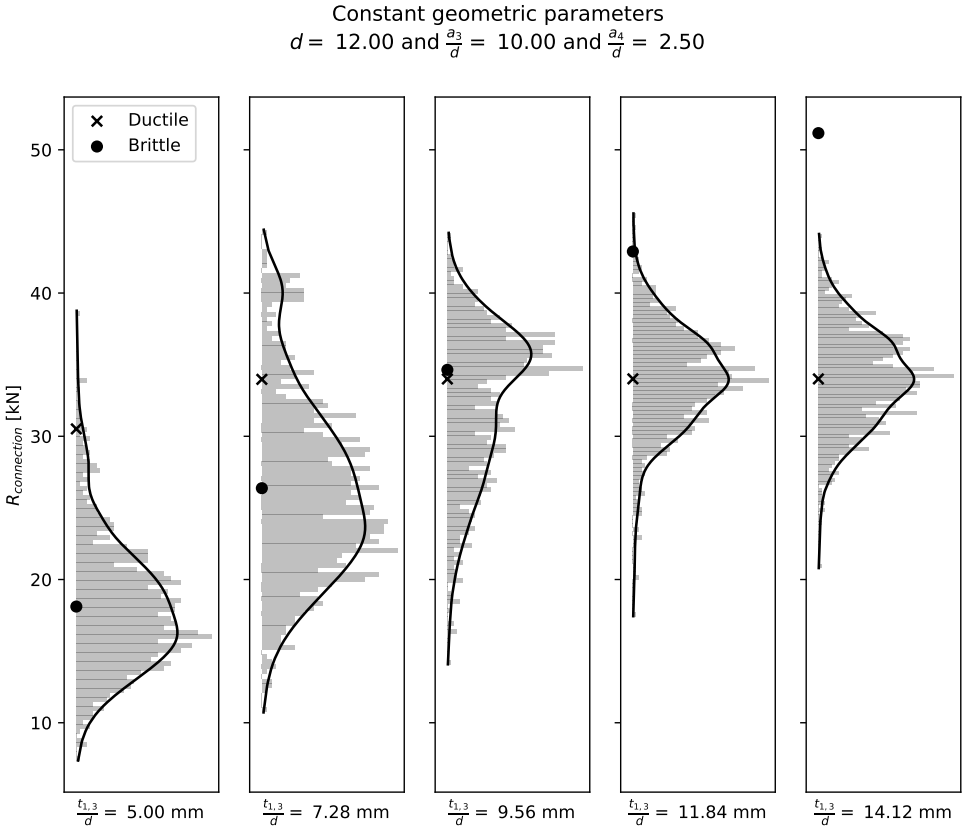

Figure 5.11: Variability of the failure capacity for a single fastener TST connection while varying $t_{1,3}$ with $d = 12mm$, $\frac{a_3}{d} = 10mm$, and $\frac{a_4}{d} = 2.5mm$. "x" denotes the mean ductile failure capacity; "o" denotes mean brittle failure capacity.

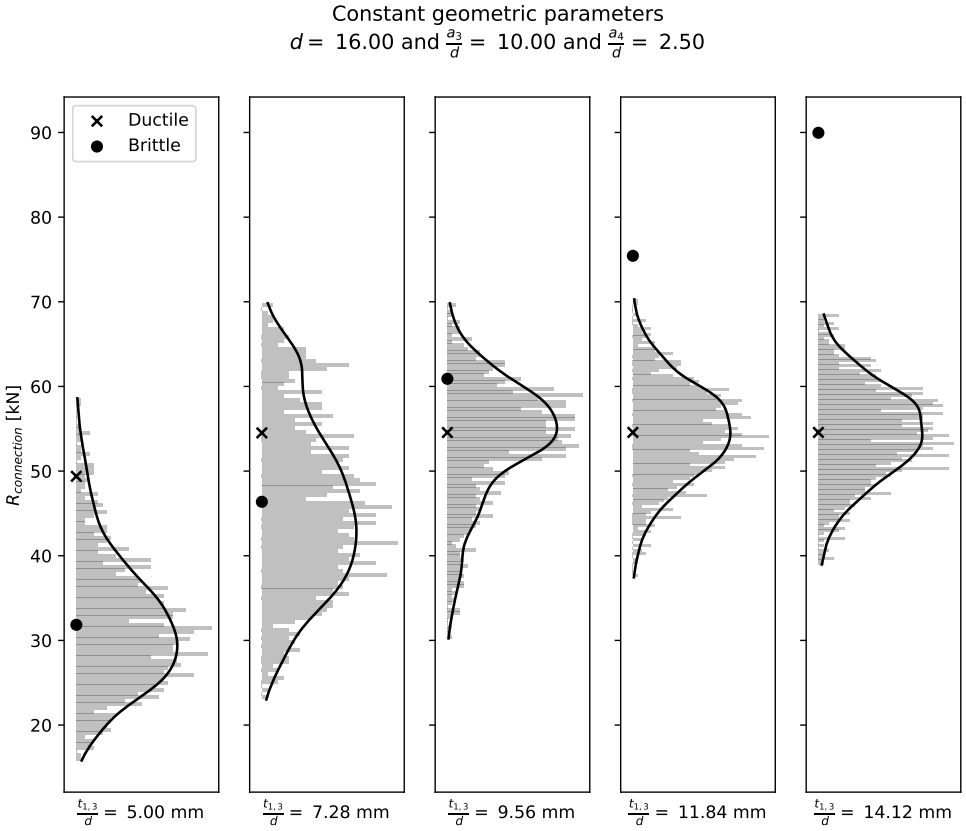

Figure 5.12: Variability of the failure capacity for a single fastener TST connection while varying $t_{1,3}$ with $d = 16mm$, $\frac{a_3}{d} = 10mm$, and $\frac{a_4}{d} = 2.5mm$. "x" denotes the mean ductile failure capacity; "o" denotes mean brittle failure capacity.

The smaller $\frac{t_{1,3}}{d} = 7.74$ subplot in each of the three figures 5.10, 5.11, and 5.12 tends towards a bimodal distribution with equal likelihood of brittle and ductile failure to occur.

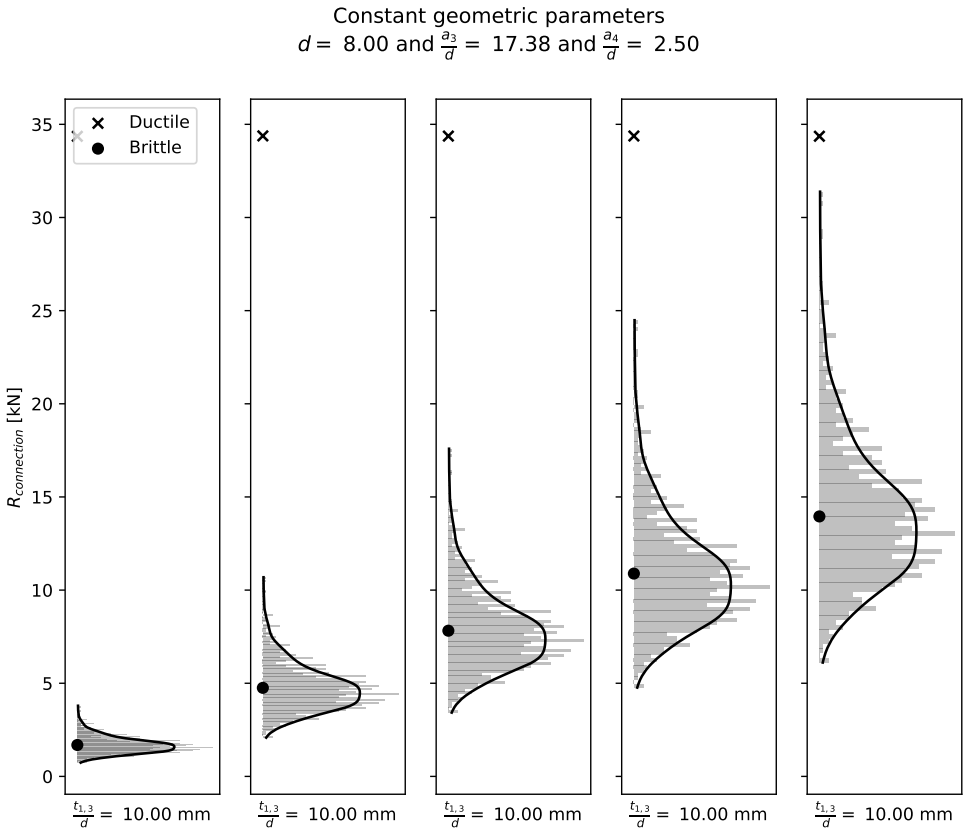

Figure 5.13: Variability of the failure capacity for a single fastener TST connection while varying a_3 with $d = 8mm$, $\frac{t_1}{d} = 10mm$, and $\frac{a_4}{d} = 2.5$. "x" denotes the mean ductile failure capacity; "o" denotes mean brittle failure capacity.

Similarly to the figures 5.10 to 5.12 displaying the failure capacity distributions due to material variability as a function of varying the timber thickness, $\frac{t_{1,3}}{d}$, the figures 5.13 to 5.15 describe very similar distributions and similar conclusions can be inferred. Just as when $\frac{t_{1,3}}{d}$ is varied, varying $\frac{a_3}{d}$ results in small end-spacing values generating lognormal distributions representing brittle failure (leftmost subplot) while large end-spacing values generate distributions which appear to exhibit normally distributed properties (two rightmost subplots). It should be noted that larger values to $\frac{a_3}{d}$ would likely appear more and more normally distributed; however, the trend towards normality still appears in figures 5.13 to 5.15 despite the second to rightmost subplot appearing more log-normally distributed than normally distributed.

Considering the mid-range values of $\frac{a_3}{d}$ as 5.92 and 9.74 (subplots second and third from the left) over all three figures 5.13 to 5.15 as a series similar to the subplots discussed in the preceding paragraphs when $\frac{t_{1,3}}{d}$ was varied, the bimodal distribution appears for a fastener diameter, $d = 8mm$, but with a larger $\frac{a_3}{d} = 9.74$. In the preceding discussion on the effect of varying $\frac{t_{1,3}}{d}$, the bimodal distribution appeared in contrast for a fastener diameter of $d = 16mm$ but for the smaller $\frac{t_{1,3}}{d} = 7.74$.

In other words, the transition from lognormal brittle failure distribution to normal ductile failure distribution passes through a bimodal distribution at some intermediate values of d, $\frac{t_{1,3}}{d}$, and

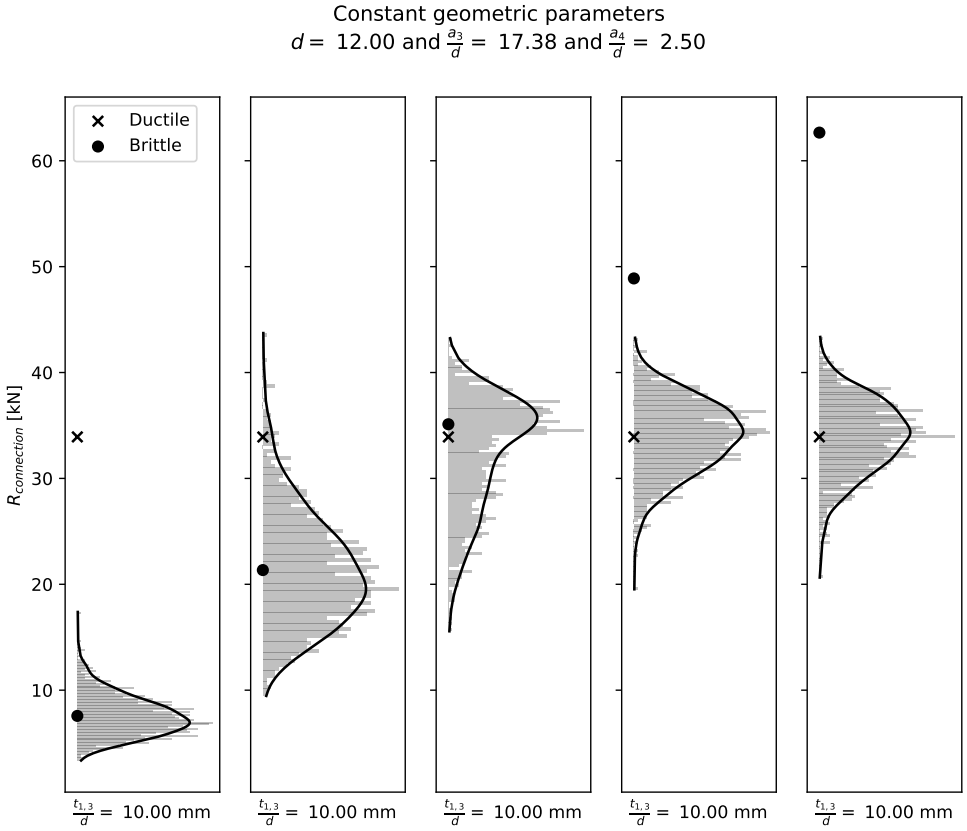

Figure 5.14: Variability of the failure capacity for a single fastener TST connection while varying a_3 with $d = 12mm$, $\frac{t_1}{d} = 10$, and $\frac{a_4}{d} = 2.5$. "x" denotes the mean ductile failure capacity; "o" denotes mean brittle failure capacity.

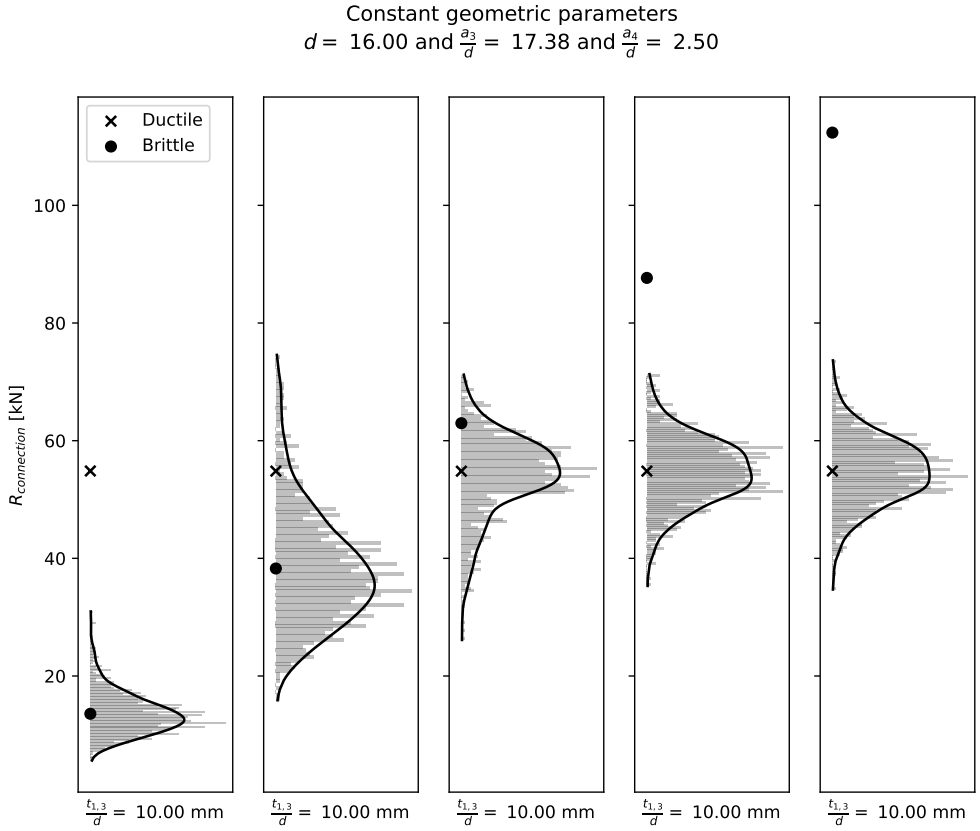

Figure 5.15: Variability of the failure capacity for a single fastener TST connection while varying a_3 with $d = 16mm$, $\frac{t_1}{d} = 10$, and $\frac{a_4}{d} = 2.5$. "x" denotes the mean ductile failure capacity; "o" denotes mean brittle failure capacity.

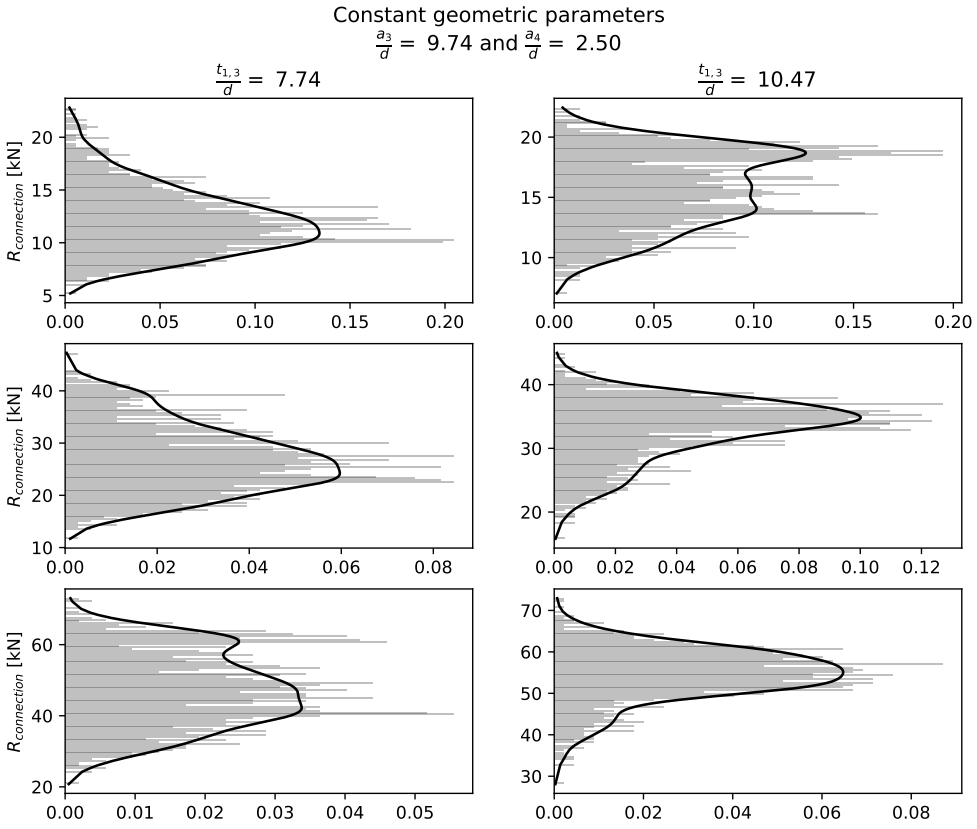

Figure 5.16: Transition of failure capacity distribution from a pure brittle to a pure ductile failure mode for intermediate values of the geometric parameters $\frac{t_{1,3}}{d}$ and $\frac{a_3}{d}$.

$\frac{a_3}{d}$ as depicted in figure 5.16 for example. Furthermore, keeping either $7.74mm \leq \frac{t_{1,3}}{d} \leq 10.47$ or $5.92 \leq \frac{a_3}{d} \leq 9.74$ constant within these intermediate ranges and increasing d if starting from a pure brittle failure or decreasing the d if starting from a pure ductile failure can be a proxy for increasing either $\frac{t_{1,3}}{d}$ or $\frac{a_3}{d}$ itself.

A consequence of this variation in failure capacity due to both variation in geometric parameters and natural material variation is first that the coefficient of variation of brittle failure modes is significantly higher than ductile failure modes. Additionally, the size effect phenomenon is not present for the single fastener TST connections studied in this thesis since the volume of these connections is sufficiently close to the reference volume of $0.01m^3$ defined by the Probabilistic Model Code [48]. Secondly, including both variation in geometric parameters and the natural material variation of wood suggests that their exist certain ranges of normalized timber member thickness, $\frac{t_{1,3}}{d}$ and normalized end-spacing, $\frac{a_3}{d}$, where brittle and ductile failure are both probable failure modes to occur resulting in a complex non-parametric/bimodal failure capacity distribution.

5.2.2 Multiple fastener connections

For multiple fastener connections, a parametric study is also performed to provide further understanding of the relationship between brittle and ductile failure modes as well as how the coefficient of variation is affected. As described in section 4.1, the multiple fastener connections which are considered consist of TST connections with either 1 or 5 fastener rows and 2 or 4 fasteners within a row of fasteners. Additionally, 1 or 2 internal steel plate TST connections are considered. To begin only a single internal steel plate is considered with multiple fasteners.

The effect of adding fasteners to a row of fasteners is shown in figures 5.17 and 5.18 for a single internal steel plate TST connection. As with the single fastener TST connections, connections with a end-spacing, $\frac{a_3}{d}$, less than 2.1 exhibit largely brittle failure regardless of the fastener spacing, $\frac{a_1}{d}$, or the number of fasteners, $n_c \times n_r$. For small $\frac{a_3}{d} \leq 2.1$ values, small $\frac{a_1}{d}$ values, and few fasteners in a row, n_c, the probability of brittle failure does become less than 100% but only for large $\frac{t_{1,3}}{d}$. Overall, the trend with increasing end-spacing, $\frac{a_3}{d}$, for a given number of fasteners within a row, n_c, follows the same trend as single fastener connections (previous section 5.2.1) while increasing the number of fasteners, n_c, per fastener row only extends the region where the probability of brittle failure governs to larger timber thicknesses, $\frac{t_{1,3}}{d}$, by comparing figures 5.17 and 5.18.

The volumes presented on each subplot refer to the mean connection volume of all the TST connections used to generate each subplot since the timber member thickness, $t_{1,3}$ is varied. Figure 5.17 includes volumes which are sufficiently close to the reference volume suggested by the Probabilistic Model Code [48] that no significant difference between the including the size effect phenomenon and not including it is observed. However, beginning already with figure 5.18 some differences between the model including the size effect and the model disregarding the size effect can be observed. As well, only connections with geometric properties that result in the splitting failure mechanism to govern the capacity will the size effect be explicitly observed in the figures within this section. That means that for subplots of figure 5.18 where the black and dark gray lines diverge, the size effect is present which also means that those TST connections will have a higher likelihood of splitting failure behaviour as computed by the failure model described in section 4.3.

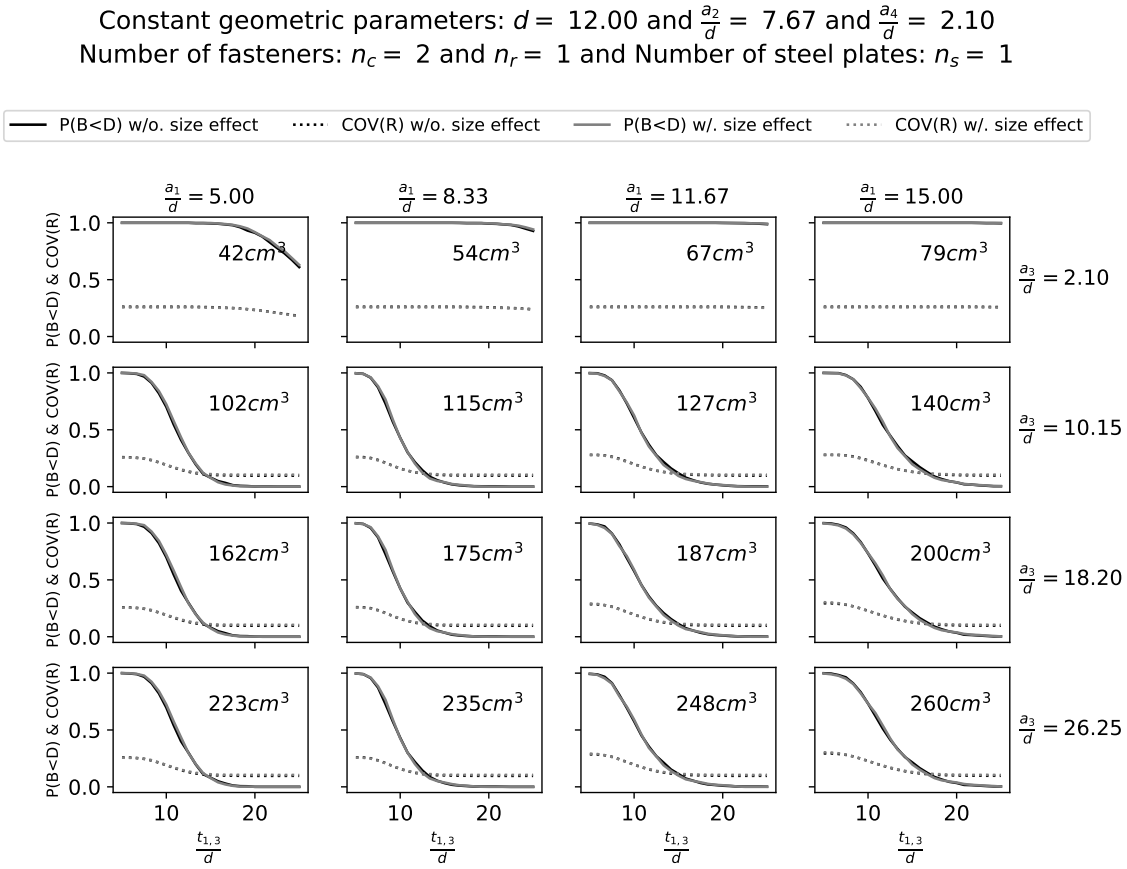

Figure 5.17: P(B<D) and COV(R) as a function of $\frac{t_{1,3}}{d}$ while fastener spacing $\frac{a_1}{d}$ and fastener end-spacing $\frac{a_3}{d}$ are discretely varied for $n_c = 2$, $n_r = 1$, and $n_s = 1$. Size effect is included.

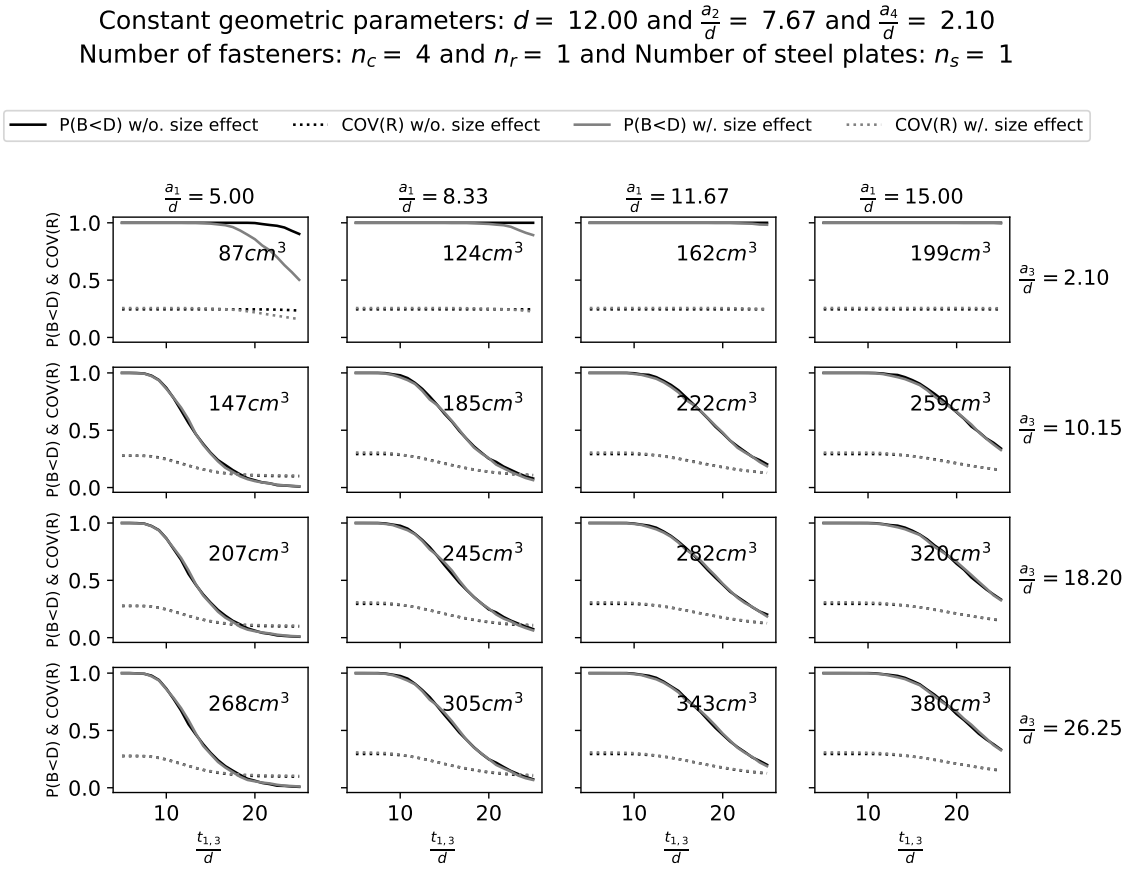

Figure 5.18: P(B<D) and COV(R) as a function of $\frac{t_{1,3}}{d}$ while fastener spacing $\frac{a_1}{d}$ and fastener end-spacing $\frac{a_3}{d}$ are discretely varied for $n_c = 4$, $n_r = 1$, and $n_s = 1$. Size effect is included.

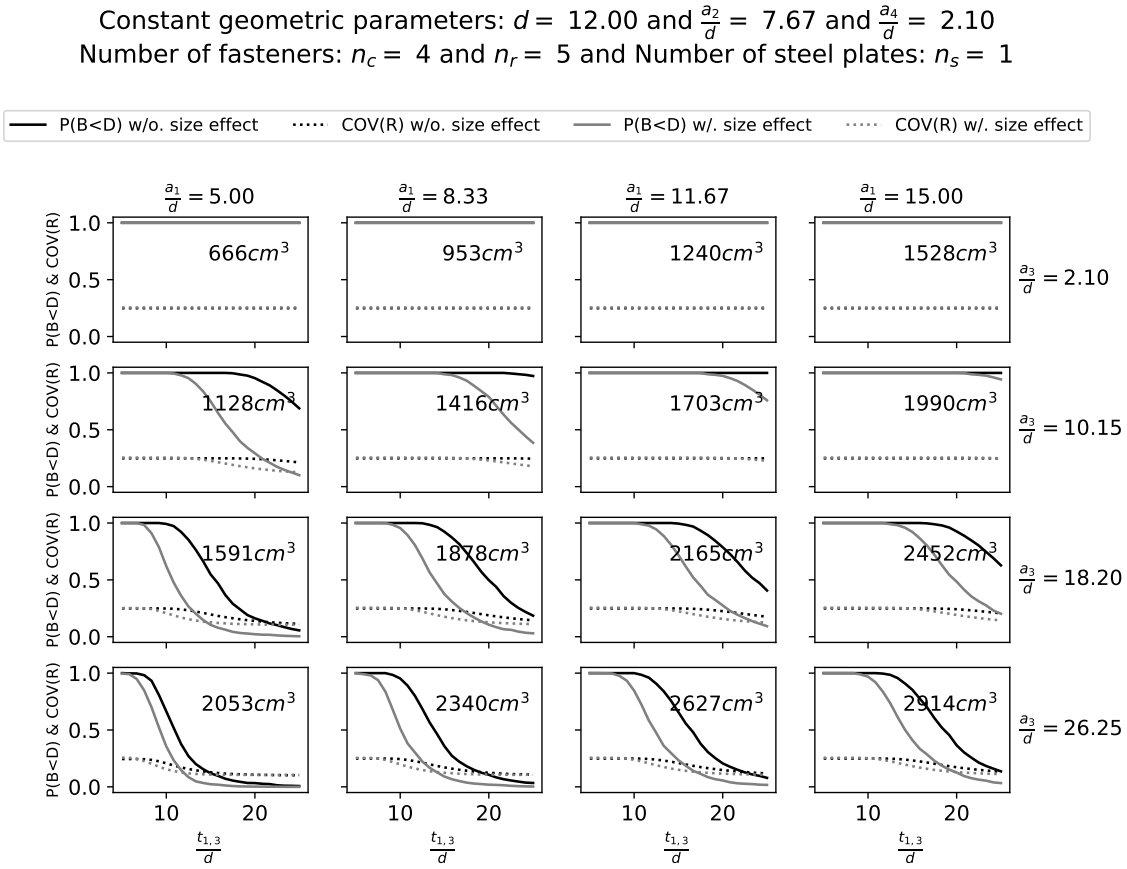

Figure 5.19: P(B<D) and COV(R) as a function of $\frac{t_{1,3}}{d}$ while fastener spacing $\frac{a_1}{d}$ and fastener end-spacing $\frac{a_3}{d}$ are discretely varied for $n_c = 4$, $n_r = 5$, and $n_s = 1$. Size effect is included.

The second effect tested by the parametric analysis of multiple fastener, single internal steel plate TST connections is the effect of adding additional rows of fasteners. Figures 5.18 and 5.19 show the result of connections with 1 and 5 rows of fasteners as $\frac{t_{1,3}}{d}$ continuously varies while $\frac{a_1}{d}$ and $\frac{a_3}{d}$ discretely vary among subplots. The trends described above for both single fastener TST connections and multiple fasteners within a single row TST connections with respect to variation with geometric properties are similar. By adding additional rows of fasteners, the volume of the connection increases at a faster rate than simply adding to the number of fasteners in one row which causes the size effect to significantly affect the failure capacity for larger $\frac{t_{1,3}}{d}$ as the splitting failure mechanism model used in this thesis is directly proportional to the tensile strength perpendicular-to-grain, $f_{t,90}$. The reduction in the $f_{t,90}$ strength due to increasing volume of multiple fastener row TST connections is counteracted by increasing the timber member thickness as shown in figure 5.19 to actually minimize the probability of brittle failure for thicker timber members, $t_{1,3}$ when the size effect is taken into consideration. More important than the size effect in all TST connections including the multiple fastener row connections are the geometric spacing between fasteners on the risk of brittle failure. However, the size effect should still be included in a complete design model to recognize that thicker timber members for multiple fastener row TST connections are governed by ductile failure behaviour typically desired in design.

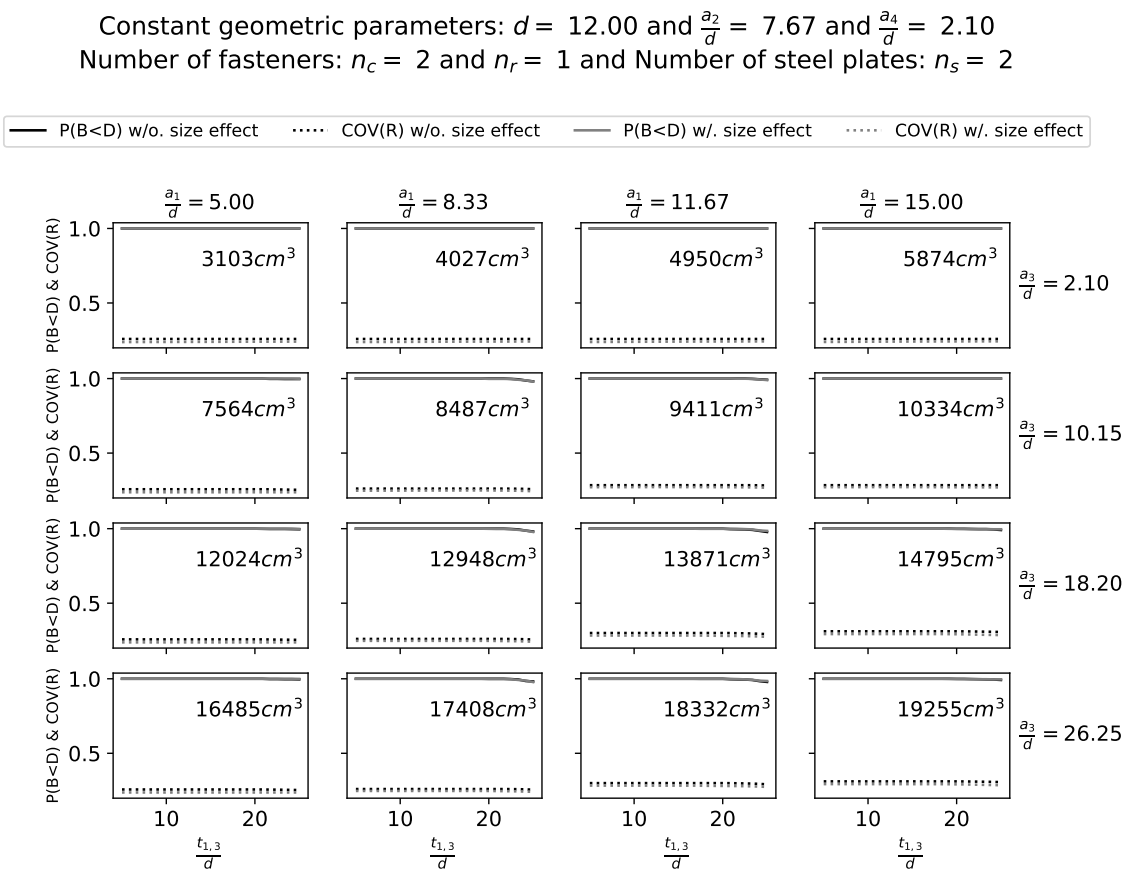

Figure 5.20: P(B<D) and COV(R) as a function of $\frac{t_{1,3}}{d}$ while fastener spacing $\frac{a_1}{d}$ and fastener end-spacing $\frac{a_3}{d}$ are discretely varied for $n_c = 2$, $n_r = 1$, and $n_s = 2$. Size effect is included.

Additional, impact of adding internal steel plates is also considered; however, for the same variation of timber thickness, $\frac{t_{1,3}}{d}$, from 5 to 25 these larger connections predict only brittle failure to occur regardless of the fastener spacing, a_1, and end-spacing, a_3, as evident in figure 5.20. This suggests that multiple internal steel plate TST connections are not suitable for evaluation

using the failure model described by this thesis due to their larger connection volumes. For that reason figures displaying the results of multiple internal steel plate TST connections are not included in this thesis. The methodology of the crude Monte Carlo simulation of the failure capacity of TST connections can be used in further research with a improved failure model to better represent multiple internal steel plate connections.

6

Conclusion

The aim of this thesis was to provide a analysis of the design of high capacity mass timber dowel-type connections with internal steel plates which are useful connection techniques in tall timber structures such as the Mjøsa Tower. A thorough review of the existing design methodology of dowel-type timber connections is presented in chapter 2 while the literature is reviewed for design models to explicitly account for brittle failure mechanisms in chapter 3. A failure model is presented within a probabilistic framework in chapter 4 to evaluate the differences in failure capacity between brittle and ductile failure modes. A heavy emphasis is placed on the methodology of the failure model evaluation rather than emphasizing the form of the failure model itself because the current state-of-the-art understanding of especially brittle failure mechanisms in the literature is not yet conclusive of brittle structural behaviour of timber dowel-type connections. Thus, the emphasis on considering both variation in geometric parameters and natural material variability within the proposed modelling methodology is used to describe a approach to allow for brittle failure models to be reliably and robustly integrated into existing ductile failure models in existing design standards (e.g. [3, CSA O86-14] [4, EC5] [5, NDS 2012]). The main two specific areas of focus of this thesis are the comparison of embedment strength, f_h, models and the relationship between brittle failure and ductile failure of TST connections largely using the probability of brittle failure less than ductile failure, $P(B < D)$.

6.1 Comparison of embedment strength models

$$f_h = A\rho^B d^C \tag{6.1}$$

Firstly, four models to calculate the embedment strength, f_h, of timber are compared. It is concluded that the form of the embedment strength equation which best represents the material property is described by equation 6.1 first presented in the literature by [42, Leijten et al.]. By this conclusion, it is shown that the embedment strength, f_h, is not sufficiently described as a function of linear predictors of timber density, ρ, and fastener diameter, d. As described by equation 6.1, the embedment strength, f_h, requires non-linear predictors to accurately express the embedment behavior of wood. As such, existing linear equations of f_h could potentially predict unreliable and unsafe values when used in design.

In timber connections, a significant challenge in developing a accurate model to represent the embedment strength of wood is a consequence of a non-linear relationship between the embedment behaviour of wood, the fastener diameter, and the wood grain orientation. In

particular, as the wood grain orientation approaches perpendicular-to-grain loading of fastener-type connections, they show a hardening effect dependent on fastener diameter, d. When considering the definition of the yield point using the two most common test methodologies (e.g. [46, 47, EN 383]) of the embedment strength, f_h, further complexity is added. The former approach captures the hardening effect by considering the embedment strength, f_h, as a ultimate strength while the latter approach does not rather considering the embedment strength, f_h, as a yield strength. Both approaches have their advantages and disadvantages; however as shown in this thesis, a design approach which considers both the yield strength and ultimate strength is essential to address explicit inclusion of brittle failure modes in a holistic design methodology of fastener-type timber connections.

A second challenge for the best fit model in equation 6.1 resulting from the comparison study in section 5.1 is the ability of the model to generalize to any domain of the input parameters for use with the wide and diverse range of timber materials (e.g. structural timber, engineered wood products, etc.) and fasteners which are commonly used. The model parameters are dependent on the specific type of timber material making it challenging to construct a model well suited for design. It is important to note that the description of the hardening effect of perpendicular-to-grain loading situations on the embedment behaviour of wood shows that care must be taken to define models according to equation 6.1 for both parallel- and perpendicular-to-grain loading conditions. This should not inadvertently cause inconsistencies for any off-axis embedment strengths through the use of the widely used Hankinson's formula (equation 1.1) in design (e.g. [3, CSA O86-14] [4, EC5] [5, NDS 2012]).

Given correctly calibrated model parameters, overall the best model is equation6.1 which is generally both accurate and reliable regardless of the experimental test method. For the wide scale use of this model in timber connection design, more research and calibration of the model parameters for parallel- and perpendicular-to-grain loading conditions is required or only limited range of values of the timber density, ρ, and fastener diameter, d, are applicable.

6.2 Parametric study of a complete failure model

A complete failure model is parametrically evaluated consisting of explicit failure mechanism models encompassing both ductile and brittle failure modes. Ductile failure modes are represented using the EYM derived especially for TST connections while the brittle failure mechanism models are chosen from a review of the literature. This thesis limits itself to identifying the trends with respect to the impact of varying geometric parameters on the connection failure capacity computed using crude Monte Carlo simulation of the material properties. No attempt is made to evaluate the accuracy of the failure mechanism models used. The thorough literature review is used as a basis to choose appropriate, accurate, and relevant models to TST connections for each brittle failure mechanism possible.

Evaluating the qualitative relationship between ductile and brittle failure modes is divided into two distinct groups: single fastener and multiple fastener TST connections. From the evaluation of single fastener TST connections, the inference that can be made is that current minimum end-spacing, a_3, requirements in design standards (e.g. [3, CSA O86-14] [4, EC5] [5, NDS 2012]) are too small to adequately prevent brittle failure at unexpected load levels to occur when explicit models are used to calculate brittle failure capacities. The high prevalence of connection related brittle failures in timber structures and lack of awareness of the issue of

brittle failure reported in the literature [7, 8, 9, 10] is a justifiable concern as this thesis has shown that minimum spacing values currently prescribed do not prevent all brittle failures from occurring.

This thesis has found that a fastener diameter normalized end-spacing, $\frac{a_3}{d}$, less than 2.1 always results in a probability of brittle failure of 100% while $\frac{a_3}{d}$ greater than 21.2 always results in a probability of brittle failure of 100% regardless of the timber member thickness. Within this range, $2.1 \leq \frac{a_3}{d} \leq 21.2$, the probability of brittle failure is dependent on the timber member thickness, $t_{1,3}$. A similar trend is observed by reversing the roles of a_3 and $t_{1,3}$ where within the range of $5 < \frac{t_{1,3}}{d} < 20.8$ the probability of brittle failure is dependent on the end-spacing, a_3. These ranges of timber member thickness, $t_{1,3}$, and end-spacing, a_3, are similar to those used in high capacity TST connections such as those designed for the Mjøsa Tower. The concern is that traditional design methods overlook brittle failure modes which exist with a significant probability of occurring. This is further observed by the change in the coefficient of variation of ductile versus brittle failure modes from approximately 10% to 25%. The coefficient of variation is derived based on the governing failure capacity of each TST connection given the Monte Carlo simulation of material properties. The transition state between ductile and brittle failure mode defined by this distribution of the failure capacities of each TST connection follows a bimodal distribution where each peak corresponds to ductile and brittle failure. Thus, the TST connections with geometric parameters within this transition state are equally likely to fail in a ductile as a brittle manner.

A relatively simple addition to existing design methodologies to better account for the risk of brittle failure is to calibrate partial safety factors with respect to the degree to which brittle failure is expected disregarding the complex transition state between the ductile and brittle failure. For connections where a large risk of brittle failure is expected, the partial safety factor used could be defined on the basis of a COV of 25% while in the case of low brittle failure risk the partial safety factor would be defined on the basis of ductile failure equal to a COV of 10%. For example, in EC5 [4] that is to say the partial safety factor used would be tied to the n_{ef} parameter—implicit recognition of the risk of brittle failure—where should n_{ef} is less than a certain value the partial safety factor would be increased to further reduce the load-carrying capacity. It is, however, preferred to consider brittle failure modes explicitly in which case the partial safety factor can be more explicitly related to the risk of brittle failure especially within the transition state where both ductile and brittle failure modes are possible as the result failure capacity distribution is decidedly more complex. Furthermore, this proposed modification would have to undergo further research with regard to its suitability and feasibility.

Multiple fastener TST connections are also evaluated with respect to the relationship between the probability of either ductile or brittle failure including the variability of the governing failure capacity and the variation of the geometric parameters. Similar trends for the timber member thickness, $t_{1,3}$, and end-spacing, a_3, are observed while the additional parameter of the fastener spacing parallel-to-grain is now also varied. It is interesting to note that for a given normalized fastener spacing, $\frac{a_1}{d}$, the probability of brittle failure decreases with both increasing timber member thicknesses, t_1, and end-spacing, a_3. However, as $\frac{a_1}{d}$ increases, the probability of brittle failure first decreases before increases as the parameter a_1 increases regardless of a_3 meaning that in practical design it is of interest to increase the fastener end-spacing, a_3, while a optimum fastener spacing, a_1, is chosen to minimize the risk of brittle failure for larger timber member thicknesses, $t_{1,3}$. Fastener spacing in this optimum range of $8.33 < \frac{a_1}{d} < 11.67$ with a end-spacing, $\frac{a_3}{d}$, say greater than 26.25 would allow for the probability of brittle failure to be less than approximately 10% when normalized timber member thicknesses, $\frac{t_{1,3}}{d}$, of greater than 12 are used. It was also observed that increasing the number of fasteners in a row only serves

to increase the probability of brittle failure to larger timber member thicknesses, $t_{1,3}$, while increasing the number of fastener rows effects mostly the volume of the connection which then disproportionately increases the probability of brittle failure due to the size effect phenomenon taking force.

The size effect is shown to only affect the TST connections at significant higher connection volumes whereby the effect of reducing the tensile perpendicular-to-grain strength, $f_{t,90}$, dominates any other effect that may be a result of the impact of varying the geometric parameters. Large, high capacity connections with a high number of fastener rows actually decreases the likelihood of unexpected brittle splitting failure considerably especially if existing rules on minimum spacings are followed. These high capacity connections require explicit formulation of brittle failure mechanisms in a design model to minimize the risk of brittle failure including accounting for the reduction in tensile perpendicular-to-grain strength, $f_{t,90}$, due to their large volume of stressed timber. More advanced complete failure models are required to provide conclusions on the impact of varying geometric parameters or impact of the size effect when multiple internal steel plate connections are considered. Despite the relative simplicity of the failure model used in this thesis, the methodology of a crude Monte Carlo simulation presented provides a foundation on which to base further research and calibration efforts to modify existing design methods to include explicit brittle failure models while ensuring a required level of reliability.

Bibliography

[1] A.J.M. Jorissen and M. Fragiacomo. General notes on ductility in timber structures. *Engineering Structures*, 33(11):2987–2997, Nov 2011.

[2] J.M. Cabrero, D. Honfi, R. Jockwer, and Miguel Yurrita. A probabilistic study of brittle failure in dowel-type timber connections with steel plates loaded parallel to the grain. *Wood Material Science & Engineering*, page 1–14, Jul 2019.

[3] CSA O86. Engineering design in wood. Standard, Canadian Standards Association, Mississauga, ON, Canada, 2014.

[4] EN 1995-1-1:2004. Eurocode 5: Design of timber structures - part 1-1: General - common rules and rules for buildings. Standard, European Committee for Standardization, Brussels, BE, 2004.

[5] NDS. National design specification for wood construction. Standard, American Wood Counci, Mississauga, ON, Canada, 2012.

[6] J.M. Cabrero and M. Yurrita. Performance assessment of existing models to predict brittle failure modes of steel-to-timber connections loaded parallel-to-grain with dowel-type fasteners. *Engineering Structures*, 171:895–910, Sep 2018.

[7] S. Thelandersson and E. Frühwald. Design of safe timber structures – how can we learn from structural failures? In *40th Proceedings of the CIB-W18 Meeting, Paper 40-15-1, Bled, Slovenia*, 2007.

[8] E. Frühwald Hansson. Analysis of structural failures in timber structures: Typical causes for failure and failure modes. *Engineering Structures*, 33(11):2978–2982, Nov 2011.

[9] C. Sandhaas, J. Munch-Andersen, and P. Dietsch. *Design of connections in timber structures: a state-of-the-art report by COST Action FP1402/WG3.* 2018.

[10] M. Stepinac, J.M. Cabrero, K. Ranasinghe, and M. Kleiber. Proposal for reorganization of the connections chapter of eurocode 5. *Engineering Structures*, 170:135–145, Sep 2018.

[11] H. Liven. Personal communication, Jan 2020.

[12] A.J.M. Jorissen. *Double shear timber connections with dowel type fasteners.* PhD thesis, TU Delft, 1998.

[13] J.H.P. Quenneville and M. Mohammad. On the failure modes and strength of steel-wood-steel bolted timber connections loaded parallel-to-grain. *Canadian Journal of Civil Engi-*

neering, 27(4):761–773, Aug 2000.

[14] A. Hanhijärvi and A. Kevarinmäki. Timber failure mechanisms in high capacity dowelled connections of timber to steel. 2008.

[15] P. Zarnani and P. Quenneville. Wood block tear-out resistance and failure modes of timber rivet connections: A stiffness-based approach. *Journal of Structural Engineering*, 140(2):04013055, Feb 2014.

[16] K.W. Johansen. Theory of timber connections. *International Association for Bridge and Structural Engineering*, 9:249–262, 1949.

[17] G.W. Trayer. The bearing strength of wood under bolts. Technical report, United States Department of Agriculture, 1932.

[18] L.A. Soltis, F.K. Hubbard, and T.L. Wilkinson. Bearing strength of bolted timber joints. *Journal of Structural Engineering*, 112(9):2141–2154, Sep 1986.

[19] A. Meyer. Die tragfähigkeit von nagelverbindungen bei statischer belastung. *Holz als Roh- und Werkstoff*, 15(2):96–109, Feb 1957.

[20] J. Köhler. A probabilistic framework for the reliability assessment of connections with dowel type fasteners. In *38th Proceedings of the CIB-W18 Meeting, Paper 38-7-2, Karlsruhe, Germany*, 2005.

[21] B.H. Xu, A. Bouchaïr, M. Taazount, and E.J. Vega. Numerical and experimental analyses of multiple-dowel steel-to-timber joints in tension perpendicular to grain. *Engineering Structures*, 31(10):2357–2367, Oct 2009.

[22] J.M. Cabrero and M. Yurrita. A review of the existing models for brittle failure in connections loaded parallel to the grain. Technical report.

[23] Swedish Wood. Design of timber structures: Structural aspects of timber construction. Last accessed Mon Jan 27 15:15:11 2020.

[24] H.J. Blaß and C. Sandhaas. *Ingenieurholzbau: Grundlagen der Bemessung*. KIT Scientific Publishing, 2016.

[25] S.T. Marcin. Load distribution in bolted joints, c.e. 103. In *Fritz Laboratory Reports, Paper 1729, Lehigh University*, 1960.

[26] C.O. Cramer. Load distribution in multiple-bolt tension joints. *Journal of the Structural Division*, 1968.

[27] G. Lantos. Load distribution in a row of fasteners subjected to lateral load. *Wood Science*, 1(3):129–136, 1969.

[28] T.L. Wilkinson. Load distribution among bolts parallel to load. *Journal of Structural Engineering*, 112(4):835–852, Apr 1986.

[29] H.J. Blass. Load distribution in nailed joints. In *23th Proceedings of the CIB-W18 Meeting, Paper 23-7-2, Lisbon, Portugal*, 1990.

[30] C.J. Mettem and A.V. Page. Load distributions in multiple-fastener bolted joints in european whitewood glulam, with steel side plates. In *25th Proceedings of the CIB-W18 Meeting, Paper 25-7-12, Ahus, Sweden*, 1992.

[31] A. Jorissen. Multiple fastener timber connections with dowel type fasteners. In *30th Proceedings of the CIB-W18 Meeting, Paper 30-7-5, Vancouver, Canada*, 1997.

[32] J. Sjödin and E. Serrano. A numerical study of methods to predict the capacity of multiple steel-timber dowel joints. *Holz als Roh- und Werkstoff*, 66(6):447–454, Aug 2008.

[33] J. Sjödin, E. Serrano, and B. Enquist. An experimental and numerical study of the effect of friction in single dowel joints. *Holz als Roh- und Werkstoff*, 66(5):363–372, Aug 2008.

[34] L. Damkilde P. Hoffmeyer M.U. Pedersen, C.O. Clorius and L. Esklidsen. Dowel type connections with slotted-in steel plates. In *32th Proceedings of the CIB-W18 Meeting, Paper 32-7-8, Graz, Austria*, 1999.

[35] J.L. Jensen and P. Quenneville. Experimental investigations on row shear and splitting in bolted connections. *Construction and Building Materials*, 25(5):2420–2425, May 2011.

[36] L.R.J. Whale and I. Smith. The derivation of design clauses for nailed and bolted joints ineurocode5. In *19th Proceedings of the CIB-W18 Meeting, Paper 19-7-6, Florence, Italy*, 1986.

[37] L.R.J. Whale, I. Smith, and H.J. Larsen. Design of nailed and bolted joints-proposals for the revision of existing formulae in draft eurocode 5 and the cib code. In *20th Proceedings of the CIB-W18 Meeting, Paper 20-7-1, Dublin, Ireland*, 1987.

[38] J. Ehlbeck and H. Werner. Design of joints with laterally loaded dowels. proposals for improving the design rules in the cib code and the draft eurocode 5. In *21th Proceedings of the CIB-W18 Meeting, Paper 21-7-4, Parksville, Canada*, 1988.

[39] T.L. Wilkinson. Dowel bearing strength. Technical report, US Department of Agriculture, Forest Service, Forest Products Laboratory, 1991.

[40] K. Sawata and M. Yasumura. Determination of embedding strength of wood for dowel-type fasteners. *Journal of Wood Science*, 48(2):138–146, Apr 2002.

[41] S. Kennedy, A. Salenikovich, W. Munoz, M. Mohammad, and D. Sattler. Design equations for embedment strength of wood for threaded fasteners in the canadian timber design code. In *World Conference on Timber Engineering*, 2014.

[42] A.J.M. Leijten, J. Köhler, and A. Jorissen. Review of probability data for timber connections with dowel-type fasteners. In *37th Proceedings of the CIB-W18 Meeting, Paper 37-7-12, Edinburgh, Scotland*, 2004.

[43] M. Havbro Faber, J. Köhler, and J. Dalsgaard Sorensen. Probabilistic modeling of graded timber material properties. *Structural Safety*, 26(3):295–309, Jul 2004.

[44] Canadian Wood Council. *Wood design manual*. Canadian Wood Council, 99 Bank Street, Suite 400, Ottawa Ontario, K1P 6B9.

[45] I. Smith, L.R.J. Whale, C. Anderson, B.O. Hilson, and P.D. Rodd. Design properties

of laterally loaded nailed or bolted wood joints. *Canadian Journal of Civil Engineering*, 15(4):633–643, Aug 1988.

[46] EN 383:2007. Timber structures - test methods - determination of embedding strength and foundation values for dowel type fasteners. Standard, European Committee for Standardisation, Brussels, BE, 2007.

[47] ASTM International. Standard test method for evaluating dowel-bearing strength of wood and wood-based products. Technical report, ASTM International, West Conshohocken, PA.

[48] Joint Committee on Structural Safety. Probabilistic model code. Technical report, JCSS, 2006.

[49] H.J. Blaß, A. Bienhaus, and V. Krämer. Effective bending capacity of dowel-type fasteners. In *33th Proceedings of the CIB-W18 Meeting, Paper 33-7-5, Delft, The Netherlands*, 2000.

[50] P. Zarnani and P. Quenneville. New design approach for controlling brittle failure modes of small-dowel-type connections in cross-laminated timber (clt). *Construction and Building Materials*, 100:172–182, Dec 2015.

[51] J.L. Jensen, U.A. Girhammar, and P. Quenneville. Brittle failure in timber connections loaded parallel to the grain. *Proceedings of the Institution of Civil Engineers - Structures and Buildings*, 168(10):760–770, Oct 2015.

[52] R. Jockwer. Impact of varying material properties and geometrical parameters on the reliability of shear connections with dowel type fasteners. In *3rd International Network on Timber Engineering Research, Paper 49-7-1, Graz, Austria*, 2016.

[53] R. Jockwer, G. Fink, and J. Köhler. Assessment of existing safety formats for timber connections – how probabilistic approaches can influence connection design in timber engineering. 2017.

[54] J.L. Jensen and P. Quenneville. Fracture mechanics analysis of row shear failure in dowelled timber connections. *Wood Science and Technology*, 44(4):639–653, Nov 2009.

[55] P. Quenneville and P. Zarnani. Proposal for the connection chapter of the new zealand design of timber structures. 2017.

[56] P. Quenneville. Predicting the failure modes and strength of brittle bolted connections. In *Proceedings of the 5th World Conference on Timber Engineering (WCTE), Montreux, Switzerland*, volume 2, pages 137–144, 1998.

[57] M. Mohammad and J.H.P. Quenneville. Bolted wood steel and wood-steel-wood connections: verification of a new design approach. *Canadian Journal of Civil Engineering*, 28(2):254–263, Apr 2001.

[58] J.L. Jensen and P. Quenneville. Fracture mechanics analysis of row shear failure in dowelled timber connections: asymmetric case. *Materials and Structures*, 44(1):351–360, Jun 2010.

[59] M.A.H. Mohammad, P. Quenneville, and I. Smith. Bolted timber connections: investigations on failure mechanism. In *Proceedings of the International Conference of IUFROS*, volume 5, pages 18–20, 1997.

[60] J.M. Cabrero and M. Yurrita. Performance of the different models for brittle failure in the parallel-to-grain direction for connections with dowel-type fasteners. In *5th International Network on Timber Engineering Research, Paper 51-7-12, Tallinn, Estonia*, 2018.

[61] W. Weibull. *A Statistical Theory of the Strength of Materials*. Handlingar / Ingeniörsvetenskapsakademien. Generalstabens litografiska anstalts förlag, 1939.

[62] Wikipedia. Weibull distribution. Page Version ID: 957059377 `https://en.wikipedia.org/w/index.php?title=Weibull_distribution&oldid=957059377`, May 2020. Last accessed Sun May 17 2020.

[63] I. Miller and J.E. Freund. *Probability and statistics for engineers.* Prentice-Hall, Inc., 1977.

[64] R.O. Foschi and J.D. Barrett. Consideration of size effects in longitudinal shear strength foruncracked beams. In *13th Proceedings of the CIB-W18 Meeting, Paper 13-6-2, Otaniemi, Finland*, 1980.

[65] R.O. Foschi. Longitudinal shear design of glued laminated beams. In *18th Proceedings of the CIB-W18 Meeting, Paper 18-10-2, Beit Oren, Israel*, 1985.

[66] F. Colling. Influence of volume and stress distribution on the shear strength and tensile strength perpendicular to grain. In *19th Proceedings of the CIB-W18 Meeting, Paper 19-12-3, Florence, Italy*, 1986.

[67] F. Rouger and T. Fewell. Size effects in timber: Novelty never ends. In *27th Proceedings of the CIB-W18 Meeting, Paper 27-6-2, Sydney, Australia*, 1994.

[68] J.D. Barrett. Effect of size on tension perpendicular-to-grain strength of douglas-fir. *Wood and Fiber Science*, 6(2):126–143, 2007.

[69] Python Software Foundation. Python language reference, version 3.7.6. Available at https://www.python.org.

[70] S. Kennedy. Withdrawal and embedding resistance of fasteners in timber and clt panels. Master's thesis, Master's Thesis. Université Laval, Quebec, CA, 2014.

[71] J. Ehlbeck and H. Werner. Softwood and hardwood embedding strength for dowel-type fasteners. In *25th Proceedings of the CIB-W18 Meeting, Paper 25-7-2, Åhus, Sweden*, 1992.

[72] B. Vreeswijk. Verbindungen in hardhout. Master's thesis, Faculty of Civil Engineering, TU Delft, 2003.

7

Appendices

A

Embedment strength comparison study

The figures described by section 5.1 are generated from scripts and functions publicly available in the source code repository at the following GitLab link. The source code within this repository is licensed according to the GNU General Public Version 2 License (GPLv2).

- Repository structure:

  bin
  LICENSE
  pyembedstrength
  README.org
  setup.py

- Scripts

  cumulative_embedment_strength_plot.py
  cumulative_embedment_strength_plot_v2.py
  feature_selection.py
  linear_regression_plot.py
  regression_plot.py

- Functions

  core.py
  ___init___.py
  linfig.py
  presentation_plot.py
  seabornFig2Grid.py

B

Single fastener TST connections

Input files containing the geometry parameters required to replicate the analyses presented in chapter 5 of single fastener and internal steel plate TST connections are listed here. Additionally, the parameters to define the material properties are provided as additional input files to the analyses conducted within this thesis in the JSON formatted input files. Furthermore, the three scripts to replicate the analyses presented are listed according to filename here.

1. `single_fastener.py` used to generate results regarding the probability of brittle failure over ductile failure. Geometric input parameter files relevant to this script are:

   - `series-probabilityBlessD-SF-vary-t1.json`

   ```
   {
       "name": "series-probabilityBlessD-SF-vary-t1",
       "type of connection": "tst",
       "geometrical parameters": {
           "d": [12, 12, 1],
           "t1": [5, 25, 50],
           "t2": [10, 10, 1],
           "nc": [1, 1, 1],
           "nr": [1, 1, 1],
           "a1": [0, 0, 1],
           "a2": [0, 0, 1],
           "a3": [2.1, 21.116, 4],
           "a4": [2.5, 2.5, 1],
           "ns": [1, 2, 2]
       },
       "material parameters": {
           "material data": "material_data.csv",
           "correlation matrix": "correlationmatrix.csv"
       }
   }
   ```

2. `single_fastener_distplots.py` used to generate results regarding the statistical distribution of the resulting governing failure capacity per TST connection. Geometric input parameter files relevant to this script are:

   - `series-distplots-SF-d8-vary-t1.json`
   - `series-distplots-SF-d12-vary-t1.json`

- `series-distplots-SF-d16-vary-t1.json`
- `series-distplots-SF-d8-vary-a3.json`
- `series-distplots-SF-d12-vary-a3.json`
- `series-distplots-SF-d16-vary-a3.json`

3. `single_fastener_pickdistplots.py` used to generate results regarding the statistical distributions of the governing failure capacity of 6 specific TST connections of certain geometric parameters. Geometric input parameter files relevant to this script are:
   - `series-pickdistplots-SF-vary-t1.json`

All of the programming code is available publicly in the repository at the following GitLab link. The code developed within this thesis is licensed under a GNU General Public version 2 License found within the source code repository.

- Repository structure:

  bin/
  LICENSE
  pyconnect/
  README.org
  requirements.txt
  setup.py

- Scripts:

  base_mech_strength_timber.py
  multiple_fastener.py
  single_fastener_distplots.py
  single_fastener_pickdistplots.py
  single_fastener.py
  weibull_distribution_plot.py

- Functions:

  connection.py
  core.py
  derived_parameters.py
  failure_equations.py
  ___init___.py
  inputs.py
  material.py
  plotting.py
  posdef.py
  version.py

The input parameter files are included below as a part of this appendix.

```
{
    "name": "series-probabilityBlessD-SF-vary-t1",
```

```
    "type of connection": "tst",
    "geometrical parameters": {
        "d": [12, 12, 1],
        "t1": [5, 25, 50],
        "t2": [10, 10, 1],
        "nc": [1, 1, 1],
        "nr": [1, 1, 1],
        "a1": [0, 0, 1],
        "a2": [0, 0, 1],
        "a3": [2.1, 21.116, 4],
        "a4": [2.5, 2.5, 1],
        "ns": [1, 2, 2]
    },
    "material parameters": {
        "material data": "material_data.csv",
        "correlation matrix": "correlationmatrix.csv"
    }
}

{
    "name": "series-SF-d8-vary-t1",
    "type of connection": "tst",
    "geometrical parameters": {
        "d": [8, 8, 1],
        "t1": [5, 15.95, 25],
        "t2": [10, 10, 1],
        "nc": [1, 1, 1],
        "nr": [1, 1, 1],
        "a1": [0, 0, 1],
        "a2": [0, 0, 1],
        "a3": [10, 10, 1],
        "a4": [2.5, 2.5, 1],
        "ns": [1, 1, 1]
    },
    "material parameters": {
        "material data": "material_data.csv",
        "correlation matrix": "correlationmatrix.csv"
    }
}

{
    "name": "series-SF-d12-vary-t1",
    "type of connection": "tst",
    "geometrical parameters": {
        "d": [12, 12, 1],
        "t1": [5, 15.95, 25],
        "t2": [10, 10, 1],
        "nc": [1, 1, 1],
        "nr": [1, 1, 1],
        "a1": [0, 0, 1],
```

```
        "a2": [0, 0, 1],
        "a3": [10, 10, 1],
        "a4": [2.5, 2.5, 1],
        "ns": [1, 1, 1]
    },
    "material parameters": {
        "material data": "material_data.csv",
        "correlation matrix": "correlationmatrix.csv"
    }
}

{
    "name": "series-SF-d16-vary-t1",
    "type of connection": "tst",
    "geometrical parameters": {
        "d": [16, 16, 1],
        "t1": [5, 15.95, 25],
        "t2": [10, 10, 1],
        "nc": [1, 1, 1],
        "nr": [1, 1, 1],
        "a1": [0, 0, 1],
        "a2": [0, 0, 1],
        "a3": [10, 10, 1],
        "a4": [2.5, 2.5, 1],
        "ns": [1, 1, 1]
    },
    "material parameters": {
        "material data": "material_data.csv",
        "correlation matrix": "correlationmatrix.csv"
    }
}

{
    "name": "series-SF-d8-vary-a3",
    "type of connection": "tst",
    "geometrical parameters": {
        "d": [8, 8, 1],
        "t1": [10, 10, 1],
        "t2": [10, 10, 1],
        "nc": [1, 1, 1],
        "nr": [1, 1, 1],
        "a1": [0, 0, 1],
        "a2": [0, 0, 1],
        "a3": [2.1, 17.38, 5],
        "a4": [2.5, 2.5, 1],
        "ns": [2, 2, 1]
    },
    "material parameters": {
        "material data": "material_data.csv",
        "correlation matrix": "correlationmatrix.csv"
```

```
    }
}

{
    "name": "series-SF-d12-vary-a3",
    "type of connection": "tst",
    "geometrical parameters": {
        "d": [12, 12, 1],
        "t1": [10, 10, 1],
        "t2": [10, 10, 1],
        "nc": [1, 1, 1],
        "nr": [1, 1, 1],
        "a1": [0, 0, 1],
        "a2": [0, 0, 1],
        "a3": [2.1, 17.38, 5],
        "a4": [2.5, 2.5, 1],
        "ns": [1, 1, 1]
    },
    "material parameters": {
        "material data": "material_data.csv",
        "correlation matrix": "correlationmatrix.csv"
    }
}

{
    "name": "series-SF-d16-vary-a3",
    "type of connection": "tst",
    "geometrical parameters": {
        "d": [16, 16, 1],
        "t1": [10, 10, 1],
        "t2": [10, 10, 1],
        "nc": [1, 1, 1],
        "nr": [1, 1, 1],
        "a1": [0, 0, 1],
        "a2": [0, 0, 1],
        "a3": [2.1, 17.38, 5],
        "a4": [2.5, 2.5, 1],
        "ns": [1, 1, 1]
    },
    "material parameters": {
        "material data": "material_data.csv",
        "correlation matrix": "correlationmatrix.csv"
    }
}

{
    "name": "series-SF-vary-t1-specialized",
    "type of connection": "tst",
    "geometrical parameters": {
        "d": [8, 16, 3],
        "t1": [7.74, 10.47, 2],
```

```
        "t2": [10, 10, 1],
        "nc": [1, 1, 1],
        "nr": [1, 1, 1],
        "a1": [0, 0, 1],
        "a2": [0, 0, 1],
        "a3": [9.74, 9.74, 1],
        "a4": [2.5, 2.5, 1],
        "ns": [1, 1, 1]
    },
    "material parameters": {
        "material data": "material_data.csv",
        "correlation matrix": "correlationmatrix.csv"
    }
}
```

C

Multiple fastener TST connections

Additional input files containing the geometry parameters of the analyses of multiple fastener TST connections are included within this second appendix. The material property input parameter files remain the same as described in the previous appendix B. The script used to generate and analyze the results of the multiple fastener TST connections studied is named `multiple_fastener.py` with the input geometry file named `series-MF.json`. Similar to appendix B, the scripts may be found in the same public source code repository as in the previous appendix (GitLab link).

```
{
    "name": "series-probabilityBlessD-MF-ns1",
    "type of connection": "tst",
    "geometrical parameters": {
        "d": [12, 12, 1],
        "t1": [5, 25, 25],
        "t2": [10, 10, 1],
        "nc": [2, 4, 2],
        "nr": [1, 5, 2],
        "a1": [5, 15, 4],
        "a2": [, 15, 4],
        "a3": [2.1, 26.25, 4],
        "a4": [0.9, 4.5, 4],
        "ns": [2, 2, 1]
    },
    "material parameters": {
        "material data": "material_data.csv",
        "correlation matrix": "correlationmatrix.csv"
    }
}
```

```
{
    "name": "series-probabilityBlessD-MF-ns1",
    "type of connection": "tst",
    "geometrical parameters": {
        "d": [12, 12, 1],
        "t1": [5, 25, 25],
        "t2": [10, 10, 1],
        "nc": [2, 4, 2],
        "nr": [1, 5, 2],
```

```
        "a1": [5, 15, 4],
        "a2": [7.67, 7.67, 1],
        "a3": [2.1, 26.25, 4],
        "a4": [2.1, 2.1, 1],
        "ns": [1, 1, 1]
    },
    "material parameters": {
        "material data": "material_data.csv",
        "correlation matrix": "correlationmatrix.csv"
    }
}

{
    "name": "series-probabilityBlessD-MF-ns2",
    "type of connection": "tst",
    "geometrical parameters": {
        "d": [12, 12, 1],
        "t1": [5, 25, 25],
        "t2": [10, 10, 1],
        "nc": [2, 4, 2],
        "nr": [1, 5, 2],
        "a1": [5, 15, 4],
        "a2": [7.67, 7.67, 1],
        "a3": [2.1, 26.25, 4],
        "a4": [2.1, 2.1, 1],
        "ns": [2, 2, 1]
    },
    "material parameters": {
        "material data": "material_data.csv",
        "correlation matrix": "correlationmatrix.csv"
    }
}
```